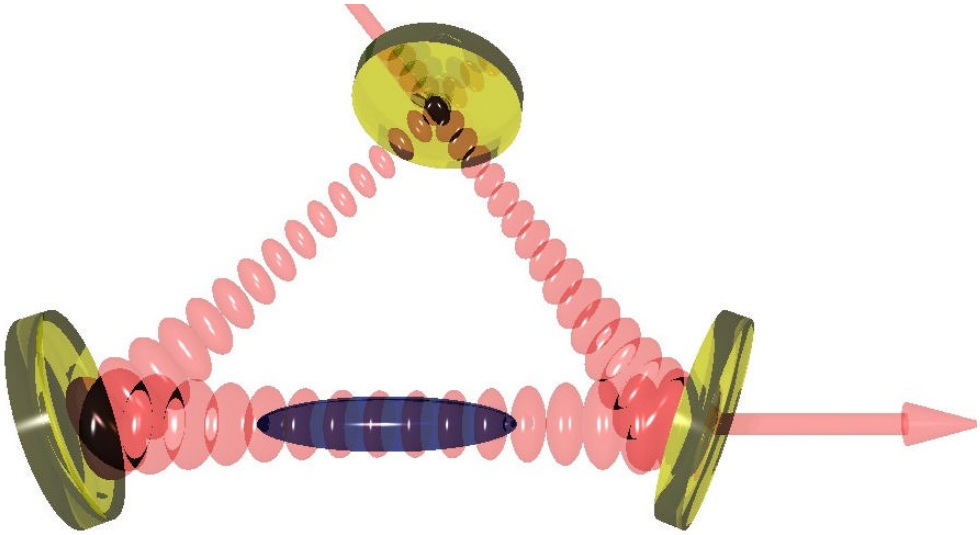

Aulas em Física para pós-graduação

Advanced Optics and Electronics laboratory

Ph.W. Courteille
Universidade de São Paulo
Instituto de Física de São Carlos
15 de maio de 2017

Sumário

Capítulo 0

Preface

This manual has been extracted from a more comprehensive script on *Advanced Optics and Electronics Laboratory* used for the graduate lab course SFI5888 offered by the Instituto de Física de São Carlos of the Universidade de São Paulo.

The quantum optical tinker course addresses to graduate students. The course's aim to introduce the student to the toolbox of experimental atom and quantum optics. Not only he should familiarize with the basic components (i.e., lenses, acousto-optic modulators, etc.) of modern quantum optics, but also test their use in complex experimental apparatuses. The student is thus working right from the beginning on a far-reaching project, such as an intensity stabilization for a laser or an information transfer system based on lasers with heterodyne detection, to the realization of which he uses quantum optical components. He will learn in addition to Gaussian optics and interferometry, which represent main topics of the course, how to develop simple electronic circuits and servo controls with operational amplifiers, how to deal with radio frequency components, and how to use the essential measurement tools (oscilloscopes, multimeters, power meters and spectrum analyzers).

Every component of the quantum optical kit has its particularities and problems, and a minimum of theoretical background is essential. It is therefore important that the student prepares himself to the course through this script, the literature indicated in this script, or information from the internet. The internet plays a particularly important role in the gathering of information, for example when data sheets for specific components are needed. Nevertheless, just as for conventional courses, the focus of the course clearly lies in practice. The setups and experiments are, however, not fixed, but can be varied according to the student's interests. The tinker course is complemented by tours in quantum optics research laboratory, in which a student has the opportunity to convince himself, that the devices and techniques he gets to know, are actually used in a modern research laboratory.

The quantum optical tinker course offers the student the opportunity to probe and to train his soft skills, such as his ability to work in a team. The groups consist of up to four people, who split and share their assigned tasks in order to solve them in the most efficient way. Just like in a small research group, for each project a project manager and a secretary will a assigned. The group should jointly hold a laboratory book, in which the realized experimental setups, the calibration curves, the measurements and evaluations are documented. A certificate will be issued, if at least two projects are drafted.

0.1 Organization of the course

The script was written for the course *Advanced Optics and Applied Electronics laboratory* (SFI5888) offered by the Instituto de Física de São Carlos (IFSC) of the Universidade de São Paulo (USP). The course is addressed to graduate Physics students. The script is a preliminary version and

subject to ongoing correction and modifications. Notifications of errors and suggestions for improvement are always welcome. The script incorporates exercises with solutions that can be obtain from the author.

Informations and announcements with respect to the course will be published on our website: http://www.ifsc.usp.br/ strontium/ $->$ Teaching $->$ SFI5888

The evaluation of the student will be based on a written test and a seminar on a topic chosen by the student.

0.2 Equipment

The lab course has been given in lab with the following equipment:

qnty	estim. price [Euro]	device
1×	10000	ECDL at 670 nm with current drive and temperature stabilization
1×	2000	optical isolator
1×	1400	power meter
2×	1600	$\lambda/2$, $\lambda/4$, PBS, non-PBS
1×		electronic supply (mixers, VCOs, quartzs, ...)
1×	200	1 W radiofrequency amplifier
1×	500	frequency generator
10×	300	broadband mirrors
10×	1000	mirror mounts and posts
1×	200	piezo-electric transducer
1×		fast photodetector
2×		photodiodes FFD 100 (Perkin Elmers)
1×		scanning Fabry-Perot
1×	500	optical fiber
1×	2000	acousto-optic modulator
1×	4000	electro-optic modulator
1×	300	function generator
2×	400	power supplies ($\pm$15 V, $\pm$25 V, +5 V)
2×		oscilloscope
1×		spectrum analyzer
1×		tools (soldering station, Allan wrenches, lens cleaning tissues, ...)
1×		National Instruments interface board
1×		computer (with internet access and Matlab)
1×		laser printer

0.3 Recommended bibliography

H. Kogelnik and X.Y. Li, Appl. Opt. **5**, 155 (1966), *Laser beams and resonators*
M. Born, 6.ed. Pergamon Press New York (1980), *Principles of Optics*
P. Horowitz and W. Hill, Cambridge University Press (2001), *The Art of Electronics*
A. Yariv,, John Wiley & Sons (1989), *Quantum Electronics*
A. Yariv and P. Yeh, Wiley, *Optical waves in crystals*
U. Tietze & Ch. Schenk, Springer-Verlag, *Halbleiterschaltungstechnik*
O. Föllinger, Hüsing-Verlag, Heidelberg, *Regeltechnik*

R.W.P. Drever, J.L. Hall, F.V. Kowalski, J. Hough, G.M. Ford, A.J. Munley, and H.W. Ward, Appl. Phys. B **31**, 97 (1983), *Laser Phase and Frequency Stabilization Using an Optical Resonator*

Capítulo 1

Gaussian optics and the polarization of light

The objective of this part of the course is to introduce the trainee into the basics of *Gaussian optics* and *polarizations optics*. The student will learn to transform the diameter and the divergence of a Gaussian beam using lenses and telescopes and to analyze and manipulate the polarization of a laser beam.

1.1 Introduction to Gaussian optics

1.1.1 Wave equation and beam parameters

At first sight, one might think that the propagation of laser light is well described by the laws of geometrical optics. On closer inspection it turns out, however, that laser beams behave in many respects more like plane waves with their energy is concentrated near an optical axis. The electro-magnetic fields satisfy the *wave equation*,

$$k^2 u + \nabla^2 u = 0 \ . \tag{1.1}$$

For waves propagating in z direction, $u = \psi(x, y, z)e^{-ikz}$, one obtains a Schrödinger-like equation [11],

$$2ik\frac{\partial \psi}{\partial z} - \frac{\partial^2 \psi}{\partial x^2} - \frac{\partial^2 \psi}{\partial y^2} = 0 \ , \tag{1.2}$$

where $\partial^2\psi/\partial z^2$ has been neglected.

To describe a *Gaussian beam*, we choose an exponential ansatz and introduce two parameters, which can vary along the propagation axis z: $P(z)$ is a complex phase shift and $q(z)$ a complex parameter, whose imaginary part describes the diameter of the beam. The ansatz

$$\psi = e^{-i\left[P(z)+k(x^2+y^2)/2q(z)\right]} \tag{1.3}$$

leads to[1]

$$0 = (q' - 1)\frac{ik(x^2 + y^2)}{q^2} - 2iP' + \frac{2}{q} \ . \tag{1.4}$$

In order for Eq. (1.4) to hold for all x and y, we need $q' = 1$ and $P' = \frac{-i}{q}$. Integrating q', we find

$$q = q_0 + z \ . \tag{1.5}$$

[1] See script of the course "Interação Luz-Matéria" from the same author.

It is useful to introduce real beam parameters,

$$\frac{1}{q} \equiv \frac{1}{R} - i\frac{\lambda}{\pi w^2} \ . \tag{1.6}$$

Inserting these into Eq. (1.2),

$$\psi = e^{-iP - i\frac{k(x^2+y^2)}{2R} - \frac{(x^2+y^2)}{w^2}} \ , \tag{1.7}$$

it becomes clear that $R(z)$ is the radius of curvature and $w(z)$ the beam diameter. Evaluating q_0 at the position of the focus (waist of the beam), where $R = \infty$, we obtain from (1.5) and (1.6)

$$w^2(z) = w_0^2\left[1 + \left(\frac{\lambda z}{\pi w_0^2}\right)^2\right] \quad \text{and} \quad R(z) = z\left[1 + \left(\frac{\pi w_0^2}{\lambda z}\right)^2\right] \ . \tag{1.8}$$

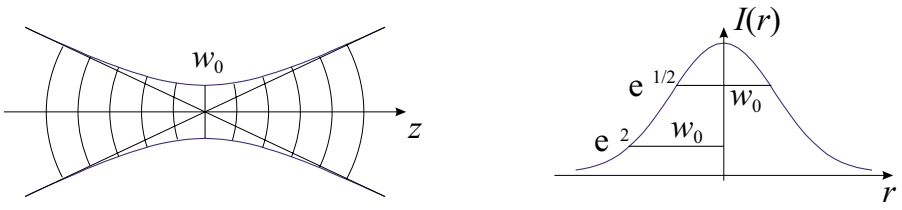

Figura 1.1: (Left) Propagation of the beam along the optical axis. (Right) Cross section of a gaussian laser beam.

1.1.2 Transfer matrices

For the practical work with Gauss beams it is helpful to introduce transfer matrices, which describe the transformation of a Gauss beam through optical components along the optical axis. The matrix

$$\mathbf{M} = \begin{pmatrix} a & b \\ c & d \end{pmatrix} \tag{1.9}$$

transforms the beam parameter q in the following way:

$$q(z) = \frac{aq(0) + b}{cq(0) + d} \ . \tag{1.10}$$

Transfer matrices allow to calculate, how the parameters R and w transform along the optical axis across the optical elements or in free space. The most common optical elements are lenses, crystals, prisms, mirrors and cavities. For example, the matrix for propagation in free space of a beam over a distance d is,

$$\mathbf{M} = \begin{pmatrix} 1 & d \\ 0 & 1 \end{pmatrix} \tag{1.11}$$

and the matrix for transformation through a thin lens with focal distance f,

$$\mathbf{M} = \begin{pmatrix} 1 & 0 \\ -1/f & 1 \end{pmatrix} \ . \tag{1.12}$$

It is interesting to note that the transfer matrices are the same as those, which in classical beam optics transform the vector, whose components are the distance of the beam from the optical axis y and its divergence $y'(z)$:

$$\begin{pmatrix} y(z) \\ y'(z) \end{pmatrix} = \mathbf{M} \begin{pmatrix} y(0) \\ y(0) \end{pmatrix} \ . \tag{1.13}$$

1.1.2.1 Ex: Tasks and learning goals

In order to test our understanding of Gaussian optics, we will derive a few useful formulae:

1. Consider a Gaussian beam characterized by its parameter $q(0)$ transformed by two lenses located at distances z_1 and z_2 along the optical axis.

1.2 Experimental characterization of a Gaussian beam

Once a Gaussian beam has been characterized at a given position z, the transfer matrix formalism allows us to calculate its shape at any position along the optical axis. In this section, we will study the propagation of a Gaussian beam through free space (see Eqs. (1.8)) and its transformation through a thin lens with focal distance f. For the latter one, we obtain directly after the lens,

$$\frac{1}{R(z \searrow 0)} = \frac{1}{R(z \nearrow 0)} - \frac{1}{f} \ . \tag{1.14}$$

1.2.0.2 Ex: Tasks and learning goals

In this exercise, we will learn to measure the beam parameters characterizing a Gaussian beam.

1. Measure the phase profile of a helium-neon laser. To this end fix a razor blade on a translation stage and move it sideways into the beam. From the power of the partially blocked beam $\int_F I(x,y)dxdy$, where F is the cross section of the unblocked part of the beam, $w(z)$ can be determined.
2. Focus the beam with a lens. Measure the beam diameter at another location. Compare with the prediction of Gaussian optics.
3. Set up a 1:3 telescope and verify that the outgoing beam is collimated.
4. Derive the formulae (1.7) using the beam matrices from Ref. [11].

Solução: *Example for the experimental determination of a Gaussian beam. We fit the integral*

$$\begin{aligned} \frac{\tilde{P}}{P} &= \int_{-\infty}^{\tilde{x}} \int_{-\infty}^{\infty} \frac{2}{\pi w(z)^2} e^{-2r^2/w(z)^2} dxdy \\ &= \frac{2}{\sqrt{\pi} w(z)^2} \int_{-\infty}^{\sqrt{2}\tilde{x}/w(z)} e^{-\xi^2} d\xi = \frac{1}{2}\left[\mathrm{erf}\left(\tilde{x}\sqrt{z}/w(z)\right) + 1\right] \end{aligned} \tag{1.15}$$

to the measured data by varying only $w(z)$.

Further reading:
*H. Kogelnik and X. Y. Li, Proc. of the IEEE **54**, 1312 (1966). Laser Beams and Resonators.*

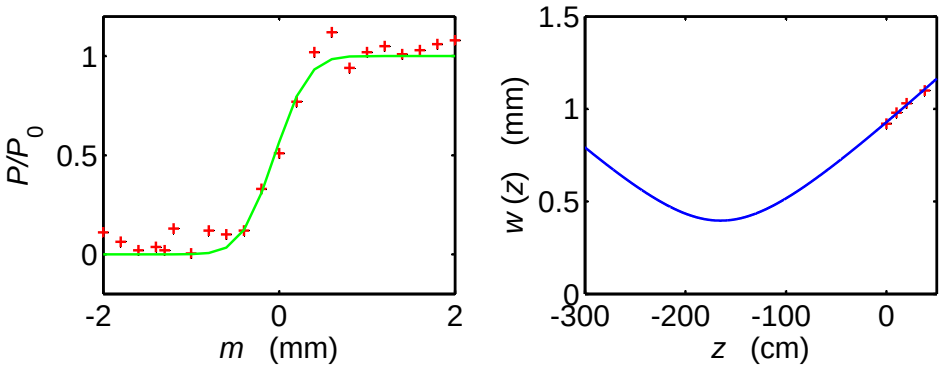

Figura 1.2: (a) Adjustment of an error function for a measured beam profile. (b) Adjustment of a laser beam propagation using Gaussian optics.

1.3 Introduction to polarization optics

A laser usually has a well-defined polarization, e.g. , linear or circular. The polarizations can be transformed into one another through a *quarter waveplate* ($\lambda/4$) or a *half waveplate* ($\lambda/2$) by a Fresnel rhomb or other birefringent elements. Superpositions of polarizations can be separated by a *polarizing beam splitter*.

The degree of freedom of polarization is often used for separating counterpropagating light fields, e.g. in ring lasers, by means of elements called *optical diode* or *optical isolator*. The elements consist of a Faraday rotator and $\lambda/2$ waveplate. Another practical example is the use of $\lambda/4$ in double passage. An incoming beam can be separated from a returning beam by using a $\lambda/4$ blade and a polarizing beam splitter.

1.3.1 Jones matrices

The term *polarization* is defined in relation to a fixed coordinate system, while the term *helicity* denotes the direction of rotation of the polarization vector with respect to the direction of propagation of the light beam. The polarization of a beam propagating in z-direction can easily be expressed by a vector of complex amplitude,

$$\mathbf{E}(\mathbf{r},t) = \begin{pmatrix} a \\ b \\ 0 \end{pmatrix} e^{i\mathbf{kr}-i\omega t} = \begin{pmatrix} 1 \\ e^{-i\phi}|b|/|a| \\ 0 \end{pmatrix} |a| e^{i\mathbf{kr}-i\omega t} \ . \tag{1.16}$$

The angle $\phi = \arctan \frac{\operatorname{Im} ab^*}{\operatorname{Re} ab^*}$ determines the polarization of the light beam. A polarization is linear when $\phi = 0$ and circular when $\phi = \pi/2$. $|b|/|a|$ is, hence, the degree of ellipticity. A polarization rotator for linearly polarized light (e.g., a sugar solution) is described by the following *Jones matrix (*we will restrict to the x-y-plane)

$$M_{rotator}(\phi) = \begin{pmatrix} \cos\phi & \sin\phi \\ -\sin\phi & \cos\phi \end{pmatrix} \ , \tag{1.17}$$

where ϕ is the rotation angle. For the Faraday rotator the sign of the rotation angle depends on the propagation direction of the laser beam. A *polariser* projects the polarization onto a specific axis. In the case of the x-axis Jones's matrix is,

$$M_{polarisador} = \begin{pmatrix} 1 & 0 \\ 0 & 0 \end{pmatrix} \ . \tag{1.18}$$

If the rotation angle is ϕ,

$$M_{polarisador}(\phi) = \begin{pmatrix} \cos\phi & \sin\phi \\ -\sin\phi & \cos\phi \end{pmatrix} \begin{pmatrix} 1 & 0 \\ 0 & 0 \end{pmatrix} \begin{pmatrix} \cos\phi & \sin\phi \\ -\sin\phi & \cos\phi \end{pmatrix}^{-1} .$$

Other components, such as electro-optical modulators or phase plates are birefringent crystals, which act only on one of the two optical axes. If only the y axis is optically active, the Jones's matrix is,

$$M_{\theta\text{-waveplate}} = \begin{pmatrix} 1 & 0 \\ 0 & e^{i\theta} \end{pmatrix} . \tag{1.19}$$

For $\theta = 2\pi/n$ we obtain a λ/n-waveplate. When we rotate the waveplate and therefore the optically inactive axis to an angle ϕ, the Jones matrices are,

$$\begin{aligned} M_{\theta\text{-waveplate}}(\phi) &= \begin{pmatrix} \cos\phi & \sin\phi \\ -\sin\phi & \cos\phi \end{pmatrix} \begin{pmatrix} 1 & 0 \\ 0 & e^{i\theta} \end{pmatrix} \begin{pmatrix} \cos\phi & \sin\phi \\ -\sin\phi & \cos\phi \end{pmatrix}^{-1} \\ &= \begin{pmatrix} \cos^2\phi + e^{i\theta}\sin^2\phi & -\sin\phi\cos\phi + e^{i\theta}\sin\phi\cos\phi \\ -\sin\phi\cos\phi + e^{i\theta}\sin\phi\cos\phi & \sin^2\phi + e^{i\theta}\cos^2\phi \end{pmatrix} . \end{aligned} \tag{1.20}$$

In most cases, we use quarter waveplates $\lambda/4$,

$$M_{\lambda/4}(\phi) = \begin{pmatrix} \cos^2\phi + i\sin^2\phi & (-1+i)\sin\phi\cos\phi \\ (-1+i)\sin\phi\cos\phi & \sin^2\phi + i\cos^2\phi \end{pmatrix} \tag{1.21}$$

and half waveplates $\lambda/2$,

$$M_{\lambda/2}(\phi) = \begin{pmatrix} \cos 2\phi & -\sin 2\phi \\ -\sin 2\phi & -\cos 2\phi \end{pmatrix} . \tag{1.22}$$

Combinations of $\lambda/2$ waveplates and *Faraday rotator*s are used as *optical isolator*, also called *optical diode*.

1.3.2 Fresnel formulae

Reflection and transmission of a beam of light at a surface depend on the polarization of the light and the angle of incidence. They are described by the *Fresnel formula*:

$$\left(\frac{E_{0t}}{E_{0i}}\right)_s = t_s = \frac{2\sin\beta\cos\alpha}{\sin(\alpha+\beta)} \tag{1.23}$$

$$\left(\frac{E_{0r}}{E_{0i}}\right)_s = r_s = -\frac{\sin(\alpha-\beta)}{\sin(\alpha+\beta)} \tag{1.24}$$

$$\left(\frac{E_{0t}}{E_{0i}}\right)_p = t_p = \frac{2\sin\beta\cos\alpha}{\sin(\alpha+\beta)\cos(\alpha-\beta)} \tag{1.25}$$

$$\left(\frac{E_{0r}}{E_{0i}}\right)_p = r_p = \frac{\tan(\alpha-\beta)}{\tan(\alpha+\beta)} . \tag{1.26}$$

The angles of incidence and transmission are related by Snell's law: $n_1\sin\alpha = n_2\sin\beta$.

The Brewster angle α_B is reached, when $\alpha_B + \beta = 90°$, i.e., when following Snell's law,

$$n_1\sin\alpha_B = n_2\sin(90°) = n_2\cos\beta \tag{1.27}$$

$$\tan\alpha_B = \frac{n_2}{n_1} . \tag{1.28}$$

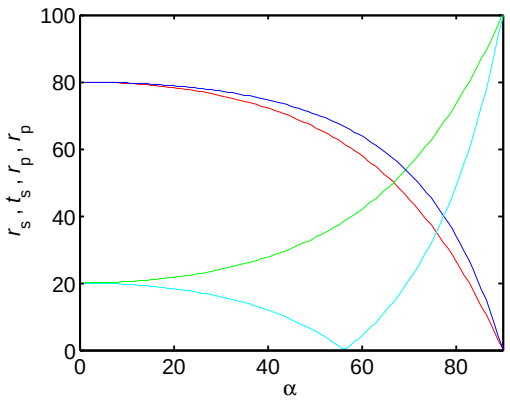

Figura 1.3: Formulae de Fresnel.

1.3.2.1 Ex: Tasks and learning goals

In order to test our understanding of the Jones matrix formalism, we will solve the following problem:

1. Consider a linearly polarized laser beam passing twice through a $\lambda/4$, first in direction of the optical axis, the second time in opposite direction. Calculate the final polarization.

1.4 Measuring the polarization of a laser beam

How to rotate the polarization of a linearly polarized light beam in an electronically controlled way, i.e., tune ϕ arbitrarily in the polarization vector $\begin{pmatrix}\cos\phi\\ \sin\phi\end{pmatrix}$? Consider a Mach-Zehnder interferometer. The two arms contain $\lambda/4$ waveplates making the polarizations circular, but in opposite senses. One of the arms additionally has a piezo displacing the phase of the wave. The recombined wave is then,

$$\begin{pmatrix}1\\ i\end{pmatrix} + \begin{pmatrix}1\\ -i\end{pmatrix} e^{i\phi} = (1+e^{i\phi}) \begin{pmatrix}1\\ \frac{i-ie^{i\phi}}{1+e^{i\phi}}\end{pmatrix} = (1+e^{i\phi}) \begin{pmatrix}1\\ \frac{\sin\phi}{1+\cos\phi}\end{pmatrix} . \tag{1.29}$$

The fact that the polarization vector is purely real shows that the polarization is linear.

1.4.0.2 Ex: Tasks and learning goals

In this part of the course, we will analyze and manipulate the polarization of a helium-neon laser.

1. Determine the polarization of a helium-neon laser. Sketch the transmitted intensity through a polarizing filter as a function of the angle of the filter in a polar diagram.

2. Mirrors can change the polarization of light and, for example, transform a linear polarization to elliptical. Determine the degree of ellipticity for a given mirror. How does a mirror transform the polarization and the helicity of a reflected laser beam?

3. Create circularly polarized light through a $\lambda/4$ blade and check the quality of the circular polarization.

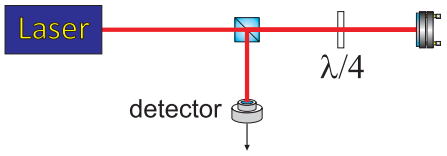

Figura 1.4: Separation of counterpropagating beams through polarization optics.

4. Use a $\lambda/4$ blade to separate a beam of light from a counterpropagating beam.

5. Characterize an optical insulator. Optimize its extinction.

6. Construct an electrically controllable polarization rotator based on a Mach-Zehnder interferometer with two $\lambda/4$ blades and one piezo.

7. Measure the transmission by a glass plate as a function of the angle of incidence for two orthogonal polarizations and determine the Brewster angle.

8. Mirrors can change the polarization of a light beam and, for example, transform a linear polarization into elliptical. Determine the degree of ellipticity for a given mirror.

Capítulo 2

Electronics and radiofrequency

For the control and regulation of important quantum optical devices, such as EOMs, AOMs, laser diodes, photodiodes, piezos etc., *electronic circuit*s are necessary. The aim of this chapter is to provide practical know-how in the basics of electronics.

2.1 Introduction to electronic circuits

2.1.1 Passive electronic components

Electronic components which are characterized by a fixed impedance are called *passive*. The most common devices are resistors, capacitors, and inductances. For their handling, it is useful to be able to identify their impedance from their labeling.

The values of the resistances of resistors are generally codified by colored rings. The first ring to be considered is the one closest to a terminal. In case of 4 rings, the first two rings are to be considered as digits, the third ring gives the exponent 10. With five rings, the first three are digits and the forth gives the exponent of 10. The last ring, in both cases specifies the tolerance of the value of the resistance.

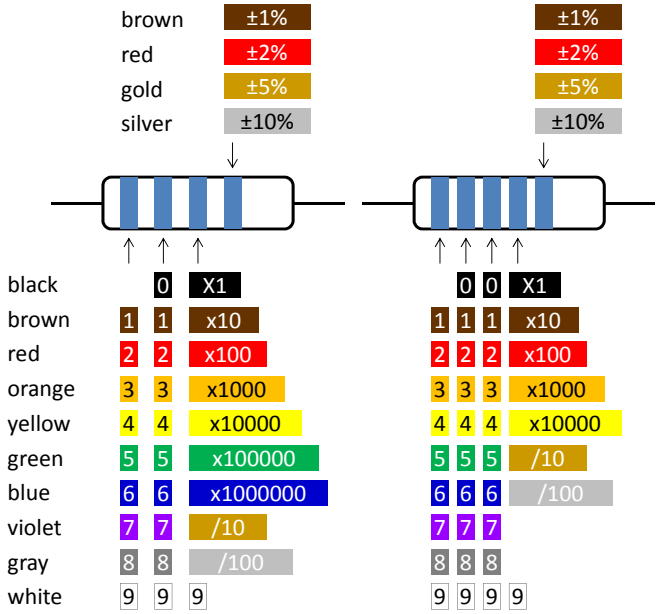

Figura 2.1: Color code for resistors with 4 and 5 rings.

There are various types of capacitors depending on the employed materials for the dielectric medium (paper, ceramics, polyester, electrolyte made of aluminum and electrolyte made of

tantalum). Electrolyte capacitors have a defined polarity, and an reversion of their voltage supply can result in their explosion. The value of the capacitance is generally written on their body, as well as their maximum allowed operating voltage. Also the polarity of electrolyte capacitors is always indicated (although there can be some confusion with regard to the physical and technical direction of the current flow). Ceramic and polyester capacitors can have their values either written in letters or color coded. The color code sequence is similar to that of resistors, with the first two digits devoted to the digits, the third to the multiplier exponent, the forth to the tolerance, and the fifth for the maximum voltage. In case of printed numbers, the first two numbers represent the first two digits, and the third one represents the numbers of 0 before the decimal point. In all cases (colors or digits), the value is given in picoFarads. With more modern serigraphic techniques, some capacitors have their values printed directly in Farads (micro, nano and pico). In these cases, the letter denoting the unit also serves to mark the decimal point. For example, 2n2 means 2.2 nF.

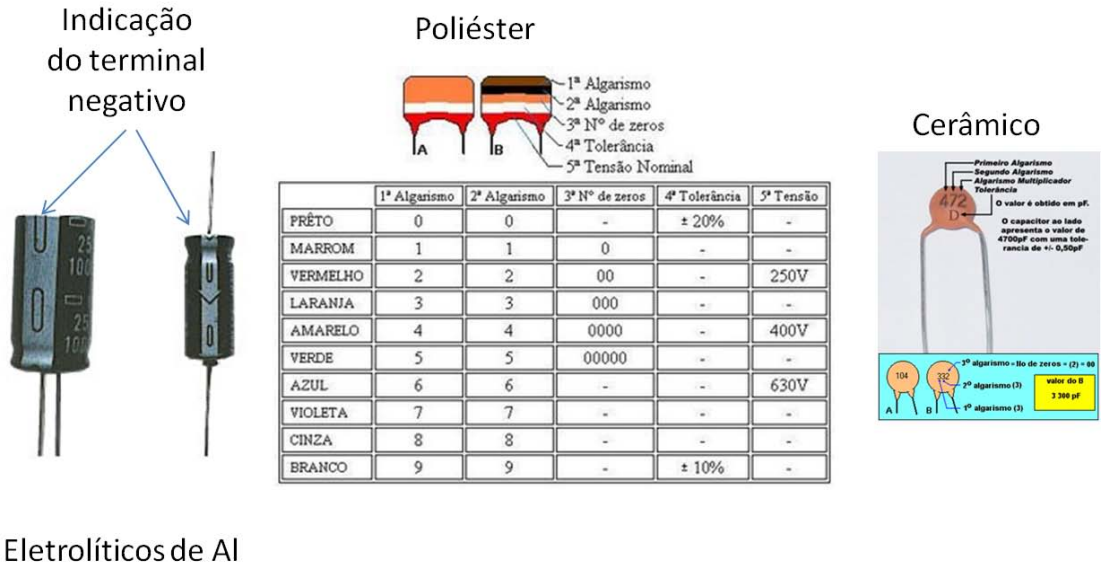

	1ª Algarismo	2ª Algarismo	3ª Nº de zeros	4ª Tolerância	5ª Tensão
PRÊTO	0	0	-	± 20%	-
MARROM	1	1	0	-	-
VERMELHO	2	2	00	-	250V
LARANJA	3	3	000	-	-
AMARELO	4	4	0000	-	400V
VERDE	5	5	00000	-	-
AZUL	6	6	-	-	630V
VIOLETA	7	7	-	-	-
CINZA	8	8	-	-	-
BRANCO	9	9	-	± 10%	-

Figura 2.2: (Left) Electrolyte aluminum capacitors. (Center) Polyester capacitor and color code. (Right) Ceramic capacitor.

2.1.2 Active electronic components and the *pn*-junction

Diodes, transistors, photodiodes, operational amplifiers are called *active components*, because their current-to-voltage curve is non-linear, their response $I = I(U)$ cannot be described by a single constant value, but depends on the applied voltage.

Most active components are many of *semiconductor* characterized by a relatively large band gap between the valence band and the conduction band. By appropriate doping of the material with donors (p-type) or acceptors (n-type)

The most basic semiconductor, which is the *diode* consists of a junction of two types of semiconductors:

During this course we will work a lot with *operational amplifiers* (OpAmp), which are integrated circuits designed to amplify input signals with characteristics that are entirely determined by external components. This feature makes them easy to use and extremely versatile.

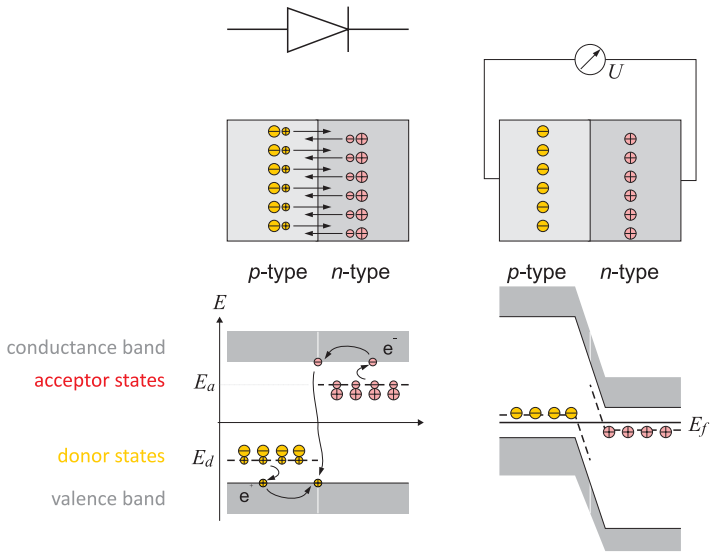

Figura 2.3: (Left) Schematic symbol of an OpAmp; (Right) Pin layout of a standard OpAmp.

OpAmps are generally found encapsulated in DIL type housings (dual in line), which means that they have two lines of 4 pins. The sequence of pins is numerated in counter-clockwise orientation, and they have a mark on the side of pin 1. It is always recommend to obtain the datasheet of the OpAmp since, despite a usual pin compatibility ensured by the various OpAmp manufacturers, deviations are frequent.

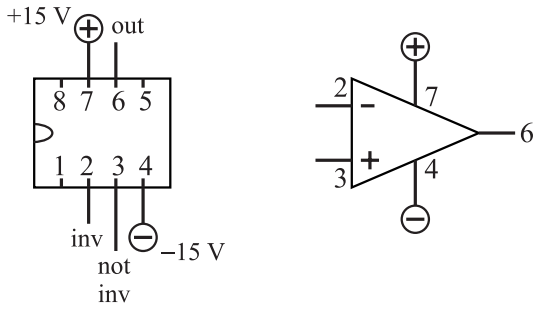

Figura 2.4: (Left) Schematic symbol of an OpAmp; (Right) Pin layout of a standard OpAmp.

2.1.3 Electronic circuits

Amplification or control circuits are nowadays mostly realized with *operational amplifiers* (*OpAmp*). The advantage of an OpAmp compared to circuits based on transistors is, that their properties are almost independent of their internal structure. Hence, their properties can be personalized via an external feedback realized with external components. The input of an OpAmp does not require current. OpAmps amplify the voltage difference between the non-inverting input (+) and the inverting (-). For most practical matters we can assume, that the OpAmp has infinite amplification and negligible input impedance.

OpAmps can be used as *inverting amplifiers* or *non-inverting amplifiers*. Using *Kirchhoff's*

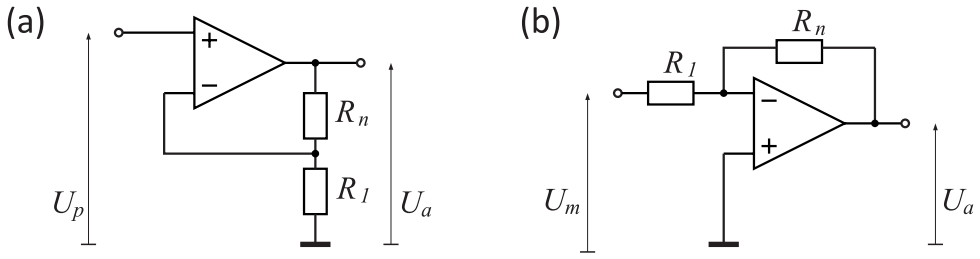

Figura 2.5: (Left) Principle scheme of a standard OpAmp. (Center) Non-inverting amplifier. (Right) Inverting amplifier.

rules for the *loops* and *nodes* of the circuit, we find for a non-inverting amplifier,

$$\frac{U_e}{R_1} = -\frac{U_a}{R_1 + R_n} \quad , \quad G = 1 + \frac{R_n}{R_1} \; . \tag{2.1}$$

This becomes clear noting that, since no voltage is dropped between the inputs (+) and (-), the input voltage must be equal to the voltage drop at R_1. And since the non-inverting input does not deliver current, the currents traversing the resistances R_n and R_1 must be equal. For the inverting amplifier, we find,

$$\frac{U_a}{R_n} = -\frac{U_e}{R_1} \quad , \quad G = -\frac{R_n}{R_1} \; . \tag{2.2}$$

This becomes clear noting that, since the input (-) does not drag current, the currents traversing the resistances R_n and R_1 must cancel each other.

Changing the resistances R to inductances L or capacitances C, it becomes possible to influence the frequency response of the amplifying circuit. The impedance are,

$$Z_L = iL\omega \quad , \quad Z_C = \frac{1}{iC\omega} \; . \tag{2.3}$$

For the calculation of the amplification wit complex impedances, we just take the absolute value of the gain G.

Further reading:
U. Tietze & Ch. Schenk, Halbleiterschaltungstechnik, Springer-Verlag
P. Horowitz & W. Hill, Die hohe Schule der Elektronik, Elektor Verlag

2.1.3.1 Ex: Tasks and learning goals

Here, we will learn how to use OpAmps: We will start mounting a 10-fold inverting amplifier on a breadboard and then modify the external passive components, such as to build a low-pass filter.

1. Assemble on a breadboard a simple inverting amplifier using an OpAmp. Use 10 kΩ resistors at the input aim for an amplification factor of 10.
2. Test the circuit with a frequency generator and an oscilloscope.
3. Modify the circuit such as to obtain a low-pass filter with $f_g = 50$ kHz bandwidth and test the circuit again.

Datasheets:
For the VCO see appendix data sheet Fig. 8.12

2.2 Photodiodes

Our first task is to construct a *photo detector*. The central part of a photodetector is the photodiode. We have at our disposal silicium pin-photodiodes of the type C30822E of the company Perkin Elmer and of the type FFD100.

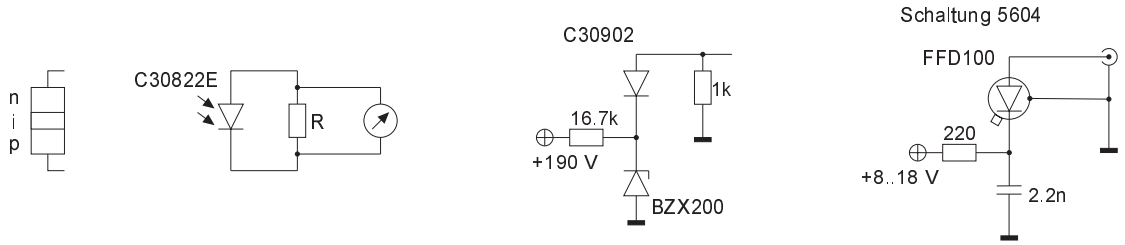

Figura 2.6: Circuit with photodiodo.

Photodiodes exploit an intrinsic photoeffect of semiconductor *pn*-junctions. In the transition region, free electrons of the *n*-type semiconductor and excess holes of the *p*-type semiconductor are drifting into the respective opposite semiconductor, where they recombine. The consequence is a transition zone with a charge carrier depletion, which acts as a barrier and has an intrinsic capacitance. The charge carrier imbalance gives rise to an electric field across the junction. The energy liberated during the recombination process can be dissipated via emission of light.

The reverse process is also possible: Via the intrinsic photoeffect, light irradiated into the *pn*-junction can lift electrons from the valence into the conduction band, thus generating pairs of charge carriers. Under the influence of the electric field across the junction, the holes flow to the edge of the p domain and the electrons flow to the n domain. This part of the current is called *drift current*. A smaller part, called the *diffusion current*, has its origin in the diffusion of the electron-hole pairs formed in the edge regions. Since these minority charge carriers have only a limited lifetime before they recombine, only the part of the current generated within a few units of the diffusion lengths near the charge carrier zone contributes. This results in an external photovoltaic voltage at the electrodes of the photodiode. If the photodiode is connected to a load, a photocurrent will flow, which is composed, as mentioned above, by the drift current of the charge carrier zone and the diffusion current from its edges.

The principal scheme of a pin diode is illustrated in Fig. 2.7(left): A weakly doped intrinsic layer separates the p and the n conductor. This reduces the capacity of the barrier. The current at short circuit is proportional to the light power. A photodiode is always operated in blocking direction. A negative offset voltage reduces the capacity of the *pn*-junction.

Despite all measures the *pn*-junction capacity remains finite. One can model the impact of the *pn*-junction capacity via a replacement diagram. The voltage drop is

$$\frac{U(\omega)}{U_0} = \frac{R_L||\frac{1}{i\omega C}}{R_i + \left(R_L||\frac{1}{i\omega C}\right)} = \frac{\frac{R_i||R_L}{R_i}}{1 + i\omega C(R_i||R_L)} \,. \tag{2.4}$$

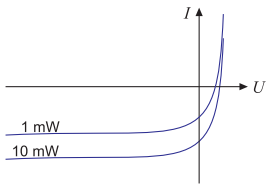

Figura 2.7: (Left) Band structure of a photodiode operated with a voltage applied in blocking direction. (Right) U-I dependence of a photodiode.

For high load resistances the frequency response obviously becomes load-independent. For small loads, $R_L < R_i$, the band width of the photodiode is dramatically increased to $\omega_g = 1/R_L C$. In the same time, however, the amplification drops to $V = R_L/R_i$.

2.2.0.2 Ex: Tasks and learning goals

In this part of the lab course, we will learn to solder and set up simple electronic circuits. We will also learn how to identify the connections of a photodiode and mount into a case with BNC connectors. Finally, we will characterize the photodiode for use in future applications. Initially, we will work without offset voltage, later we will apply a voltage and identify its impact.

1. Connect an LED to a function generator and make it blink at low frequencies adjusting the offset and the amplitude of the output voltage. Shine the light onto your photodiode and monitor the signal on an oscilloscope. Explain your observations.

2. Reduce the amplitude and adjust the offset until you observe a sinusoidal signal. Increase the frequency and explain your observations. (Note that the response of LEDs is extremely fast (MHz).) Determine the bandwidth of your detector.

3. Measure the current at short circuit. Connect a $R = 10$ kΩ resistive load in parallel to the photodiode output and measure the voltage drop into this load.

4. Characterize the photodetector with respect to its sensitivity (em A/W) by varying the load.

5. How is the frequency response of the photodiode modified by the load? Measure bandwidth as a function of the load. Adjust the load until the detector (circuit including photodiode and resistor) has a bandwidth of 10 kHz (which is sufficient for many applications).

6. Apply a 10 V voltage no sentido de bloqueio and analyze again the sensitivity and the bandwidth of your photodetector. Note that the blinking LED can be replaced by a rotating chopper wheel.

Solução: *Example of a measured characterization of a photodiode.*

Datasheets:
For the Photodiode FFD100 see appendix data sheet Fig. 8.8
For the Photodiode C30822E see appendix data sheet Fig. 8.9

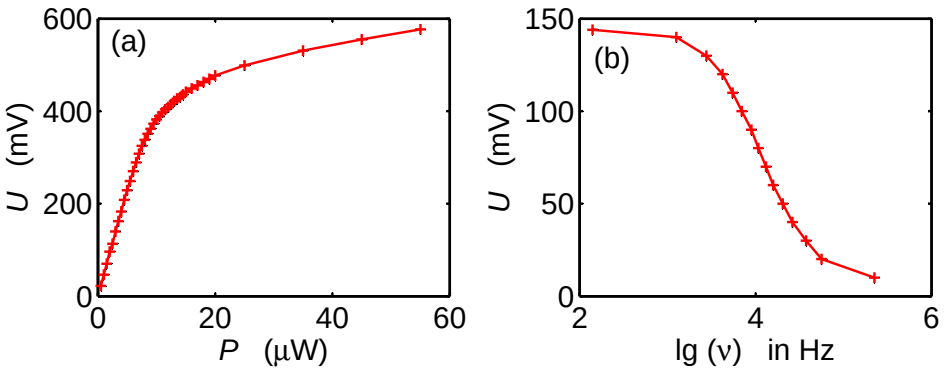

Figura 2.8: (a) Calibration of a photodiode, measured voltage as a function of the incident light power. (b) Low-pass behavior of a resistive charge of 90 kΩ.

2.3 VCOs and the generation of rf-sidebands

Voltage-controlled oscillators (*VCO*) serve to generate variable radiofrequencies. They are the basis for most function generators. A useful particularity of VCOs is the possibility modulate the frequency and phase of an optical carrier wave by modulating the control voltage of a VCO at low frequency.

The modulation of the carrier wave generates sidebands. This can be seen by expanding the signal which carries the phase modulation into a Fourier series,

$$Ae^{i\omega t+i\beta\sin\Omega t} = Ae^{i\omega t}\sum_{k=-\infty}^{\infty} J_k(\beta)e^{ik\Omega t} \simeq Ae^{i\omega t} + J_1(\beta)Ae^{i\omega t+i\Omega t} + J_{-1}(\beta)Ae^{i\omega t-i\Omega t} \tag{2.5}$$

when the *modulation index* β is small. Here, $J_{-k}(\beta) = (-1)^k J_k(\beta)$ are the Bessel functions. This is in contrast to amplitude modulation, which is described by only two symmetric sidebands,

$$A\left(1+\beta\sin\Omega t\right)e^{i\omega t} = Ae^{i\omega t}\left(1+\frac{\beta}{2i}\left(e^{i\Omega t}-e^{-i\Omega t}\right)\right) . \tag{2.6}$$

For *amplitude modulation* (*AM*) the beat signals between the carrier frequency and the two sidebands are in phase, i.e.,

$$\left|e^{i\omega t}+e^{i(\omega\pm\Omega)t}\right|^2 = 2+e^{i\Omega t}+e^{-i\Omega t} . \tag{2.7}$$

For *phase modulation* (*PM*) the beat signal are ion counter-phase, i.e.,

$$\left|e^{i\omega t}+e^{i(\omega\pm\Omega)t+i\pi/2}\right|^2 = 2+ie^{\pm i\Omega t}-ie^{\mp i\Omega t} . \tag{2.8}$$

In the case of AM, the amplitude is blurred, but the phase at zero-crossing is well defined. In the case of PM, the amplitude in the antinode is sharp, but the phase of the zero-crossing is blurred.

It is not easy to transform AM into PM, and vice versa. In fact, the phase between carrier and sidebands can be varied, for example by adding an AC voltage, $\sqrt{2}e^{i\omega t+3i\pi/4}$ to the signal; however, it is not easy to transform synchronize phases into opposite phases.

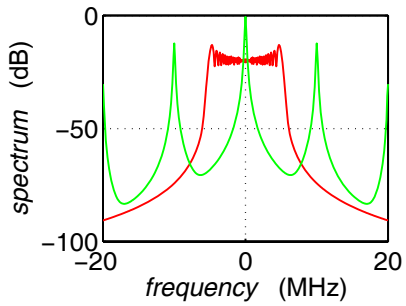

Figura 2.9: Frequency spectra of a phase-modulated carrier frequency for $\Delta\omega = 5$ MHz modulation excursion and (red) $\omega = 100$ kHz modulation frequency ($\beta = \frac{\Delta\omega}{\Omega} = 50$) and (green) $\omega = 10$ MHz modulation frequency ($\beta = 0.5$). Furthermore, a $\gamma = 100$ kHz resolution linewidth is assumed.

As shown in Eq. (2.5), the spectrum of a signal with phase modulation (PM) consists of discrete lines, called sidebands, whose amplitudes are given by Bessel functions,

$$S(\omega) = \sum_{k=-\infty}^{\infty} |A\mathcal{J}_k(\beta)|^2 \delta(\omega + k\Omega) \ . \tag{2.9}$$

In real systems, the sidebands have finite widths γ due to frequency noise or the finite resolution of the detectors. In the case of Lorentzian line profiles, we have,

$$S(\omega) = \sum_{k=-\infty}^{\infty} |A\mathcal{J}_k(\beta)|^2 \frac{\beta^2}{(\omega - k\Omega)^2 + \beta^2} \ . \tag{2.10}$$

2.3.0.3 Ex: Tasks and learning goals

In this exercise, we will understand the origin of sidebands as we'll see them emerge from a modulation spectrum when we gradually increase the modulation index.

1. Take a VCO, for example, ZOS-100+ from MiniCircuits. Study the datasheet and drive the VCO with an AC voltage. Vary the amplitude and the frequency of the voltage and observe the output signal of the VCO on a spectrum analyzer.

2. Try to understand the spectrum observing the limiting cases $\Omega \gg \Delta\omega$ and $\Omega \ll \Delta\omega$. How can you read Ω and Δf from the spectra in both cases?

3. Write a MATLAB program to simulate the spectrum.

Datasheets:
For the VCO see appendix data sheet Fig. 8.3
For the variable attenuator see appendix data sheet Fig. 8.4
For the mixer see appendix data sheet Fig. 8.6

2.4 Mixer

2.5 Sample-and-hold circuit

Sample-and-hold circuit Solder on euroboard

2.6 Box-car integrator

box-car integrator Solder on euroboard

2.7 Lock-in amplifier

An *lock-in amplifier* (also called a phase-sensitive rectifier or *mixer*) is an amplifier that can measure a weak electrical signal by modulating the signal by a reference signal with a known frequency and phase. The device represents a bandpass filter with an extremely narrow bandwidth and, therefore, improves the signal-to-noise ratio (SNR). DC or AC noise components are efficiently filtered.

2.7.0.4 Ex: Tasks and learning goals

Let's now build a lock-in amplifier. The principle is illustrated in Fig. 2.10(a). The sinusoidal signal discriminated at a non-linear line is switched on and off in the lock-in by a switch. At the same time, the inverted signal (i.e., phase shifted by 180°) is turned off and on. Both signals are combined and low-pass filtered. As Fig. 2.10(b) shows, the sign of the filtered signal depends on the phase between the discriminator and the TTL signal controlling the switch.

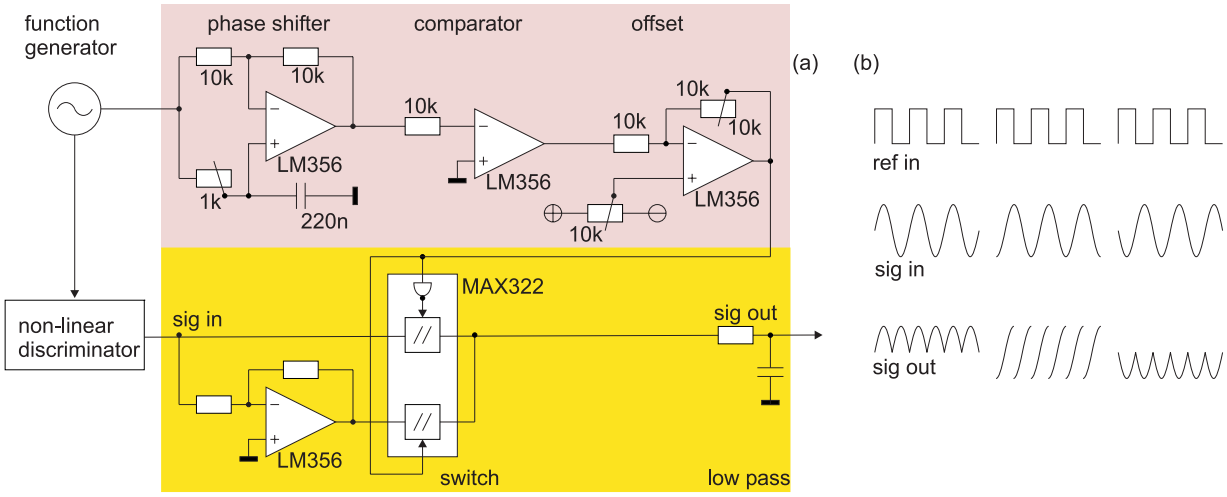

Figura 2.10: (a) Principal scheme of a lock-in amplifier. (b) Mode of operation.

1. Create the circuit sketched in Fig. 2.10(a) on a circuit board and test it by varying the phase between the modulated output signal and the TTL signal provided by a function generator.

Datasheets:

For the operational amplifier see appendix data sheet Fig. 8.11
For the switch see appendix data sheet Fig. 8.10

Capítulo 3

Quantum optics and quantum electronics

The objective of this part of the course is to introduce the trainee into the basics of *quantum electronics*. He will learn, how to match the light modes in optical cavities and fibers, and to phase-match the wavefronts of two laser beams in order to detect their frequency beating with a photodetector. Furthermore, he will learn how to handle a piezo-electric transducer, an electro-optic modulator, and an acousto-optic modulator.

3.1 Optical fiber

An *optical fiber* is a waveguide in which light is guided by internal total reflection. The total reflection occurs inside layers with different refractive indices.

3.1.0.5 Ex: Tasks and learning goals

Here we will learn to couple a laser beam into an optical fiber.

1. Optimize its position and the focus o the beam.

3.2 Piezo-electric actuator

The piezo-electricity effect describes the reciprocal action between mechanical pressure (from Greek: piézein - press) and electrical voltage in solids. It is based on the phenomenon that occurs in the regular deformation of certain piezoelectric materials: at the surface occur displacements of electric charges criating microscopic dipoles inside the unit cells. The sum over all the unit cells of the crystal leads to a macroscopically measurable electrical voltage. The deformation should be directed, which means, that the pressure is not applied from all sides on the crystal, but for example only on opposite sides.

On the other hand, by applying an electric voltage, a crystal (or piezo-ceramic element) may be deformed. Like any other solid body, piezo-electric crystals can execute mechanical vibrations. In a *piezo-electric actuator* (or piezo transducer PZT), these vibrations can be electrically excited. The frequency of the vibrations depend only on the speed of sound (which is a constant of the material) and the dimensions of the actuator. Therefore, actuators are also suitable for realizing oscillators (for example, quartz crystals). The piezo-electric effect can only occur in non-conductive materials (e.g., lead titanate zirconate).

When a voltage is applied to the piezo-ceramic in the direction of polarization, we observe an expansion in this direction and a perpendicular contraction. Depending on the employed

material and the coefficient for piezo-electric strain d, stretches up to $\Delta l/l = 0.15\%$ can be obtained:

$$\Delta l = dEl_0 \ , \tag{3.1}$$

where l_0 is the length of the actuator and $E = U/l_0$ the amplitude of the electric field. The elongation effect is therefore proportional to the field strength and the overall length of the actuator. To achieve large stretches with manageable electrical voltages, actuator discs are often stacked (mechanical circuit in series and electric circuit in parallel).

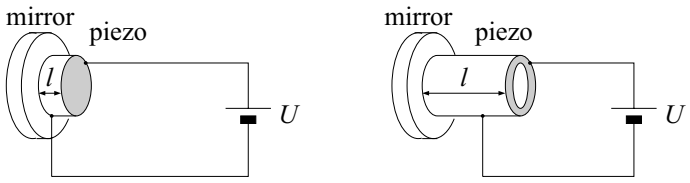

Figura 3.1: Principle of a piezo actuator. (Left) Piezo disc. (Right) Ring piezo.

Negative voltages with respect to the orientation of the discs cause a contraction. However, negative voltages can also cause a change in the polarization state of the piezo and should therefore be avoided! In electrical circuits, piezoelectric actuators introduce a capacitance with a relative dielectric constant between 600 and 5000 and an internal resistance of about 10^8 Ω depending on the material.

3.2.0.6 Ex: Tasks and learning goals

Here we will construct a mechanically stable Mach-Zehnder or Michelson type interferometer.

1. Mount one of the mirrors of the interferometer on a piezo. Optimize the phase matching of the beams until you get visible interference patterns.

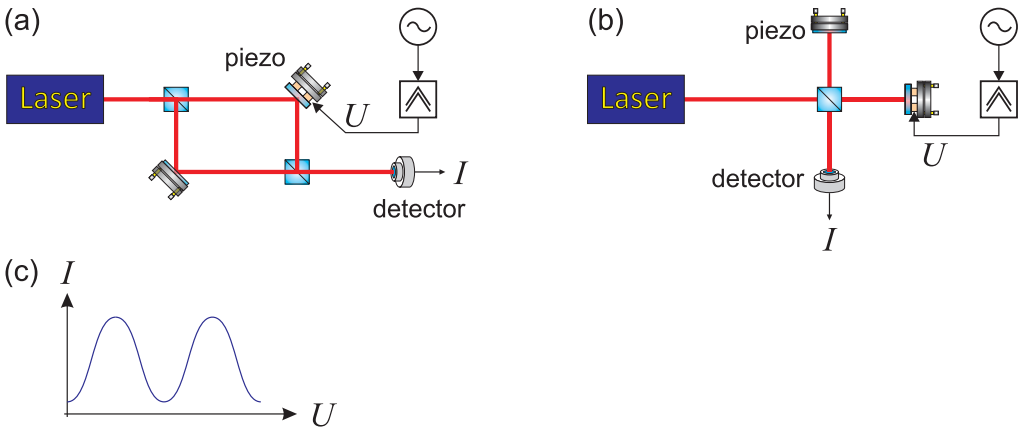

Figura 3.2: Setup for testing a piezo using (a) a Mach-Zehnder interferometer or (b) a Michelson interferometer. The interference signal I observed as a function of the voltage U applied to the piezo allows to measure the voltage expansion coefficient.

2. Vary the voltage applied to the piezo-electric actuator and measure the voltage expansion coefficient d.

3.3 Optical resonator

Optical cavities consist of an arrangement of mirrors reflecting the light beams in such a way, that they form a closed path. Since light that entered the cavity is performing there many round trips before it is transmitted again or absorbed, the light power is considerably enhanced, i.e. cavities can store light.

Light which is to resonate in the cavity must satisfy the boundary condition, that the mirror surfaces coincide with standing wave nodes. Therefore, in a cavity with length L only a discrete spectrum of wavelengths $\lambda = NL$ can be resonantly amplified, where N is a natural number. Because of this property, cavity are often used as frequency filters or optical spectrum analyzers: Only frequencies $\nu = N\delta_{fsr}$ are transmitted, where $\delta_{fsr} = c/2L$ is the free spectral range of the cavity.

Cavities are characterized on one hand by their geometry, i.e. the curvature and the distance of their mirrors, and on the other hand by their finesse, which is given by the reflectivity of their mirrors. Let us first study the finesse. Regarding the cavity as a multipass interferometer [**?**], we can derive expression for the reflected and transmitted intensity as a function of frequency.

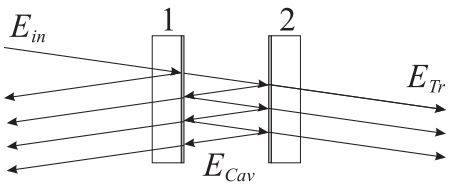

Figura 3.3: Multiple interference in an optical cavity.

The so-called *Airy formulae f*or transmission and reflection are,

$$I_{refl} = I_{in}\frac{(2F/\pi)^2\sin^2(\Delta/2\delta_{fsr})}{1+(2F/\pi)^2\sin^2(\Delta/2\delta_{fsr})} \quad \text{and} \quad I_{trns} = I_{in}\frac{1}{1+(2F/\pi)^2\sin^2(\Delta/2\delta_{fsr})}\ , \tag{3.2}$$

where R is the reflectivity of a mirror and $\delta = 4\pi L/\lambda = 2\pi\nu/\delta_{fsr}$. The transmission curve of a cavity has a finite transmission bandwidth $\Delta\nu$, which depends on the reflectivity of the mirrors. The finesse of a cavity is defined by

$$F \equiv \frac{2\pi\delta_{fsr}}{\kappa} = \frac{\pi\sqrt{R}}{1-R}\ . \tag{3.3}$$

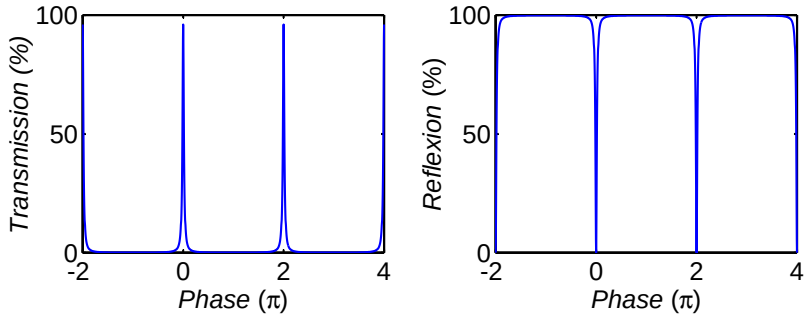

Figura 3.4: Transmission and reflection through a resonator.

The geometry of a cavity must satisfy certain conditions, in order to be stable [11]. Besides the main longitudinal modes a cavity possesses transverse modes of the order TEM_{mn}, whose frequencies are given by

$$\nu/\delta_{fsr} = (q+1) + \frac{m+n+1}{\pi} \arccos \sqrt{\left(1-\frac{L}{\rho_1}\right)\left(1-\frac{L}{\rho_2}\right)} \,. \tag{3.4}$$

A *confocal cavity* with degenerate transversal modes, $\rho_1 = \rho_2 = L$, is particularly suited as optical spectrum analyzer.

The diameter of the beam waist in the cavity is

$$w_0 = \sqrt[4]{\left(\frac{\lambda}{\pi}\right)^2 \frac{L(\rho_1 - L)(\rho_2 - L)(\rho_1 + \rho_2 - L)}{(\rho_1 + \rho_2 - 2L)^2}} \,. \tag{3.5}$$

For an optimal coupling of the light into the cavity the Gaussian laser beam must be matched to the cavity's geometry of the cavity, i.e. diameter and divergence of the laser beam must be adapted to the cavity mode with a suitable arrangement of lenses.

For the realization of the project prior knowledge of 1. Gaussian beams (see Sec. 1.2), 2. photodetectors (see Sec. 2.2), and 3. piezo-electric transducers (see Sec. 3.2) is required.

Further reading:
*H. Kogelnik and X. Y. Li, Proc. of the IEEE **54**, 1312 (1966). Laser Beams and Resonators.*
W. Demtröder, Laser spectroscopy, Springer-Verlag.

3.3.0.7 Ex: Tasks and learning goals

Optical cavities are frequently used as *optical spectrum analyzers*. For this application, it is helpful to simplify the intrinsic mode spectrum of the cavity by using a confocal design, where all transerse modes are degenerated. In this part of the course, we will set up an optical cavity and characterize it by its free spectral range and its finesse. Then we will analyze its mode spectrum and modify its geometry to make it confocal.

1. Couple a laser beam into a cavity as shown in Fig. 3.5. The cavity provided by this tinker course consists of a plane incoupler ($\rho_1 = \infty$, $R_1 = 98\%$) and a high reflector ($\rho_2 = 25$ mm, $R_2 = 99.8\%$). Position the mirror at a distance L, where the cavity is stable. Calculate the free spectral range, the finesse, the diameter of the beam waist.

2. Detune the frequency of the diode laser by scanning the piezo transducer of the laser cavity. Observe the mode spectrum of the laser in the transmission signal of the cavity. Measure its free spectral range and the finesse of the cavity.

3. Match the laser beam to the cavity. In order to do this (a) measure the diameter of the diode laser beam, (b) determine the lens which can be used to focus down to the beam waist of the cavity. How does the transmission spectrum change upon the beam matching?

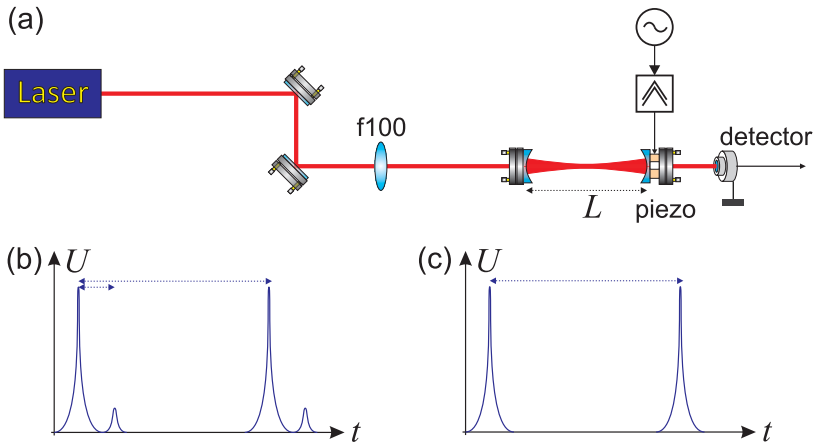

Figura 3.5: Setup for aligning a confocal resonator.

3.4 Diode laser

A *diode laser* exhibits, in comparison to other laser types, the advantage of a very small size and a compact design. They are, in general, easy to handle and can be controlled conveniently via current and temperature. However, they also have the disadvantage of a large beam divergence and a broad emission spectrum. The beam divergence can be compensated by a collimation optics in front of the laser diode. In order to narrow the emission spectrum the light is partially reflected from a grating. The first reflection order is fed back to the laser diode. The diode laser and the grating represent a cavity, which restricts the emission spectrum to a single mode. The frequency of the mode can be manipulated via the inclination of the grating. For very fine adjustment of the grating inclination and hence high frequency resolution the grating is mounted on a piezo transducer. This type of laser is called *extended cavity diode laser* (*ECDL*).

The temperature has an impact on the band structure of the *pn*-transition of the laser diode and hence on the frequency. Therefore, it is stabilized via a Peltier element, which is mounted underneath the laser diode holder. The degree of freedom is used for tuning the laser frequency in wide steps.

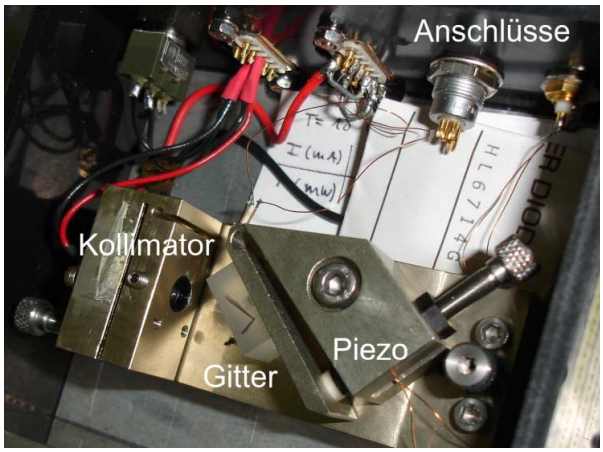

Figura 3.6: Vista lateral de um ECDL.

3.4.0.8 Ex: Tasks and learning goals

Here we will construct a diode laser in Littmann configuration.

1. Take a laser diode, a Peltier cooler, a thermistor, a piezo transducer, and a diffraction grating. Put everything together.

2. Optimize the threshold. Analyze the emission spectrum with an optical spectrum analyzer.

3.5 Electro-optic modulator

An *electro-optic modulator* is an optical device with which, by an applied voltage, the phase, frequency, amplitude or direction of a light beam can be modulated. Modulation bandwidths in the GHz regime are possible. In the simplest case, the EOM consists of a crystal (e.g., lithium niobate), whose refractive index depends on the amplitude of the local electric field. That is, when a lithium niobate crystal is exposed to an electric field the speed of light propagation is reduced. One can thus control the phase of a light beam at the output of a crystal by inserting it into a plate capacitor and applying a voltage. The phase shift of the light depends linearly on the applied voltage.

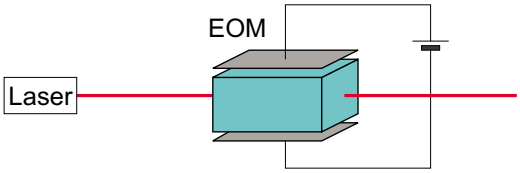

Figura 3.7: Modulador elétro-óptico.

EOMs are often used to generate sidebands in a monochromatic laser beam. They are also used as *Pockels cell*, i.e., as a voltage-controlled phase-plate. The Pockels effect produces in a medium a *birefringence*, which depends linearly on the applied electric field. This is in contrast to the *Kerr effect*, in which the birefringence depends in a quadratic form of the electric field.

Suppose the optically inactive axis is x. In this case, the influence of EOM on the polarization of a laser beam is described by

$$M_{EOM}(\theta) = \begin{pmatrix} 1 & 0 \\ 0 & e^{i\theta} \end{pmatrix} . \tag{3.6}$$

For operation as a Pockels cell, the EOM is inserted between two polarizers crossed by $\pm 45°$,

$$M_{Pockels}(\theta) = M_{polarizer}(-\pi/4) \begin{pmatrix} 1 & 0 \\ 0 & e^{i\theta} \end{pmatrix} M_{polarizor}(\pi/4) , \tag{3.7}$$

where the Jones matrix of the polarizer comes from the equation (1.19). Now we get,

$$M_{Pockels}(0) = \begin{pmatrix} 0 & 0 \\ 0 & 0 \end{pmatrix} \quad \text{and} \quad M_{Pockels}(\pi) = \begin{pmatrix} \frac{1}{2} & -\frac{1}{2} \\ \frac{1}{2} & -\frac{1}{2} \end{pmatrix} . \tag{3.8}$$

That is, an incident beam of light, $E = \frac{1}{\sqrt{2}} \begin{pmatrix} 1 \\ 1 \end{pmatrix}$, linearly polarized with a polarization rotated by 45°, is completely blocked or transmitted through the Pockels cell, depending on the phase shift θ.

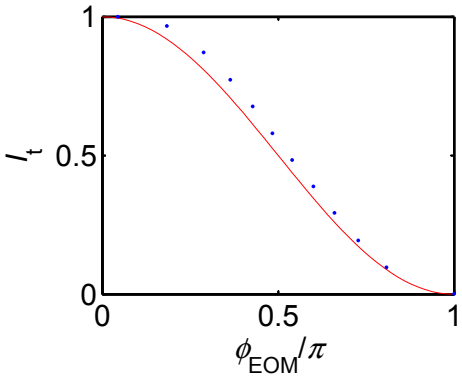

Figura 3.8: Effect of a Pockels cell. The solid line was calculated with the Eq. (3.7), the dotted was measured experimentally.

3.5.0.9 Ex: Tasks and learning goals

Here we will learn to operate an EOM as Pockels cell and as phase modulator.

1. Align a laser beam through an electro-optic modulator. Supply a voltage between 0 V and 500 V to the EOM. Test its operation by beating the ordinary with the extraordinary beam. Modulate the supply voltage at a low frequency.

2. Set up a Mach-Zehnder interferometer by phase-matching the exit beam of the EOM with a part of the input beam.

3. The interferometer provides a mean to convert a phase modulation into an amplitude modulation. Describe this feature theoretically using the Eqs. (2.7) and (2.8).

4. Use the EOM as a Pockels cell. Rotate the EOM by 45° around the optical axis. Probe the polarization of the outgoing beam with a polarization filter.

5. Modulate the EOM and show that the light acquires sidebands.

3.6 Optical phase modulation

The frequency and the phase of a laser beam can be influenced and modulated similarly to radiofrequency signals. We can therefore use the calculation of Sec. 2.3 completely, only changing the carrier frequency to be the frequency of the light. In particular, *phase modulation* imprints sidebands onto a monochromatic laser beam.

Technically the phase can be modulated by means of electro-optical modulators or by periodic modulation of the current which controls a diode laser. In the second case, the laser current can be easily modulated by inductive coupling by an *bias-T*.

3.6.0.10 Ex: Tasks and learning goals

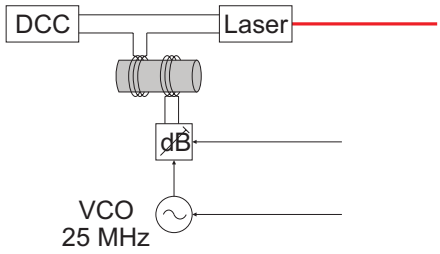

Figura 3.9: Modulação de fase de um laser de diodo.

1. Apply the required voltages to a VCO (MiniCircuits, ZOS100), until it generates a variable frequency between 40 and 60 MHz. Attenuate the power with a variable attenuator up to -20 dBm. Check the amplitude and frequency with a spectrum analyzer.
2. Add a bias-T to the power supply of a laser diode. Observe the transmission spectrum of a Fabry-Pérot cavity for various frequencies and modulation amplitudes. Determine the modulation index. Use the known distance of the sidebands to estimate the finesse of the Fabry-Pérot cavity.

Datasheets:
For the VCO see appendix data sheet Fig. 8.3
For the power divider see appendix data sheet Fig. 8.5
For the mixer see appendix data sheet Fig. 8.6

3.7 Acousto-optic modulator

The *acousto-optic modulator AOM* permits fast frequency and amplitude variations of a laser beam. Because it does not incorporate mechanical parts, it works without fatigue. AOMs are used, for instance, in laser printers, where the gray tone of a pixel can be adjusted via the intensity of the laser beam, while its position (rows and columns) is varied by a rotating mirror and the drum propagating the paper sheet.

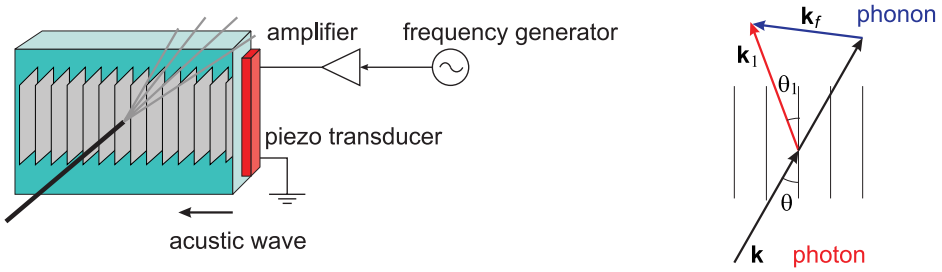

Figura 3.10: (Left) Principle of the acousto-optic modulator. (Right) Scheme of the diffraction in an acousto-optic modulator: A photon with wavevector k is scattered by a phonon with wavevector k_1 resulting in a photon with wavevector k_f.

The acousto-optic modulator consists of a piece of crystal (or glass) excited by an acoustic wave with frequency f produced by a piezo-electric transducer (see Sec. 3.7) mounted perpendicularly to propagation direction of the laser beam. The sound waves propagate through the

crystal as density fluctuations periodically changing the refraction index n. The incident light is diffracted through Brillouin scattering at the spatial modulation of the refraction index. In a wave picture, the process can be interpreted as Bragg scattering of a light wave (with its wavelength inside the crystal $\lambda_n = 2\pi/k_n = c/n\nu$) from a density grating. c/n is the propagation velocity of light inside the crystal. Since phonons (with their wavelength $\lambda_f = 2\pi/k_f = c_f/f$, where c_f is the sound velocity in the crystal) are quantized and can only be emitted and absorbed entirely, the frequency of the first-order diffraction is $\nu_1 = \nu + f$. In case of an ideal adjustment of the Bragg angle, the *Bragg condition* results in $\theta_1 = \theta$ (see Fig. 3.10),

$$\sin\theta = \frac{k_f}{2k} = \frac{f\lambda_n}{2c_f} \ . \tag{3.9}$$

Since the laser beam is refracted when it enters the crystal, the relation between the incidence and exit angle is given by *Snell's law*, $\sin\alpha = n\sin\theta$. With this, the Bragg condition can be written,

$$\sin\alpha = \frac{f\lambda}{2c_f} \ . \tag{3.10}$$

The angle between the 0^{th} and the 1^{st} order is, hence, 2α.

In a corpuscular picture, the process can be understood as a *four-wave mixing* (*4WM*) between photons and phonons. The deflection of the laser beam is a consequence of momentum, $\mathbf{k}_1 = \mathbf{k} + \mathbf{k}_f$. The frequency shift corresponds exactly to the Doppler shift induced by the Brillouin scattering (absorption and reemission of a phonon in reverse direction), and we obtain a relationship that is equivalent to the Bragg condition,

$$f = \nu_1 - \nu = 2\nu\frac{c_f\sin\theta}{c/n} \ . \tag{3.11}$$

From the Bragg condition, knowing the deflection angle and the (fixed) frequency shift, we can calculate the sound velocity. A typical value is $c_f \simeq 4200$ m/s.

Further reading:
A. Yariv, Quantum Electronics, Wiley
A. Yariv and P. Yeh, Optical waves in crystals, Wiley

3.7.0.11 Ex: Tasks and learning goals

Fig. 3.11 illustrates the setup, use, and test of an AOM. It is recommended familiarizing with the operation principle of a *voltage-controlled oscillator* (*VCO*) (see Sec. 2.3) and a voltage-controlled *variable attenuator*. We will also learn how to use a spectrum analyzer.

1. Optimize a diffraction efficiency of the AOM. What are the impacts of the Bragg angle, the radiofrequency power, and the laser beam diameter.

2. Measure the deflection angle as a function of the applied radiofrequency. Based on this result, calculate the sound velocity in the crystal.

3. Measure the diffraction efficiency as a function of the applied radiofrequency power at a fixed Bragg angle. Repeat the measurement optimizing the Bragg angle for every value of the radiofrequency.

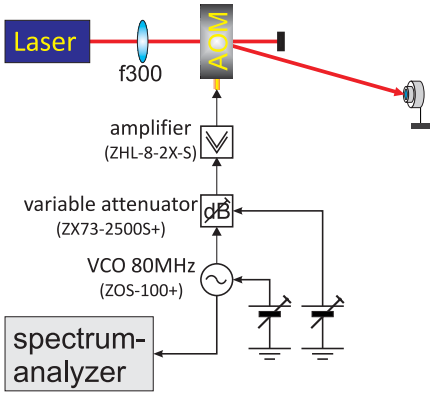

Figura 3.11: Setup for testing an acousto-optic modulator.

4. Reduce the radiofrequency power using the variable voltage-controlled attenuator. Determine the diffraction efficiency as a function of radiofrequency power.

Solução: *The curves exhibited in Fig. 3.12 were obtained with ...*

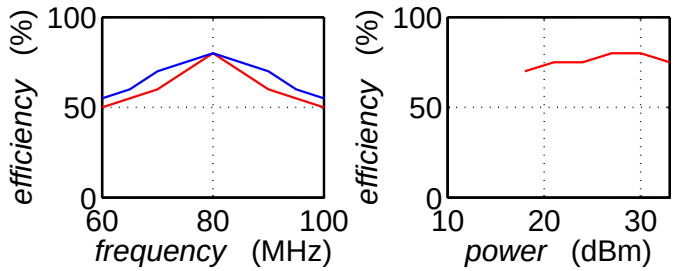

Figura 3.12: Example of measured efficiency curves.

Data sheets:
For the VCO see appendix data sheet Fig. 8.3
For the AOM see appendix data sheet Fig. 8.7

Capítulo 4

Laser interferometry and heterodyne methods

In this part of the lab course (Sec. 4.1 to 4.2) we will construct and use interferometers. Interferometers have versatile applications such as 1. for the detection of very small length variations (as for example caused by gravitational waves), 2. as vibration and inertial sensors, or in 3. the transmission of information (radio).

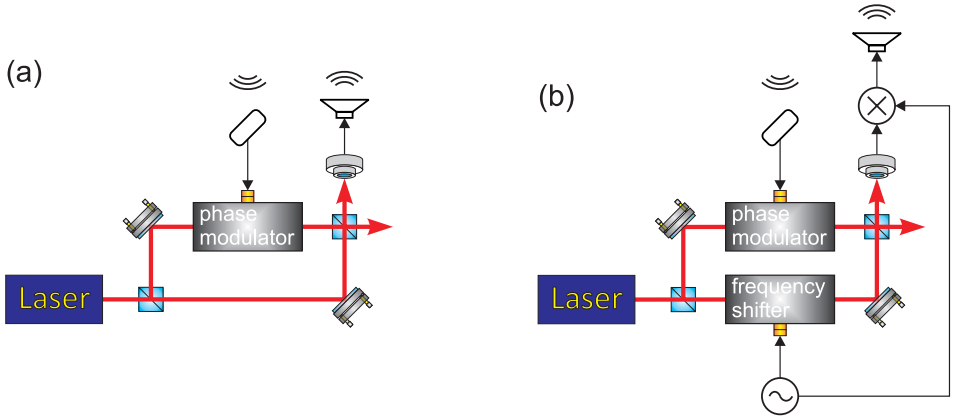

Figura 4.1: Principle scheme of the homo- and heterodyning technique at the example of a Mach-Zehnder interferometer.

4.1 Measurement of a frequency beat

Interferometry is always based on the splitting and recombination of a wave, e.g., a laser beam or a matter wave. The recombination of laser beams is always a little technical challenge, as it requires a perfect phase matching of the Gaussian laser modes. Let us consider two plane waves $E_1 = Ae^{i\omega_1 t}$ and $E_2 = Ae^{i\omega_2 t}$ impinging on a photodiode. We suppose that they are phase-matched, such that their wavevectors are parallel. The photodiode then generates a *beat signal* $I = |E_1 + E_2|^2 = AB[2 + 2\cos(\omega_1 - i\omega_2)t]$.

In practice, laser beams are usually not plane waves, but have a finite diameter and radius of curvature. In order to get a high contrast signal, a good phase-matching of the beams is important in order to obtain a strong photodiode signal.

4.1.0.12 Ex: Tasks and learning goals

In this exercise, we will ...

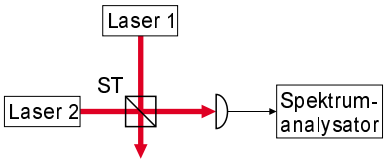

Figura 4.2: Principle of a beat frequency measurement.

1. Take two independent lasers operating at nearly the same frequency (within $\sim$ 1 GHz) and overlap them at a (non-polarizing) beam splitter.

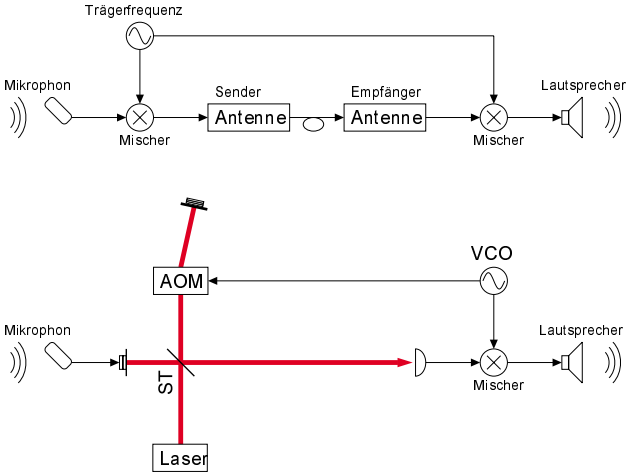

Figura 4.3: Analogy between radio transmission and heterodyne techniques with a laser.

2. Focus one of the ports of the beam splitter on a photodetector with large band width ($\sim$ 1 GHz).
3. Analyze the beat signal on a spectrum analyzer.
4. Focus a helium-neon laser onto a fast photodetector and determine the free spectral range of the laser resonator.

4.2 Radiofrequency techniques and the transfer of information

4.2.1 Homodyne method

For the *homodyne method* the field amplitude of a laser beam, E_i, with frequency, $\omega = ck$, is divided by a beam splitter (reflectivity $R = |\eta|^2 \simeq 50\%$) into a reference beam (reflexão por um meio opticamente diluído) and a probe beam,

$$\begin{aligned} E_r &= -\eta E_i \\ E_p &= (1 - i\eta) E_i \ . \end{aligned} \tag{4.1}$$

The reference beam traverses two times the distance L_r, which can be varied by a piezo,

$$E_r' = E_r e^{2ikL_r} \ . \tag{4.2}$$

The probe beam traverses two times the path L_p,

$$E'_p = E_p e^{2ikL_p} \ . \tag{4.3}$$

The beams are recombined on a beam splitter and sent to a photodetector, whose signal is,

$$\begin{aligned} I &\propto \left|(1-i\eta)E'_r + \eta E'_p\right|^2 \\ &= \left|(1-i\eta)E_r e^{2ikL_r} + \eta E_p e^{2ikL_p}\right|^2 \\ &= |(1-i\eta)\eta E_i|^2 \left|-e^{2ikL_r} + e^{2ikL_p}\right|^2 \ . \end{aligned} \tag{4.4}$$

Hence,

$$I \propto \left|-e^{2ikL_r} + e^{2ikL_p}\right|^2 = 2 - e^{2ik(L_p-L_r)} - e^{-2ik(L_p-L_r)} = 2 - 2\cos 2k\,(L_p - L_r) \ . \tag{4.5}$$

4.2.2 Heterodyne method

The *heterodyne method* is similar to the homodyne one, except that the probe beam is frequency-shifted (e.g., by double-passage through an AOM operated at frequency Ω,

$$E'_p = E_p e^{2ikL_p + 2i\Omega t} \ . \tag{4.6}$$

O photodetector signal generated by the beams after their recombination at the beam splitter is,

$$\begin{aligned} I &\propto \left|(1-\eta)E_r e^{2ikL_r} + \eta E_p e^{2ikL_p+2i\Omega t}\right|^2 \\ &= \left|-(1-\eta)\eta E_i e^{2ikL_r} + \eta(1-\eta)E_i e^{2ikL_p+2i\Omega t}\right|^2 \\ &= |(1-\eta)\eta E_i|^2 \left|-e^{2ikL_r} + e^{2ikL_p+2i\Omega t}\right|^2 \ . \end{aligned}$$

This signal is now de demodulated with the double of the AOM frequency,

$$Ie^{2i\Omega t} \propto \left|-e^{2ikL_r} + e^{2ikL_p+2i\Omega t}\right|^2 e^{2i\Omega t} = 2e^{2i\Omega t} - e^{2ik(L_p-L_r)+4i\Omega t} - e^{-2ik(L_p-L_r)} \ . \tag{4.7}$$

A low-pass filter cuts all ac-components of the signal,

$$I_{tp} \propto -e^{-2ik(L_p-L_r)} \ .$$

Now, we consider a sinusoidal modulation of the reference path, $L_r \to L_r + M\sin ft$, and expand the amplitude of the reference field in a Fourier serie,

$$e^{2ik(L_r+M\sin ft)} = e^{2ikL_r}\left[J_0(2kM) + J_1(2kM)e^{ift} + J_{-1}(2kM)e^{-ift}\right] \ . \tag{4.8}$$

Hence,

$$\begin{aligned} Ie^{2i\Omega t} &\propto -e^{2ik(L_r-L_p)}\left[J_0(2kM) + J_1(2kM)e^{ift} - J_1(2kM)e^{-ift}\right] \\ &\to J_1(2kM)2i\sin ft \simeq kM2i\sin ft \ . \end{aligned} \tag{4.9}$$

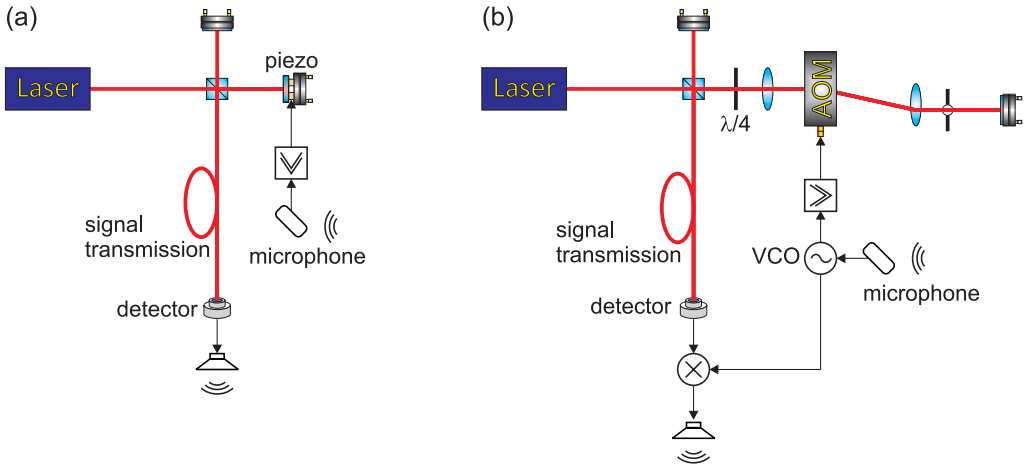

Figura 4.4: Homo- and heterodyning with a Michelson interferometer.

4.2.2.1 Ex: Tasks and learning goals

In this exercise, we will ...

1. Set up a Michelson interferometer.

4.3 Laser gyroscope

Time interval for the two directions,

$$\Delta t = 4A\Omega/c^2 \ . \tag{4.10}$$

$A \simeq 0.5$ m^2 is the area included within the ring resonator, $\Omega \simeq 2\pi/24$ h the rotation velocity due to the earth's rotation. The path difference is, consequently,

$$\Delta L = c\Delta t \ , \tag{4.11}$$

of the order of magnitude of femtometers. The frequency shift is,

$$\Delta\nu = \nu\Delta L/L = \frac{4A}{\lambda L}\ \Omega \ , \tag{4.12}$$

The gyroscope is self-rotating

$$N = \int_0^t \Delta f dt = \frac{4A}{\lambda L}\ \theta \ , \tag{4.13}$$

4.3.0.2 Ex: Tasks and learning goals

1. Pre align the mirrors of the laser gyroscope using an auxiliary laser beam.

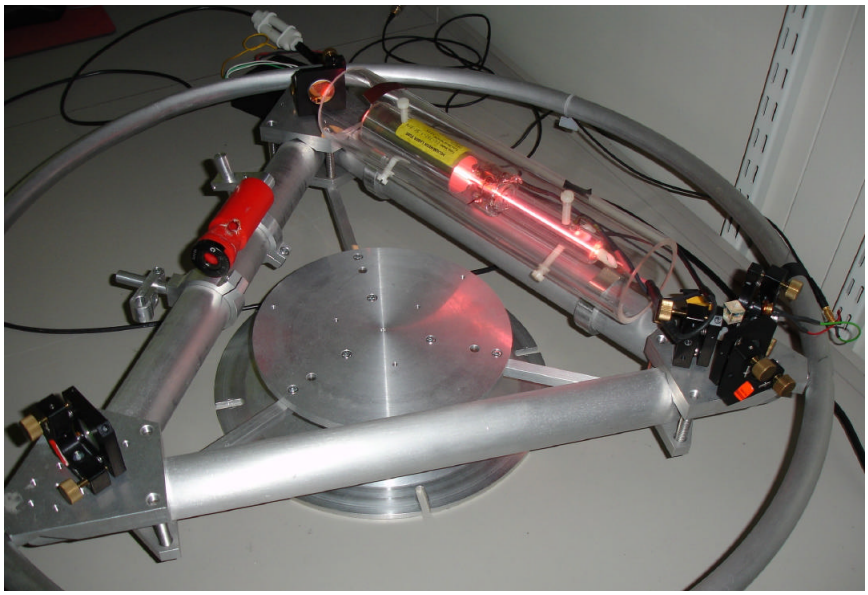

Figura 4.5: Laser giroscope.

4.4 Laguerre-Gaussian light modes

Light beams not only possess polarization, but can also have orbital angular momentum. This property of light can impressively demonstrated at the so-called *Laguerre-Gaussian mode*s.

These modes can be produced by means of masks resembling *Fresnel zone plate*. Fresnel zone plates are masks consisting of concentric sequences of bright (transmitting) and dark (absorbing) rings. The diameters of the rings are selected in such a way that the diameters of the rings defined by the bright rings interfere constructively at a certain distance f_1 on the optical axis and form a "focus"there. For this purpose, the distance d_n of the n^{th} ring must satisfy the condition,

$$d_n = \sqrt{(f_1 + n\lambda)^2 - f_1^2} \simeq \sqrt{2f_1 n\lambda}\ . \tag{4.14}$$

For a given zone plate there are other focuses at smaller distances,

$$f_k = \frac{d_n^2 - k^2 n^2 \lambda^2}{2kn\lambda} \simeq \frac{d_n^2}{2kn\lambda} = \frac{f_1}{k}\ . \tag{4.15}$$

In order to separate the beams diffracted by the zone plate into a given focus from those diffracted into other focuses or not being diffracted at all, we pass the beam through an iris diaphragm localized at the desired focus and recollimate the beam by means of a lens, as shown in Fig. 4.6.

The phase profile of the beam can be viewed interferometrically (see Fig. 4.6) by overlapping a plane wave laser beam. With a *neutral density filter* the intensities of the overlapping beams can be adjusted to maximize the contrast.

Now, for realizing Laguerre-Gaussian light modes, we use Fresnel zone plates with spiral patterns, instead of concentric rings. In contrast to the Gaussian mode, the Laguerre-Gauß modes exhibit an intensity minimum on the optical axis (doonat mode). Their phase profiles can be viewed by interferometry.

Further reading: *L. Allen, M. W. Beijersbergen, R. J. C. Spreeuw, and J. P. Woerdman,*

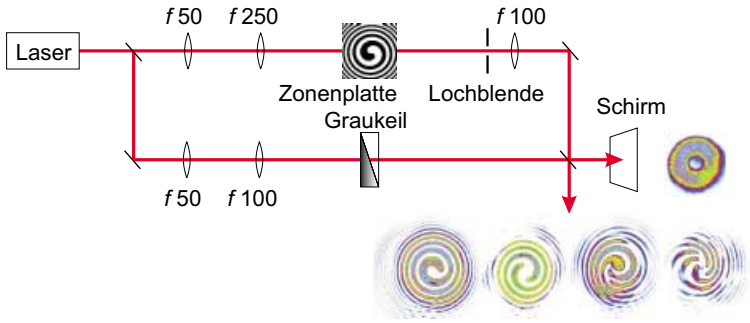

Figura 4.6: Creation of Laguerre-Gaussian modes.

Phys. Rev. A ***45****, 8185 (1992). Orbital Angular Momentum of Light and the Transformation of Laguerre-Gaussian Laser Modes.*

4.4.0.3 Ex: Tasks and learning goals

In this exercise, we will...

1. Construct the interferometer sketched in Fig. 4.6 using adequate Fresnel zone plates. What do you observe in the diffracted beam and in the interferogram, when instead of filtering the principal focus f_1 you filter a higher order focus?

2. Pass a Laguerre-Gauß laser beam through a $\lambda/2$ waveplate. How does the angular orbital momentum change when you change the rotation? What happens upon reflection from a mirror?

3. Slightly misalign the mode-matching between the Laguerre-Gauß beam and the Gaussian reference beam until you observe multiple fringes. What do you observe?

Capítulo 5

Laser spectroscopy

In this chapter (Sec. 5.1 to 5.2), we will try various spectroscopic techniques applied to atomic or cavity resonances.

5.1 Saturation spectroscopy

One of the most popular spectroscopic technique is *saturation spectroscopy*, as it is simple, robust, and allows to avoid Doppler-broadening. There are, however, many possible implemen-

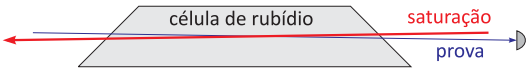

Figura 5.1: Scheme for saturated absorption spectroscopy.

tations of saturation spectroscopy, f.ex. *frequency modulation spectroscopy* or *modulation transfer spectroscopy*, which we will present in the following.

5.1.1 Lamb-dip spectroscopy

The scheme known as *Lamb-dip spectroscopy* and which is illustrated in Fig. 5.1, consists in a cell filled with a gas (for example, atomic rubidium whose resonance frequency is $\omega_0 = ck = 2\pi c/780$ nm and decay rate is $\Gamma = (2\pi)$ 6 MHz) and two laser beams with the same frequency ω, but propagating in opposite directions. One is called the saturating beam, the other probe beam.

Maxwell's one-dimensional and normalized velocity distribution is,

$$\rho(v)dv = \sqrt{\frac{m}{2\pi k_B T}} e^{-mv^2/2k_B T} dv \ .$$

The gas has $T = 300$ K temperature, where the partial pressure of rubidium is about $P = 10^{-1}$ mbar. We assume a cell length of $L = 10$ cm. The probe laser intensity is below saturation, such that the optical cross section for an atom moving with velocity v is,

$$\sigma(v) = \frac{6\pi}{k^2} \frac{\Gamma^2}{4(\omega - \omega_0 - kv)^2 + \Gamma^2} \ .$$

The saturating laser has high intensity. Let us suppose here, $\Omega \equiv 10\Gamma$, where Ω is the Rabi frequency caused by the saturating laser. In this way, it creates a population of N_e atoms in the excited state. Since this population is missing in the ground state, $N_g = N - N_e$, the absorption is reduced for the probe beam by a factor,

$$\frac{N_e}{N} = \frac{2\Omega^2}{4(\omega - \omega_0 + kv)^2 + 2\Omega^2 + \Gamma^2} \ .$$

We will now calculated the spectrum of the optical density for the probe laser, $OD(\omega) = Ln\int_{-\infty}^{\infty}\frac{N_g-N_e}{N}\sigma(v)\rho(v)dv$, and the light intensity transmitted through the cell, $\frac{I}{I_0} = e^{-OD}$.

The optical density with Doppler broadening is,

$$\begin{aligned} OD(T,\omega) &= Ln(T)\int_{-\infty}^{\infty}\frac{N_g-N_e}{N}\sigma(v)\rho(v)dv \\ &= L\frac{P}{k_BT}\sqrt{\frac{m}{2\pi k_BT}}\frac{6\pi}{k^2}\int_{-\infty}^{\infty}\frac{2\Omega^2}{4(\Delta+kv)^2+2\Omega^2+\Gamma^2}\frac{\Gamma^2}{4(\Delta-kv)^2+\Gamma^2}e^{-mv^2/2k_BT}dv \ , \end{aligned}$$

with $\Delta \equiv \omega - \omega_0$. The widths of the three velocity distribution are, respectively,

$$\begin{aligned} k\Delta v &= \sqrt{\tfrac{1}{2}\Omega^2+\tfrac{1}{4}\Gamma^2} \approx (2\pi)\ 68\ \text{MHz} \qquad \text{for the saturating beam} \\ k\bar{v} &= k\sqrt{\tfrac{k_BT}{m}} \approx (2\pi)\ 217\ \text{MHz} \qquad \text{for the Doppler broadening} \\ k\Delta v &= \tfrac{1}{2}\Gamma \approx (2\pi)\ 3\ \text{MHz} \qquad \text{for the probe beam} \ . \end{aligned}$$

where $\bar{v} = \sqrt{k_BT/m}$ is the mean atomic velocity (or the *rms* width) of Maxwell's distribution. Since the spectral width of the probe laser is much smaller, we can substitutes it by a δ-function,

$$\frac{\Gamma^2}{4(\Delta-kv)^2+\Gamma^2} \longrightarrow \frac{\pi\Gamma}{2}\delta(\Delta-kv) \ ,$$

which gives

$$\begin{aligned} OD(T,\omega) &\simeq L\frac{P}{k_BT}\sqrt{\frac{m}{2\pi k_BT}}\frac{6\pi}{k^3}\int_{-\infty}^{\infty}\left(1-2\frac{2\Omega^2}{4(\Delta+kv)^2+2\Omega^2+\Gamma^2}\right)\frac{\pi\Gamma}{2}\delta(\Delta-kv)e^{-mv^2/2k_BT}dkv \\ &= L\frac{P}{k_BT}\sqrt{\frac{m}{2\pi k_BT}}\frac{6\pi}{k^3}\frac{\pi\Gamma}{2}\left(1-\frac{4\Omega^2}{8\Delta^2+2\Omega^2+\Gamma^2}\right)e^{-m(\Delta/k)^2/2k_BT} \ . \end{aligned}$$

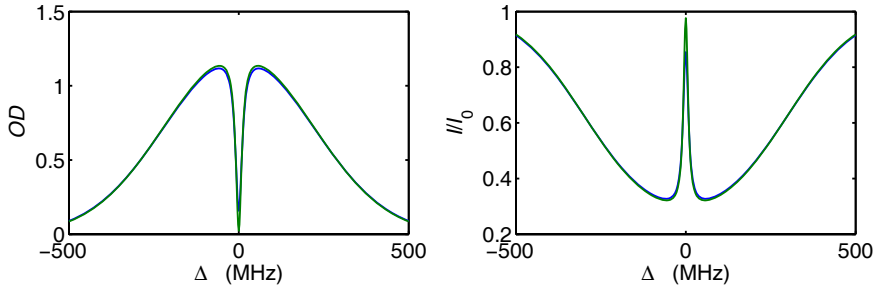

Figura 5.2: (a) Optical density and (b) absorption. (Blue) Integral formula and (green) approximation for high temperature and high saturation.

The *Lamb dip* is the narrow (Doppler-free) feauture in the center of the the spectrum exhibited in Fig. 5.2.

5.1.2 Frequency modulation and modulation transfer spectroscopy

5.1.2.1 Ex: Tasks and learning goals

In this exercise, we will spectroscopically identify the various lines of the rubidium D_2-transition of the isotopes ^{87}Rb and ^{85}Rb. The Hyperfine splittings of the ground and excited states are reproduced in Fig. 5.3.

1. Set up the optics for Lamb-dip spectroscopy as shown in Fig. 5.2.

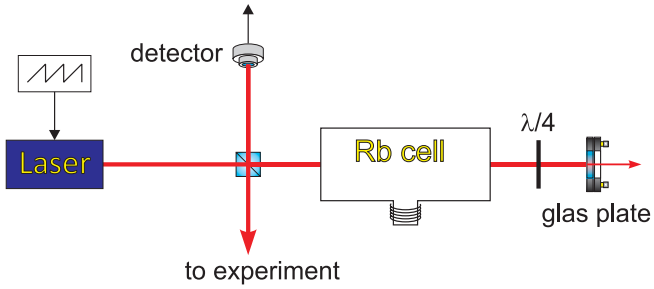

Figura 5.3: Saturation spectroscopy.

5.2 Birefringence and Hänsch-Couillaud spectroscopy

The *Hänsch-Couillaud technique* uses the *birefringence* of certain materials, devices, or gases.

5.2.1 Birefringence of a ring cavity

In a *ring cavity*, the resonance frequencies of the s-polarized and the p-polarized modes are slightly shifted from one another due to the different penetration depth of the s- and p-polarized light modes into the layers of the dielectric mirrors. For a moderate finesse of the cavity (say $\mathcal{F} = 2000$), the modes actually overlap.

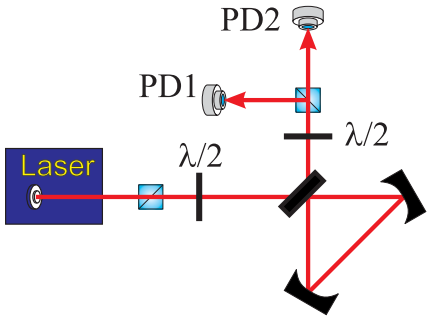

Figura 5.4

This leads to a birefringence used in the famous Hänsch-Couillaud locking scheme. The detector signal in the scheme shown in the figure may calculated via a concatenation of the Jones matrices for a $\lambda/2$-plate, the reflective response of the ring cavity, another $\lambda/2$-plate, and finally a polarizing beam splitter,

$$\begin{pmatrix} E_s \\ E_p \end{pmatrix} = \begin{pmatrix} 1 & 0 \\ 0 & 0 \end{pmatrix} \begin{pmatrix} \cos\beta & -\sin\beta \\ -\sin\beta & \cos\beta \end{pmatrix} \begin{pmatrix} \frac{1-e^{-2\pi i\omega/\delta_{fsr}+i\phi_s}}{1-R_s e^{-2\pi i\omega/\delta+i\phi_s}} & 0 \\ 0 & \frac{1-e^{-2\pi i\omega/\delta_{fsr}+i\phi_p}}{1-R_p e^{-2\pi i\omega/\delta+i\phi_p}} \end{pmatrix} \begin{pmatrix} \cos\alpha & -\sin\alpha \\ -\sin\alpha & \cos\alpha \end{pmatrix} \begin{pmatrix} E_0 \\ 0 \end{pmatrix}$$
$$= \begin{pmatrix} \frac{1-e^{-2i\pi\frac{\omega}{\delta_{fsr}}+i\phi_s}}{1-R_s e^{-2i\pi\frac{\omega}{\delta}+i\phi_s}} \cos\alpha\cos\beta + \frac{1-e^{-2i\pi\frac{\omega}{\delta_{fsr}}+i\phi_p}}{1-R_p e^{-2i\pi\frac{\omega}{\delta}+i\phi_p}} \sin\alpha\sin\beta \\ 0 \end{pmatrix} E_0 \ .$$

Calculating $|E_s|^2$ as a function of the laser frequency ω reproduces the observed curves.

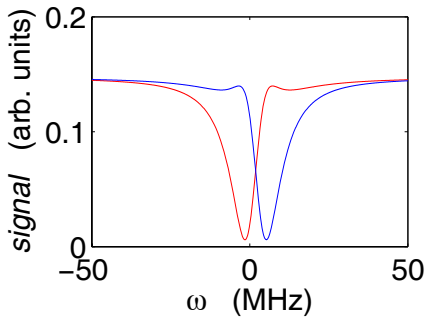

Figura 5.5

5.2.1.1 Ex: Tasks and learning goals

Birefringence can also be introduced in a standard linear optical cavity by simply inserting an interface (e.g. a glas plate) crossing the optical axis under the Brewster angle. In this exercise, we will analyze the birefringence of a such a cavity.

1.

Capítulo 6

Locking circuits

In a laboratory we are often confronted with the need to control the value of a physical parameter, f.ex., room temperature, currents and voltages, or the frequency and intensity of laser beams. The physical discipline dealing with the fundamental concepts of this field is called *control theory* and its application to development of automatic control systems is called *control engineering*.

The minimum ingredients of a control system are 1. a sensor measuring the actual value of the parameter to be controlled (e.g., a thermometer), 2. an actuator capable of correcting the value (e.g., a heater or cooler), and 3. a suitable electronics linking sensor and the actuator thus providing a feedback.

In this chapter, after a brief introduction into control theory, we will design and construct a few automatic control systems, which are common in quantum optics labs.

6.1 Introduction to control theory

Control theory is a theory that deals with influencing the behavior of dynamical systems. It is an interdisciplinary subfield of physics and engineering, which later evolved into other fields, such as social sciences.

Control systems may be thought of as having four functions: measure, compare, compute, and correct with an actuator. A standard example of a measuring unit (or sensor) is a thermometer. The comparator compares the measured value with a reference and delivers the difference to a controller, which may be implemented electronically by proportional control, PID control, bistable hysteretic control, or programmable logic control. Older controller units have been mechanical, as in a carburetor. Finally, the value computed by the controller is delivered to an actuator, which manipulates and changes a variable in the controlled system (or plant).

6.1.1 Open-loop and closed-loop (feedback) control

Fundamentally, there are two types of control loop: open loop control, and closed loop (feedback) control.

In open loop control, the control action from the controller is independent of the "process output"(or "controlled process variable"). A good example of this is a central heating boiler controlled only by a timer, so that heat is applied for a constant time, regardless of the temperature of the building. (The control action is the switching on/off of the boiler. The process output is the building temperature).

In closed loop control, the control action from the controller is dependent on the process output. In the case of the boiler analogy, this would include a thermostat to monitor the building temperature, and thereby feed back a signal to ensure the controller maintains the building at the temperature set on the thermostat. A closed loop controller therefore has a feedback loop which ensures the controller exerts a control action to give a process output the

same as the "reference input"or "set point". For this reason, closed loop controllers are also called feedback controllers.

The definition of a closed loop control system is *a control system capable of canceling the deviation of a system variable from a reference value by means of a feedback signal computed from a measured value of the variable and used to act on the system in a controlled way* [J.J. Di Steffano, A.R. Stubberud, I.J. Williams. Schaums outline series, McGraw-Hill 1967, *Feedback and control systems*]. Automatic feedback control has revolutionized all areas of manufacturing, aircraft, communications and other industries.

6.1.2 Classical control theory

To overcome the limitations of the open-loop controller, control theory introduces feedback. A closed-loop controller uses feedback to control states or outputs of a dynamical system. Its name comes from the information path in the system: process inputs (e.g., voltage applied to an electric motor) have an effect on the process outputs (e.g., speed or torque of the motor), which is measured with sensors and processed by the controller; the result (the control signal) is "fed back"as input to the process, closing the loop.

Closed-loop controllers have the following advantages over open-loop controllers:

- disturbance rejection (such as hills in the cruise control example above)
- guaranteed performance even with model uncertainties, when the model structure does not match perfectly the real process and the model parameters are not exact
- unstable processes can be stabilized
- reduced sensitivity to parameter variations
- improved reference tracking performance

In some systems, closed-loop and open-loop control are used simultaneously. In such systems, the open-loop control is termed feedforward and serves to further improve reference tracking performance.

6.1.3 Closed-loop transfer function

The output of the system $y(t)$ is fed back through a sensor measurement F to a comparison with the reference value $r(t)$. The controller C then takes the error e (difference) between the reference and the output to change the inputs u to the system under control P. This is shown in the figure. This kind of controller is a closed-loop controller or feedback controller. We will restrain here to *single-input-single-output control* systems (SISO) disregarding the possibility of having multiple and interdependent inputs and outputs.

If we assume the controller C, the plant P, and the sensor F are linear and time-invariant (i.e., elements of their transfer function $C(s)$, $P(s)$, and $F(s)$ do not depend on time), the systems above can be analyzed using the Laplace transform on the variables. This gives the following relations:

$$Y(s) = P(s)U(s) \tag{6.1}$$

$$U(s) = C(s)E(s) \tag{6.2}$$

$$E(s) = R(s) - F(s)Y(s)\ . \tag{6.3}$$

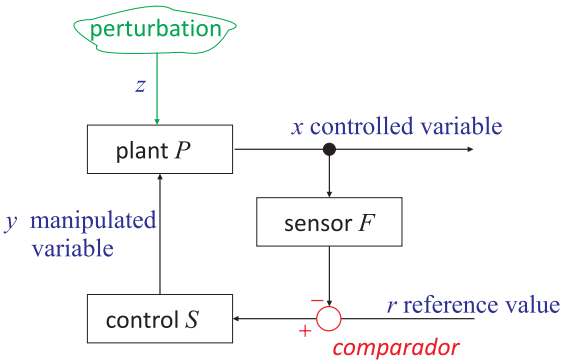

Figura 6.1: Diagram of a feedback loop.

Solving for $Y(s)$ in terms of $R(s)$ gives,

$$Y(s) = \left(\frac{P(s)C(s)}{1 + F(s)P(s)C(s)} \right) R(s) = H(s)R(s) \ . \tag{6.4}$$

is referred to as the closed-loop transfer function of the system. The numerator is the forward (open-loop) gain from r to y, and the denominator is one plus the gain in going around the feedback loop, the so-called loop gain. If $|P(s)C(s)| \gg 1$, i.e.,it has a large norm with each value of s, and if $|F(s)| \simeq 1$, then $Y(s)$ is approximately equal to $R(s)$ and the output closely tracks the reference input.

6.1.4 PID feedback control

A PID controller continuously calculates an error value $e(t)$ as the difference between a desired setpoint and a measured process variable and applies a correction based on proportional, integral, and derivative terms. PID is an acronym for Proportional-Integral-Derivative, referring to the three terms operating on the error signal to produce a control signal.

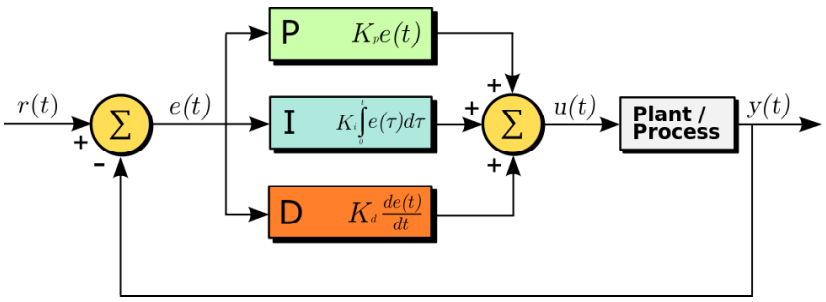

Figura 6.2: A block diagram of a PID controller in a feedback loop, $r(t)$ is the desired process value or "set point", and $y(t)$ is the measured process value. A proportional-integral-derivative controller (PID controller) is a control loop feedback mechanism control technique widely used in control systems.

The theoretical understanding and application dates from the 1920s, and they are implemented in nearly all analogue control systems; originally in mechanical controllers, and then using discrete electronics and latterly in industrial process computers. The PID controller is probably the most-used feedback control design.

Referring to the equation below;

If $u(t)$ is the control signal sent to the system, $y(t)$ is the measured output and $r(t)$ is the desired output, and tracking error $e(t) = r(t) - y(t)$, a PID controller has the general form,

$$u(t) = K_P e(t) + K_I \int e(\tau)d\tau + K_D \frac{de(t)}{dt} \ . \tag{6.5}$$

The desired closed loop dynamics is obtained by adjusting the three parameters K_P, K_P, and K_I, often iteratively by "tuning"and without specific knowledge of a plant model. Stability can often be ensured using only the proportional term. The integral term permits the rejection of a step disturbance (often a striking specification in process control). The derivative term is used to provide damping or shaping of the response. PID controllers are the most well established class of control systems: however, they cannot be used in several more complicated cases, especially if MIMO systems are considered.

Applying Laplace transformation results in the transformed PID controller equation,

$$u(s) = K_P e(s) + K_I \frac{1}{s} e(s) + K_D s e(s) \tag{6.6}$$

$$u(s) = \left(K_P + K_I \frac{1}{s} + K_D s \right) e(s) \ . \tag{6.7}$$

with the PID controller transfer function

$$C(s) = \left(K_P + K_I \frac{1}{s} + K_D s \right) \ . \tag{6.8}$$

There exists a nice example of the closed-loop system discussed above. If we take PID controller transfer function in series form

$$C(s) = K \left(1 + \frac{1}{sT_i} \right) (1 + sT_D) \tag{6.9}$$

1st order filter in feedback loop

$$F(s) = \frac{1}{1 + sT_f} \tag{6.10}$$

linear actuator with filtered input

$$P(s) = \frac{A}{1 + sT_P} \tag{6.11}$$

, A = const and insert all this into expression for closed-loop transfer function H(s), then tuning is very easy: simply put

$$K = \frac{1}{A}, T_I = T_f, T_D = T_P \tag{6.12}$$

and get $H(s) = 1$ identically.

For practical PID controllers, a pure differentiator is neither physically realizable nor desirable[6] due to amplification of noise and resonant modes in the system. Therefore, a phase-lead compensator type approach is used instead, or a differentiator with low-pass roll-off.

6.1.5 Linear and nonlinear control theory

Linear control theory applies to systems made of devices which obey the superposition principle, which means roughly that the output is proportional to the input. They are governed by linear differential equations. A major subclass is systems which in addition have parameters which do not change with time, called linear time invariant (LTI) systems. These systems are amenable to powerful frequency domain mathematical techniques of great generality, such as the Laplace transform, Fourier transform, Z transform, Bode plot, root locus, and Nyquist stability criterion. These lead to a description of the system using terms like bandwidth, frequency response, eigenvalues, gain, resonant frequencies, poles, and zeros, which give solutions for system response and design techniques for most systems of interest.

Nonlinear control theory covers a wider class of systems that do not obey the superposition principle, and applies to more real-world systems, because all real control systems are nonlinear. These systems are often governed by nonlinear differential equations. If only solutions near a stable point are of interest, nonlinear systems can often be linearized by approximating them by a linear system using perturbation theory, and linear techniques can be used.[7]

6.1.6 Analysis techniques - frequency domain and time domain

Mathematical techniques for analyzing and designing control systems fall into two different categories:

Frequency domain: In this type the values of the state variables, the mathematical variables representing the system's input, output and feedback are represented as functions of frequency. The input signal and the system's transfer function are converted from time functions to functions of frequency by a transform such as the Fourier transform, Laplace transform, or Z transform. The advantage of this technique is that it results in a simplification of the mathematics; the differential equations that represent the system are replaced by algebraic equations in the frequency domain which are much simpler to solve. However, frequency domain techniques can only be used with linear systems, as mentioned above.

Time-domain state space representation: In this type the values of the state variables are represented as functions of time. With this model the system being analyzed is represented by one or more differential equations. Since frequency domain techniques are limited to linear systems, time domain is widely used to analyze real-world nonlinear systems. Although these are more difficult to solve, modern computer simulation techniques such as simulation languages have made their analysis routine.

In contrast to the frequency domain analysis of the classical control theory, modern control theory utilizes the time-domain state space representation, a mathematical model of a physical system as a set of input, output and state variables related by first-order differential equations. To abstract from the number of inputs, outputs and states, the variables are expressed as vectors and the differential and algebraic equations are written in matrix form (the latter only being possible when the dynamical system is linear). The state space representation (also known as the "time-domain approach") provides a convenient and compact way to model and analyze systems with multiple inputs and outputs. With inputs and outputs, we would otherwise have to write down Laplace transforms to encode all the information about a system. Unlike the frequency domain approach, the use of the state-space representation is not limited to systems with linear components and zero initial conditions. "State space"refers to the space whose axes are the state variables. The state of the system can be represented as a point within that space.[8][9]

6.2 PI servo for a current stabilization

Many applications in quantum optics require very stable high currents, for instance, in coils generating magnetic field for atomic trapping potentials. Here, we will construct a *PI servo* to para realize a *current stabilization*.

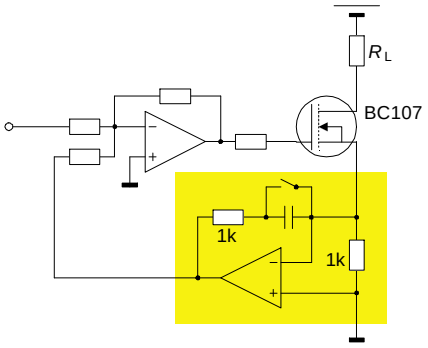

Figura 6.3: Current stabilization.

Further reading:
U. Tietze & Ch. Schenk, Halbleiterschaltungstechnik, Springer-Verlag
O. Föllinger, Regeltechnik, Hüsing-Verlag, Heidelberg

6.2.0.1 Ex: Tasks and learning goals

How to control high currents? How to dramatically increase the switching speed despite inductive loads and eddy currents?

1. Connect a resistive charge to a voltage source. Insert a *MOSFET* into the circuit and a small resistor. Control the gate of the MOSFET with a voltage and measure the current of the circuit via the voltage drop at the small resistor as a function of the gate voltage.

2. Now control the gate voltage via the voltage measured at the small resistor and measure again the dependency voltage-to-current.

6.3 Laser intensity stabilization with an AOM

The light emitted from lasers is generally subject to *frequency fluctuations* and *intensity fluctuations*, which are unacceptable for many applications. In this section we will construct an *intensity stabilization* for a laser beam.

One way of stabilizing the light intensity of a laser beam consists in using the an acousto-optic modulator, as shown in Fig. 6.4. The first Bragg diffraction order (see Sec. 3.7) is focused onto a photodiode. Intensity fluctuations of the light recorded by the photodiode are converted into voltage fluctuations, processed by an electronic circuit fed back to the AOM. The intensity of light diffracted into the first order can be controlled via the power of the radiofrequency alimenting the AOM. The control circuit can now be conceived such as to neutralize the intensity fluctuations recorded by the photodiode.

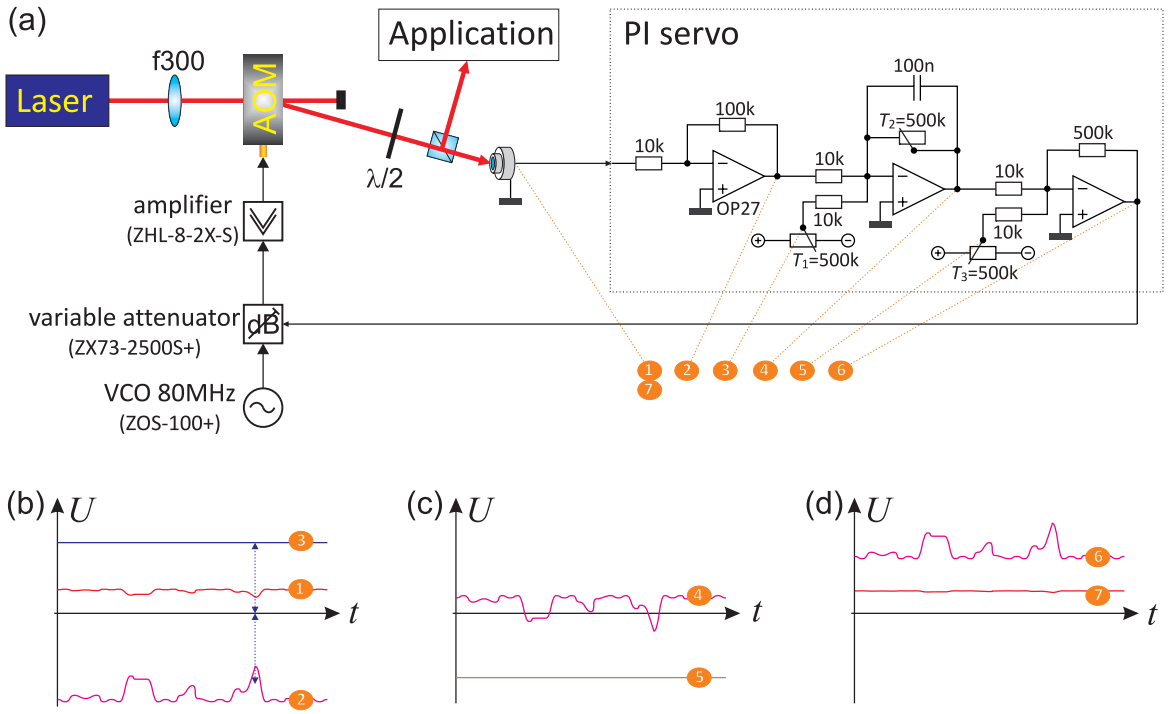

Figura 6.4: (a) Layout of the intensity control. The variable attenuator controls the amplitude of the radiofrequency driving the AOM: low voltage (0 V) increases the attenuation, high voltage (+16 V) reduces it. The sketched control circuit realizes a negative feedback, when the photodetector produces a positive signal. (b-d) Signals recorded at the test points of the circuits shown in (a). See text for explanations.

For the realization of the project prior knowledge of 1. photodetectors (see Sec. 2.2), 2. acousto-optic modulators (AOM) (see Sec. 3.7), 3. electronic circuits (see Sec. 2.1.3), and 4. control circuits (see Sec. 6.1) is required.

6.3.1 Operation principle

The idea of the intensity stabilization is illustrated in Fig. 6.4(b-d): The laser intensity scattered into the first diffraction order is recorded by a photodiode (test point 1 in the figure). The signal is then amplified (and inverted) by a first OpAmp (test point 2). The trimmer T_1 (test point 3) is now adjusted to a positive voltage compensating the DC part of the signal (2), i.e., the sum (2+3) after being inverted and amplified by the second OpAmp (test point 4), should be around zero DC. The signal (2+3) is called *error signal*, since it is this signal which tells us in which direction the control circuits has to work to counteract the power fluctuation. In the present design, the second OpAmp also incorporates the PI servo (see Sec. 6.1), which can be adjusted via the amplification of the trimmer T_2 and the capacity C.

It is now important to realize, that the variable attenuator works best around a given control voltage, which is provided by adding via the trimmer T_3 (test point 5) and a third OpAmp an appropriate offset. Furthermore, we note that variable attenuator reduces its attenuation with increasing control voltage. Thus, the control signal (test point 6) works to enhance the efficiency of the AOM, when the photodiode signals a power drop, and vice versa. As a result, the light power in the first diffraction order is stabilized, however, at a level inferior to the unstabilized

power.

6.3.2 Adjustment procedure

The trimmers of the servo circuits can be adjusted using the following procedure:

1. Observe the light intensity and its fluctuations at test point (1), set test point (4) to ground (e.g. short-circuiting the trimmer T_2), and adjust trimmer T_3 until the light intensity level is at bit lower than the lowest fluctuations.

2. Reconnect test point (4) to the circuit and adjust trimmer T_1 until the voltage at test point (4) cancels to zero.

Further reading:
U. Tietze & Ch. Schenk, Halbleiterschaltungstechnik, Springer-Verlag
O. Föllinger, Regeltechnik, Hüsing-Verlag, Heidelberg

6.3.2.1 Ex: Tasks and learning goals

We will now set up up an intensity stabilization.

1. Realize the optical setup illustrated in Fig. 6.4. Optimize the alignment of the AOM (in particular, the focus and the Bragg angle) in order to maximize the efficiency of the AOM. Take care not to saturate the photodiode, if necessary adapt the load resistance (see Sec. 2.1.). Study the data sheet of the variable attenuator.

2. Set up the electronic circuit exhibited in Fig. 6.4. Test it by observing the signals at the six test points marked in the circuit diagram. Understand and interprete the roles of the three adjustable parameters: "input offset, amplification, and output offset.

3. Incorporate the servo circuit into the optical setup as shown in Fig. 6.4. How to make sure the circuit is operating properly?

Datasheets:
For the VCO see appendix data sheet Fig. 8.3
For the variable attenuator see appendix data sheet Fig. 8.4
For the amplifier see appendix data sheet Fig. 8.2.

6.4 Frequency stabilization of a Fabry-Pérot cavity

One method of stabilizing a laser on a resonator consists in modulating the frequency slightly and then demodulating the transmission signal of the resonator at the same frequency. This is the so-called *lock-in method*. Frequency modulation of the laser beam can be done by modulating the laser diode feed current, the piezo of the extended laser cavity or using an AOM. Fig. 6.5 shows the layout of the optical assembly.

The principle of control through modulation is explained in Fig. 6.5(a). A laser beam passes twice (round-trip) through an *acousto-optic modulator* fed by a radiofrequency voltage with

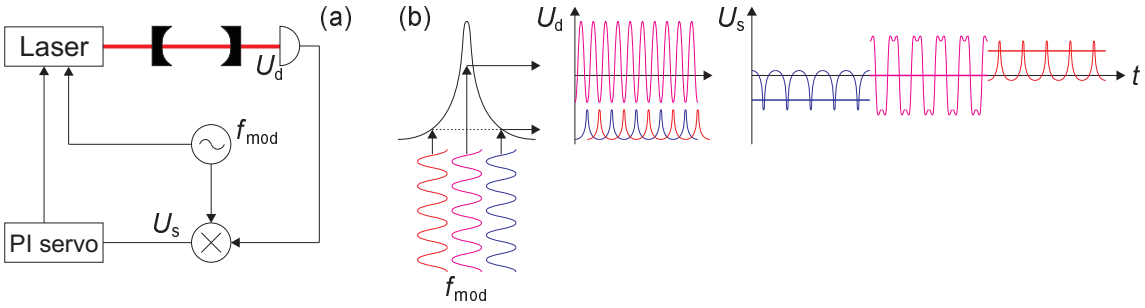

Figura 6.5: (a) Frequency stabilization to a cavity using the lock-in method. (b) Frequency-modulated signals applied to a resonance suffer a period doubling, when the signal frequency is close to resonance. By demodulating the signals discriminated at the resonance profile, we obtain, after averaging over a period, a DC voltage that is proportional to the frequency detuning.

modulated frequency, $\omega(t) = \omega_c + M \cos ft$. Here, the modulation frequency is much lower than its amplitude (or frequency excursion), $f \ll M$. The laser beam is now injected into an optical cavity and the frequency of the laser tuned near a resonance of the cavity. The dependence of the transmission on the frequency is described in good approximation of the *Airy formula* by a Lorentzian,

$$I(\omega) = \frac{\gamma^2}{4(\omega - \omega_0)^2 + \gamma^2} \ . \tag{6.13}$$

The signal transmitted through the cavity [see Fig. 6.5(b)],

$$U_d(t) = I(\omega(t)) = \frac{\gamma^2}{4\left(\omega_c + M\cos ft - \omega_0\right)^2 + \gamma^2} \ , \tag{6.14}$$

is demodulated by a lock-in amplifier [see Fig. 6.5(c)],

$$U_s(t) = U_d(t)\cos(ft + \phi) \ , \tag{6.15}$$

integrated with a locking electronics [see Fig. 6.5(d)]

$$\bar{U}_s(t) = \frac{1}{T}\int_0^T U_s(t)dt \ . \tag{6.16}$$

and used to control the piezo of the laser's extended cavity.

6.4.0.2 Ex: Tasks and learning goals

Here is, how we are going to stabilize a laser to a cavity:

1. Stabilize a helium-neon laser to a Fabry-Pérot cavity, generating a frequency modulation by modulating the laser diode current or the piezo of the extended cavity. Choose a modulation frequency in the range of $f \simeq 1$ kHz and a modulation amplitude in the range of $M \simeq 5$ MHz. Adjust the reference voltage of the control electronics until the error signal is symmetrical.
2. If you do not have a lock-in amplifier available, construct one following the project Sec. 2.7.
3. Now, do the opposite, stabilizing the optical cavity to the laser frequency using the resonator piezo as control element.
4. Vary the optical setup now modulating the frequency using an AOM (see Fig. 6.6).

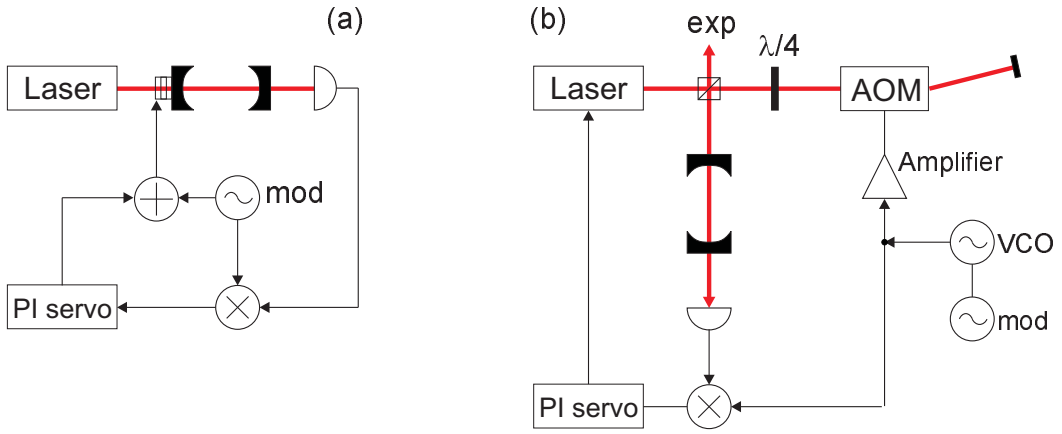

Figura 6.6: Variations on the same theme: (a) Frequency stabilization of a cavity to a laser frequency using the lock-in method. This method is often used for spectral filtering of a laser beam by a transmission etalon. (b) Frequency stabilization of a laser to a cavity using an AOM. The advantage of using an AOM compared to the scheme shown in Fig. 6.5 is, that only the beam injected into the cavity is modulated, but not the beam used for the main experiment.

6.5 Pound-Drever-Hall frequency stabilization

When the frequency of a carrier wave ω is modulated by a frequency Ω, the spectrum consists of sidebands the frequencies and phases of which can be calculated from an expansion of the wave in Bessel functions. Let N be the modulation excursion and $J_k(x)$ the Bessel function of the order k. Higher-order sidebands $k > 1$ are usually dropped in the calculation,

$$e^{i(\omega t + N \sin \Omega t)} = e^{i\omega t}[-J_1(N)e^{i\Omega t} + J_0(N) + J_1(N)e^{-i\Omega t}] \ . \tag{6.17}$$

From the latter expression, it can be seen that the spectrum of sidebands is formed by the frequencies ω and $\omega \pm \Omega$. A resonator responds to a field of incident light $E_0(\omega)$ oscillating with frequency ω by reflecting the field (R: reflectivity of mirrors, δ: free spectral range)

$$E_r(\omega) = E_0(\omega)\sqrt{R}\frac{1 - e^{-2\pi i\omega/\delta}}{1 - R\ e^{-2\pi i\omega/\delta}} \ , \tag{6.18}$$

where the amplitude and the phase of the reflected light field follow from the relation $E_r(\omega) = |E_r(\omega)|e^{i\phi(\omega)}$. Obviously the field of the reflected light is strong only, when the laser frequency is close to one mode of the resonator (when ω/δ is an integer number). By inserting Eq. (6.18) into Eq. (6.17), we obtain the response of the resonator to a field containing sidebands as a function of the frequency of light ω, of the modulation frequency Ω, and of the cavity finesse,

$$\begin{aligned} |E_{tot}|^2 &= |e^{i\omega t}[J_1(N)E_r(\omega + \Omega)e^{i\Omega t} + J_0(N)E_r(\omega) - J_1(N)E_r(\omega - \Omega)e^{-i\Omega t}]|^2 \\ &= J_0(N)J_1(N)E_r(\omega + \Omega)e^{i\Omega t} + J_0(N)J_1(N)E_r^*(\omega - \Omega)e^{i\Omega t} + ... + c.c. \ . \end{aligned} \tag{6.19}$$

The contributions of the reflected field to the current in the photodetector, $|E_r|^2$, oscillating with frequency Ω and extracted by the alternating current $e^{-i\Omega t + i\theta}$ (θ is an arbitrarily chosen phase angle), are

$$S_{PDH} = |E_{tot}|^2 e^{-i\Omega t + i\theta} = J_0(N)J_1(N)\mathrm{Re}\{e^{i\theta}[E_r^*(\omega)E_r(\omega + \Omega) - E_r(\omega)E_r^*(\omega - \Omega)]\} + ... \ . \tag{6.20}$$

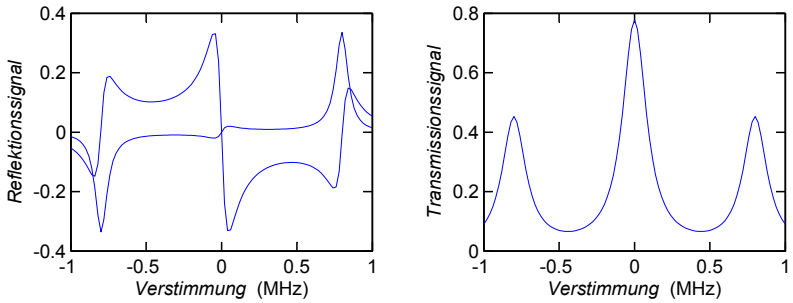

Figura 6.7: (Left) Pound-Drever-Hall reflection signal for $\theta = 0, \pi/2$. (Right) Transmission signal.

By a suitable choice of the modulation index, the pre-factor containing Bessel functions (and therefore the signal amplitude) can be maximized. That is the case, for $M \simeq 1.1$. Each of the two parts of the summation in the above equation is the result of a beating of the carrier $E_r(\omega)$ with one of the sidebands $E_r(\omega \pm \Omega)$. Only those optical sidebands being close to a mode of the resonator provide, along with the radiofrequency sidebands, contributions to the reflection signal

The dependence of the reflection signal S_{PDH} on the frequency ω is shown in Fig. 6.7(a). The antisymmetric shape and the zero-crossing slope are ideal for use as a discriminator generating an *error signal* for a frequency stabilization. This method is called *Pound-Drever-Hall method*.

6.5.0.3 Ex: Tasks and learning goals

Now we'll stabilize a laser to a cavity using the Pound-Drever-Hall technique:

1. Consider the reflected signal. To do this, separate the beam injected into the resonator from the reflected beam by means of a $\lambda/4$ waveplate and a polarizing beam splitter.
2. Now analyze the reflected signal with a fast photodetector at a spectrum analyzer.
3. Demodulate the signal with the modulation frequency. Vary the length of the cables. Optimize the slope of the error signal by a suitable choice of frequency and modulation excursion.

Further reading:

M. Born, 6.ed. Pergamon Press New York (1980), Principles of Optics
*R.W.P. Drever, J.L. Hall, F.V. Kowalski, J. Hough, G.M. Ford, A.J. Munley, and H.W. Ward, Appl. Phys. B **31**, 97 (1983), Laser Phase and Frequency Stabilization Using an Optical Resonator*

Datasheets:

For the VCO see appendix data sheet Fig. 8.3
For the power splitter see appendix data sheet Fig. 8.5
For the mixer see appendix data sheet Fig. 8.6

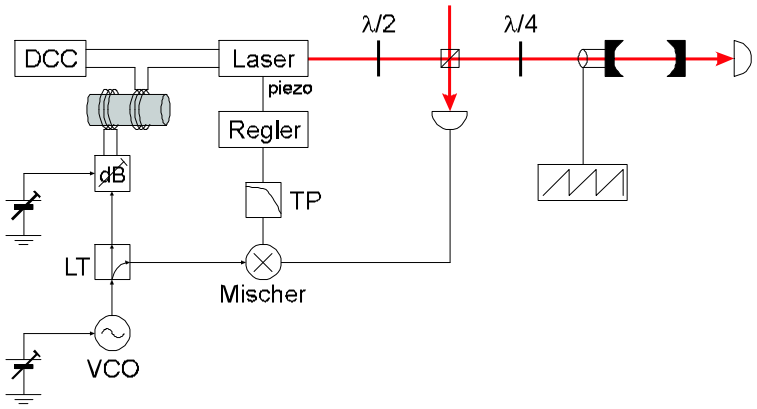

Figura 6.8: Setup of a frequency regulator following Pound-Drever-Hall. VCO: Voltage-Controlled Oscillator, LT: power splitter, dB: variable attenuator, LP: low-pass filter.

6.6 Phase locking

6.6.1 VCO and mixing

In a *phase-locked loop* one tries to synchronize a self-sustained oscillator, in general realized by a VCO, with a local oscillator. The VCO generates an ac-voltage U_{rf}, whose frequency is tuned via a dc-control-voltage U_{ct} around a center frequency ω_0. It can be modeled by,

$$\begin{aligned} U_{rf}(t) &= 2B\cos\phi(t) \\ \frac{d\phi}{dt} &= \omega_0 + KU_{ct}(t)\ . \end{aligned} \tag{6.21}$$

The local oscillator produces an ac-voltage, $U_{lo}(t) = A\sin\phi_{lo}(t)$. A mixer multiplies both signals,

$$U_d(t) = AB\left(\sin[\phi_{lo}(t) - \phi(t)] + \sin[\phi_{lo}(t) + \phi(t)]\right)\ . \tag{6.22}$$

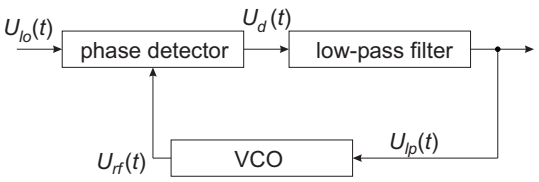

Figura 6.9: PLL.

6.6.2 Low-pass filtering

The multiplied signal U_d contains all information about frequency deviations of the VCO from the LO. To extract them, we *low-pass filter* this signal, cutting off all high frequency components, i.e. apply the filter transfer function,

$$F(p) = (1 + pRC)^{-1}\ . \tag{6.23}$$

The signal of the filter is $U_{lp}(p) \equiv F(p)U_d(p)$. In time domain, which is obtained by a Laplace transform, $F(t) = (RC)^{-1}\theta(t)e^{-t/RC}$, such that

$$U_{lp}(t) = F \star U_d(t) = \int_{-\infty}^{\infty} F(t-\tau)U_d(\tau)d\tau = \frac{e^{-t/RC}}{RC}\int_{-\infty}^{t} e^{\tau/RC}U_d(\tau)d\tau \ . \tag{6.24}$$

The derivative is obviously,

$$\begin{aligned} \frac{dU_{lp}}{dt} + \frac{U_{lp}}{RC} &= \frac{U_d(t)}{RC} \\ &= \frac{AB}{RC}\sin\left[\phi_{lo}(t) - \phi(t)\right] \ , \end{aligned} \tag{6.25}$$

inserting the above expression for U_d. Note, taht we would have obtained the same result using control theory (see Sec. 6.1).

6.6.3 Phase synchronization

The phase synchronization servo is closed by setting $U_{ct} = U_{lp}$. Thus we may substitute $U_{lp}(t)$ and define $\psi \equiv \phi - \phi_{lo}$,

$$\frac{d^2\psi}{dt^2} + \frac{1}{RC}\frac{d\psi}{dt} + \frac{KAB}{RC}\sin\psi = -\frac{d^2\phi_{lo}}{dt^2} - \frac{1}{RC}\left(\frac{d\phi_{lo}}{dt} - \omega_0\right) \ . \tag{6.26}$$

In most cases the LO frequency varies slowly, so that we may assume $\dot{\phi_{lo}} = \omega_{lo}$,

$$\frac{d^2\psi}{dt^2} + \frac{1}{RC}\frac{d\psi}{dt} + \frac{KAB}{RC}\sin\psi = -\frac{1}{RC}\left(\omega_{lo} - \omega_0\right) \ . \tag{6.27}$$

Hence, a PLL generates a signal $U_{rf}(t)$ having approximately the same (time-dependent) frequency as the local oscillator $U_{lo}(t)$. The equation is identical to that of an overdamped rotator or a resistively shunted Josephson junction [14].

The experimental implementation of phase locking of two lasers via a local oscillator is detailed in (see Details).

6.7 Phase stabilization of standing waves

Para a estabilização da fase de uma onda estacionária pode-se usar o esquema seguinte. É semelhante ao método homódino utilizado com o interferômetro de Michelson com a diferencia, que a separação e a recombinação do feixe laser são feitos em divisores de feixes diferentes.

6.8 Frequency referencing

Various new phenomena are expected in the dynamics of Bose-Einstein condensates (BEC) coupled to a high-finesse ring resonator. Examples are a strong modification of superradiant Rayleigh scattering due to recycling of the optical end-fire modes [8]⊙, collective atomic recoil lasing (CARL) from quantum degenerate gases or cavity cooling of Bose-Einstein condensates [9]⊙.

Almost all experiments involving backaction of the atoms onto the light fields require precise tuning of the cavity resonance. However, this task is non-trivial because of several contradictory

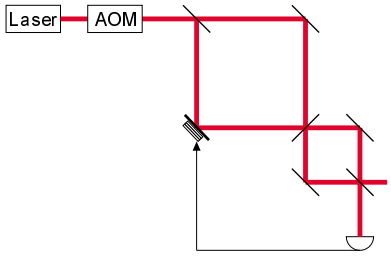

Figura 6.10: Estabilização da fase.

requirements: Collective coupling is only effective at reasonably small atom-light detunings and when the light is resonant to a cavity mode. To maintain the cavity resonant (e.g. via a servo loop) a minimum amount of light must be coupled in. Unfortunately both conditions, the small detuning and the non-vanishing light intensity result in radiation pressure which heats the atomic cloud and quickly destroys the BEC.

In order to inject a laser beam into a cavity mode, the laser must be stabilized to an eigenfrequency of the cavity. To probe the eigenfrequency it is necessary to monitor the cavity's response to an injected light field. The response can than be used to set up a servo loop, e.g. a Pound-Drever-Hall (PDH) locking scheme. For a PDH servo to operate reliably a minimum of injected light power is required. Unfortunately, this light will interact with the atoms stored inside the cavity mode and in the case of a BEC lead to its rapid destruction.

A possible way to circumvent this problem is to use *two* lasers: One is very weak, close to an atomic resonance, tunable across a cavity eigenfrequency and can readily be switched on and off. The other is very far from atomic resonance, sufficiently strong and serves to probe the cavity's free spectral range. Both lasers are phase-coherently locked together by some means, for example via a transfer cavity, using frequency mixing techniques or frequency combs. Another approach consist in probing the cavity on a higher-order $\mathrm{TEM}_{k,l}$ mode

In the following we will discuss and compare the different approaches. All of them include the locking of a Ti:sapphire laser using the Pound-Drever-Hall technique and an offset locking scheme using a phase-locked loop (PLL).

6.8.1 PLL for two laser frequencies

A tunable frequency synthesizer outputs the following signal,

$$U_{scn}(t) = A\cos\omega_{scn}t \ . \tag{6.28}$$

The output of a 100 MHz reference quartz is

$$U_{qrz}(t) = B\cos\omega_{qrz}t \ . \tag{6.29}$$

A VCO operating around 102.5 MHz is described by

$$\begin{aligned} U_{vco}(t) &= D\cos\phi_{vco}(t) \\ \frac{d\phi_{vco}}{dt} &= \omega_{vco} + KU_{ct}(t) \ . \end{aligned} \tag{6.30}$$

All three signals are multiplied at mixers

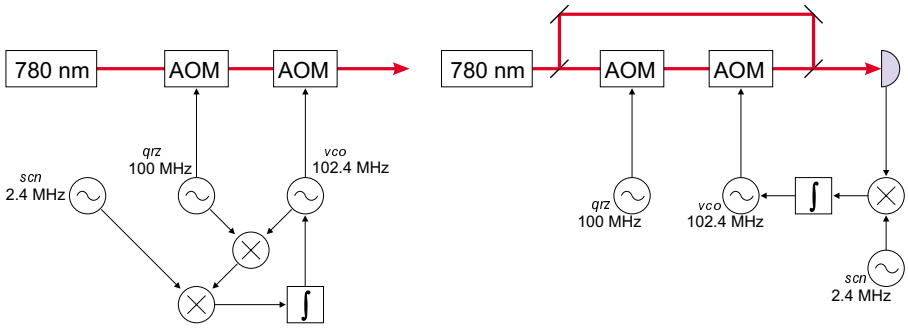

Figura 6.11: Scheme for tuning one laser with respect to a reference laser.

$$
\begin{aligned}
U_{dem}(t) &= U_{scn}(t)U_{qrz}(t)U_{vco}(t) \qquad (6.31)\\
&= A\cos\omega_{qrz}t\ B\cos\phi(t)\ D\cos\omega_{scn}t\\
&= \tfrac{ABD}{4}\sin[-\omega_{scn}t-\omega_{qrz}t+\phi(t)] + \tfrac{ABD}{4}\sin[\omega_{scn}t-\omega_{qrz}t+\phi(t)] + \tfrac{ABD}{4}\sin[-\omega_{scn}t+\omega_{qrz}t+\phi(t)] + \\
&= \tfrac{ABD}{4}\sin[(-\omega_{scn}-\omega_{qrz}+\omega_{vco})t+\phi(t)] + \dots\ ,
\end{aligned}
$$

and then filtered by a low pass

$$
\begin{aligned}
F(p) &= (1+pRC)^{-1} \qquad (6.32)\\
F(t) &= (RC)^{-1}\theta(t)e^{-t/RC}
\end{aligned}
$$

yielding,

$$
\begin{aligned}
U_{lp}(t) &= F\star U_{dem}(t) \qquad (6.33)\\
&= \frac{e^{-t/RC}}{RC}\int_{-\infty}^{t} e^{-\tau/RC}U_{dem}(\tau)d\tau\\
\frac{dU_{lp}}{dt}+\frac{U_{lp}}{RC} &= \frac{U_{dem}(t)}{RC} = \tfrac{ABD}{4RC}\sin[(-\omega_{scn}-\omega_{qrz}+\omega_{vco})t+\phi_{vco}(t)]\ .
\end{aligned}
$$

The PLLoop is closed when

$$
U_{lp}(t)\equiv U_{ct}(t) = \frac{1}{K}(\frac{d\phi_{vco}}{dt}-\omega_{vco})\ . \qquad (6.34)
$$

With the abbreviation

$$
\psi = (-\omega_{scn}-\omega_{qrz}+\omega_{vco})t+\phi_{vco}(t)\ , \qquad (6.35)
$$

one obtains

$$
\begin{aligned}
\frac{d^2\phi_{vco}}{dt}+\frac{1}{RC}\frac{d\phi_{vco}}{dt} &= \tfrac{KABD}{4RC}\sin\left[(-\omega_{scn}-\omega_{qrz}+\omega_{vco})t+\phi_{vco}(t)\right] \qquad (6.36)\\
\frac{d^2\psi}{dt}+\frac{1}{RC}\frac{d\psi}{dt}-\tfrac{KABD}{4RC}\sin\psi &= \frac{1}{RC}(\omega_{scn}+\omega_{qrz}-\omega_{vco})\ .
\end{aligned}
$$

We observe that the PLL is locking to servo oscillations. The spectrum of signal produced by the VCO exhibits sidebands as soon as the loop is closed. Their amplitude depends on the gain, their frequency varies with the offset voltage controlling the VCO.

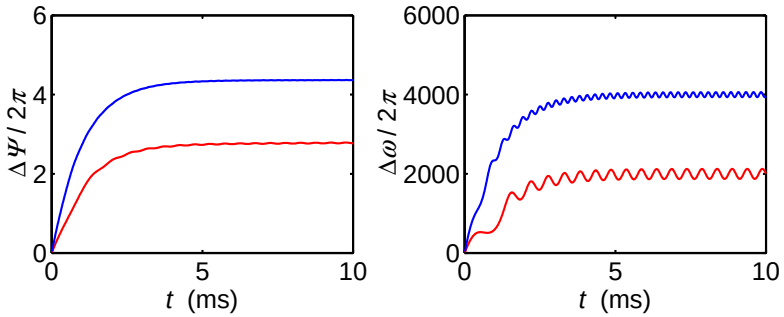

Figura 6.12: Simulation of the phase and frequency difference in a PLL.

6.8.2 Transfer cavities

A Ti:sapphire laser operating at 850 nm is locked to the ring cavity. A piezo-tunable reference cavity is now locked to the Ti:sapphire laser, and a diode laser operating at 780 nm is locked to the reference cavity. It is hopeless to try to tune the diode laser to the ring cavity resonance with acousto-optic modulators, because their tuning range is about 100 times narrower than the ring cavity's free spectral range. Therefore, we need to build up an offset locking scheme with a second diode laser, which is now used to drive the BEC.

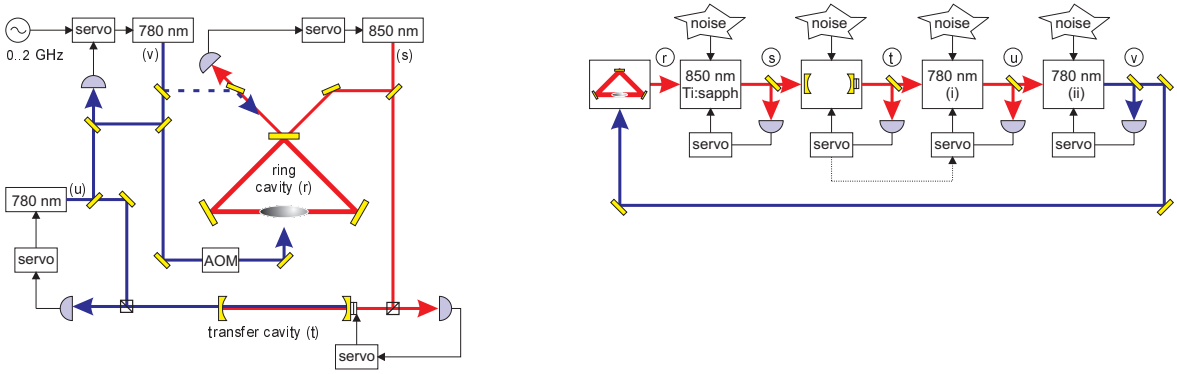

Figura 6.13: (a) The optical setup for the experiment consists of 4 servo loops. A Ti:sapphire laser (s) at 850 nm is locked to the ring cavity (r) and locks a transfer cavity (t). Now, a first 780 nm laser (u) is locked to the transfer cavity. The light of a second diode laser (v), which is offset-locked to the first one, is shone onto the BEC or alternatively coupled into the ring cavity (dashed line). (b) Schematic view of the complete locking system consistent of four consecutive loops. Each resonance or laser oscillator k is characterized by a transfer function A_k, each servo loop by a transfer function B_k. Noise is coupled in at every stage. An additional feedforward C_u relieves the servo loops in the high-frequency noise domain.

The cascaded locking servo systems must ensure a stability superior to the ring cavity transmission linewidth, i.e. better than 10 kHz. This requires the use of the Pound-Drever-Hall technique.

Thermal drifts of the ring cavity can influence the detuning Δ_c between the laser at 780 nm and the ring cavity. If the drifts are strong, the quadruple locking scheme may suffer. Let us assume for now, that the locking operates perfectly and write the resonance conditions for the

Ti:sapphire laser (ω_s), the diode lasers ($\omega_{u,v}$) and the

$$\begin{aligned} \omega_r &= n_r\delta_r \\ \omega_s &= \omega_r = n_t\delta_t \\ \omega_u &= m_t\delta_t \\ \omega_v &= m_t\delta_t + X \equiv m_r\delta_r \ . \end{aligned} \tag{6.37}$$

Thus, $X = (m_r/n_r - m_t/n_t)\omega_s$. Fluctuations of the ring cavity eigenfrequencies of $\Delta\omega_s$ translate into fluctuations of the detuning between diode laser (u) and the nearest ring cavity mode of

$$\Delta X = \frac{X}{\omega_s}\Delta\omega_s \ . \tag{6.38}$$

Hence, if the mode to which the Ti:sapphire laser is locked is chosen such that diode laser (u) also coincides with a mode, i.e. if the detuning can be chosen $X = 0$, the fluctuations will cancel out. On the other hand, assuming $X \simeq 500$ MHz and ring cavity drifts of one free spectral range, the drift of diode laser (v) can reach $\Delta\omega_v = \Delta X \simeq 800$ Hz.

6.8.3 Modeling of the locking via a transfer cavity

The whole locking scheme consists of four consecutive servo loops (see Fig. **??**). The role of the servo loops is to ensure that the diode laser (v) sits on a resonance of the ring cavity, i.e. the frequency of both fluctuate in a common mode, $\Delta\omega_p = \Delta\omega_r$.

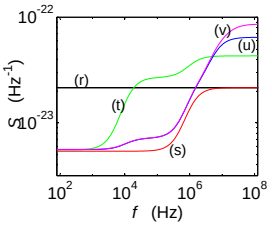

Figura 6.14: Spectral density of frequency fluctuations at different locations of the servo system: The ring cavity is strongly afflicted by acoustic noise and thermal drifts. However, we take its free spectral range as a reference, i.e. set its noise spectrum as a delta distribution. For simplicity, all noise coupled in is assumed to have a white frequency spectrum **(r)**. With respect to the ring cavity the Ti:sapphire laser exhibits frequency fluctuations **(s)**. A servo loop reduces the fluctuations below a certain bandwidth. The same happens at every consecutive step. Unfortunately, the second servo **(t)** is very slow, because the correcting element is a piezo. This can however be corrected with a feedforward, resulting in (u).

The relations of the last section are now generalized to include the impact of noise sources

$$\begin{aligned} \omega_s &= n_r\delta_r + \Delta\omega_{ns} - B_s(\omega_s - n_r\delta_r) \\ n_t\delta_t &= \omega_s + \Delta\omega_{nt} - B_t(n_t\delta_t - \omega_s) \\ \omega_u &= m_t\delta_t + \Delta\omega_{nu} - B_u(\omega_u - m_t\delta_t) - C_u(n_t\delta_t - \omega_s) \\ \omega_v &= \omega_u + \Delta\omega_{nv} - B_v(\omega_v - \omega_u) \ . \end{aligned} \tag{6.39}$$

Now let us denote by $\Delta\omega_x$ the frequency deviations with respect to the ring cavity resonance,

$$\begin{aligned}
\Delta\omega_s &\equiv \omega_s - n_r\delta_r = \frac{1}{1+B_s}\Delta\omega_{ns} \\
\Delta\omega_t &\equiv n_t\delta_t - n_r\delta_r = \Delta\omega_s + \frac{1}{1+B_t}\Delta\omega_{nt} \\
\Delta\omega_u &\equiv \omega_u - \frac{m_t n_r}{n_t}\delta_r = \frac{m_t}{n_t}\Delta\omega_s + \frac{m_t - (1+B_u)^{-1} C_u n_t}{(1+B_t)\, n_t}\Delta\omega_{nt} + \frac{1}{1+B_u}\Delta\omega_{nu} \\
\Delta\omega_v &\equiv \omega_v - \frac{m_t n_r}{n_t}\delta_r = \Delta\omega_u + \frac{1}{1+B_v}\Delta\omega_{nv} \ .
\end{aligned} \tag{6.40}$$

In the absence of noise or for perfect servos, $B_x \to \infty$, we recover the situation of the last section. However, the servos always have a finite bandwidth beyond which noise is fully coupled to the system. The weakest point of the servo chain is probably the small bandwidth of the piezo transducer of the transfer cavity, B_t. A possible way to solve this problem might be to couple fast frequency corrections via a feedforward. We see that even for small values of B_t the prefactor of the noise contribution ω_{nt} can be canceled out by a judicious choice of C_u.

Due to noise, the frequencies excursions are time-dependent, $\omega_x = \omega_x(t)$. However, we transform them into frequency space, $\omega_x = \omega_x(f)$, where f is the Fourier frequency of the noise.

6.8.4 Frequency combs

[16]⊙ [10]⊙ [6]⊙ [7]⊙ [13]⊙ [1]⊙ [15]⊙

6.9 Characterization of stability

6.9.1 Spectral density of fluctuations, Allan variance and power spectral density

In the expression $\alpha(t) = \alpha_0(t)e^{i\phi(t)}$ noise afflicts phase and amplitude. If amplitude noise can be neglected and if the frequency fluctuations only vary little from a mean value, we may write $\phi(t) \equiv \omega_0 t + \varphi(t)$ and $y(t) \equiv \dot{\varphi}/\omega_0$. For Markovian white noise the phase is δ-distributed. This means that the *autocorrelation function* of the frequency is

$$R_\phi \equiv \langle \phi^*(t)\phi(t+\tau)\rangle \equiv \lim_{T\to\infty}\int_0^T \phi^*(t)\phi(t+\tau)\rangle d\tau = D\delta(\tau) \ . \tag{6.41}$$

In that case the *spectral density of frequency fluctuations* is constant,

$$S_\phi(f) = \int_{-\infty}^{\infty} R_\phi(\tau)e^{-2\pi i f\tau}d\tau = D \ . \tag{6.42}$$

The *Allan-variance*

$$\begin{aligned}
y_k(\tau) &= \frac{1}{\tau}\int_{t_k}^{t_k+\tau} y(t)dt \\
\sigma_y^2(\tau) &= \frac{1}{N-1}\sum_{k=1}^{N} y_k^2
\end{aligned} \tag{6.43}$$

for white noise is

$$\sigma_y^2(\tau) = \frac{D}{2\tau} \ . \tag{6.44}$$

The *autocorrelation function of the field amplitude* may be calculated with

$$R_\alpha(\tau) \equiv \langle \alpha^*(t)\alpha(t+\tau)\rangle = \alpha_0^2 \langle e^{i[\phi(t+\tau)-\phi(t)]}\rangle = \alpha_0^2 e^{i\omega_0\tau}\langle e^{i\omega_0\tau y(t)}\rangle \ . \tag{6.45}$$

Note that the *first-order coherence* is just the normalized autocorrelation

$$g^{(1)}(\tau) \equiv \frac{\langle \alpha^*(t)\alpha(t+\tau)\rangle}{\langle \alpha^*(t)\alpha(t)\rangle} = \frac{R_\alpha(\tau)}{R_\alpha(0)} \ . \tag{6.46}$$

Under the assumption of a Gaussian distribution for the noise amplitude [2, 3], $\langle e^{ix}\rangle = e^{-\sigma_x^2/2}$, we get

$$R_\alpha(\tau) = \alpha_0^2 e^{i\omega_0\tau} e^{-\omega_0^2\tau^2\sigma_y^2/2} = e^{-D\omega_0^2|\tau|/4} \ . \tag{6.47}$$

To see this in detail, we note that for a *Gaussian noise process* $\langle A^{2n}\rangle = (2n)!\langle A^2\rangle^n/2^n n!$ and $\langle A^{2n-1}\rangle = 0$, so that

$$\begin{aligned} \left\langle e^{-i[\eta(t)-\eta(t+\tau)]}\right\rangle &= \sum_n \frac{1}{n!}\left\langle i^n\left[\phi(t)-\phi(t+\tau)\right]^n\right\rangle \\ &= \sum_n \frac{1}{n!}\left\langle -\tfrac{1}{2}\left[\phi(t)-\phi(t+\tau)\right]^2\right\rangle^n = e^{-\left\langle[\phi(t)-\phi(t+\tau)]^2\right\rangle/2} \ . \end{aligned} \tag{6.48}$$

Now we set $\phi(t) = \int_0^t V(t')dt'$. Then

$$\left\langle[\phi(t)-\phi(t+\tau)]^2\right\rangle = \left\langle\left[\int_0^\tau V(t')dt'\right]^2\right\rangle = \int_0^\tau\int_0^\tau \left\langle V(t')V(t'')\right\rangle dt'dt'' = 2\int_0^\tau (\tau-t)R_V(t)dt \ . \tag{6.49}$$

The autocorrelation R_V of a given spectrum $S_V(f)$ is $R_V(t) \equiv \int_0^\infty S_V(f)e^{2\pi i f t}df$. Then

$$\begin{aligned} \left\langle[\phi(t)-\phi(t+\tau)]^2\right\rangle &= 2\int_0^\infty S_V(f)\int_0^\tau (\tau-t)e^{2\pi i f t}dtdf = 2\int_0^\infty S_V(f)\left(\frac{\sin\pi f\tau}{2\pi f}\right)^2 df \\ &= \frac{S_V|\tau|}{2\pi}\int_0^\infty\left(\frac{\sin x}{x}\right)^2 dx = \frac{S_V|\tau|}{4} \ , \end{aligned} \tag{6.50}$$

where we assumed white noise.

The *power spectral density* is a Lorentzian:

$$S_\alpha(\omega) = \alpha_0^2\int_{-\infty}^\infty R_\alpha(\tau)e^{-i\omega\tau}d\tau = \frac{D^2\omega_0^4}{4(\omega-\omega_0)^2+D^2\omega_0^4} \ . \tag{6.51}$$

The *laser emission bandwidth*

$$\beta = \tfrac{1}{4}D\omega_0^2 \ . \tag{6.52}$$

Capítulo 7

Special topics

7.1 Deepening of control theory

The variation of a physical quantity (e.g., a voltage or a temperature) in time is called *signal*. In a specific environment or technical device, such a variation may cause other physical quantities to change as well. For example, the rise in temperature of an optical cavity may modify its length and its resonance frequency, while the inverse is not true. This feature is illustrated by a block diagram as shown in Fig. 7.1, where $x(t)$ denotes the variation of a physical quantity (called *input*) that causes the variation of another quantity $y(t)$ (called *output*). The precise way how $y(t)$ depends on $x(t)$ depends on the particularities of the device, which is labeled by a symbol $\mathcal{T}$ called transfer function. $\mathcal{T}$ is in fact an operator acting on functions and transforming input signals into output signals.

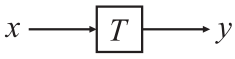

Figura 7.1: Transfer and modification of a time-dependent signal.

While we have described above the transfer of (time-varying) signals, the same feature can be treated in frequency domain via Fourier or Laplace-transforms. This script is not the right place to recapitulate the mathematics of these transforms, and we will restrict ourselves to reproducing some on the most fundamental results, as we may need them in the following.

7.1.1 Signal transfer through LTI systems without delay

For an operator $\mathcal{T}$ transforming a temporal signal $x(t)$ into a signal $y(t)$,

$$y(t) = \mathcal{T}x(t) \ , \tag{7.1}$$

to be *linear* and time-independent, we require,

$$\begin{aligned} \mathcal{T}[\alpha x_1(t) + \beta x_2(t)] &= \alpha\mathcal{T}[x_1(t)] + \beta\mathcal{T}[x_2(t)] \\ \mathcal{T}[x(t-\tau)] &= \mathcal{T}[x(t)] \star \delta(t-\tau) \ , \end{aligned} \tag{7.2}$$

where the $\star$ denotes a convolution,

$$(f \star g)(t) = \int_{-\infty}^{\infty} f(\tau)g(t-\tau)d\tau \ . \tag{7.3}$$

Such system are called *Linear Time-Independent LTI* systems [1].

[1] To be more general, also the derivative and integral of the output signal must be included (see later sections).

7.1.2 Laplace transform

We define the *Laplace transform* $\mathcal{L}$ as a linear operator acting on a signal $x(t)$ defined through,

$$\mathcal{L}... \equiv \int_{-\infty}^{0} ...e^{pt} d\tau \ . \tag{7.4}$$

The frequency variable is denoted by the imaginary quantity $p = if$. The question is now, what is the meaning of the Laplace operator?

To answer this question, we start introducing the pulse response $h(t)$ via

$$h(t) = \mathcal{T}[\delta(t)] \tag{7.5}$$

as the reaction of a system $\mathcal{T}$ to a pulse $\delta(t)$. Now, it is easy to see, that the operator $\mathcal{P}$ defined as,

$$\mathcal{P}... \equiv h(t) \star ... \ , \tag{7.6}$$

and which describes the convolution of an arbitrary input signal with the pulse response, satisfies the above linearity condition. Now calculating,

$$\mathcal{P}e^{pt} = h(t) \star e^{pt} = \int_{-\infty}^{0} h(\tau) e^{p(t-\tau)} d\tau = \mathcal{L}[h(t)] \cdot e^{pt} = (\mathcal{L}h)(p) \cdot e^{pt} \ , \tag{7.7}$$

we find that the functions e^{pt} are eigenfunctions of the operator $\mathcal{P}$ with the eigenvalues $\mathcal{L}[h(t)]$, which are just the Laplace transforms of the pulse response.

We can now expand arbitrary functions $x(t)\theta(t)$ in a Laplace series and obtain,

$$\mathcal{L}[h(t) \star x(t)] = \int_{-\infty}^{0} h(t) \star e^{pt} \ x(t) dt = (\mathcal{L}h)(p) \int_{-\infty}^{0} e^{pt} x(t) dt = (\mathcal{L}h)(p) \cdot (\mathcal{L}x)(p) \ . \tag{7.8}$$

The convolution on the left-hand side is in time domain, while the product on the right-hand side is in frequency domain.

7.1.3 Pulse and jump response from a transfer function

The transmission of a signal by an element of a control loop can be described in the temporal or spectral domain [4, 5, 12], and we can switch from one representation to another via Laplace transformation. Operators of LTI systems $\mathcal{T}$ are represented by products with spectral functions in frequency-domain, $\tilde{F}(p) \cdot ... = (\mathcal{L}F)(p) \cdot ...$ or convolutions with time-varying functions in time-domain, $F(t) \star ...$,

$$\begin{aligned} y(t) &= \mathcal{T}x(t) \\ \overset{transf.\ Laplace}{\longrightarrow} \quad \tilde{y}(p) &= \tilde{F}(p) \cdot \tilde{x}(p) \\ \overset{transf.\ Laplace}{\longrightarrow} \quad y(t) &= F(t) \star x(t) \ . \end{aligned} \tag{7.9}$$

In practice, the function $\tilde{F}(f)$ can be determined by feeding a sinusoidal signal with amplitude $x(p)$ into the system, measuring $y(p)$ (which is a complex number) [2], and calculating

$$F(p) = \frac{y(p)}{x(p)} \ . \tag{7.10}$$

[2] From now on, we will drop the tilde $\sim$ on transfer functions and amplitudes, when it is clear that we are in frequency-domain.

The transitory behavior $F(t)$ can in practice be extracted via an adequate choice of the test function, f.ex., the response to a pulse:

$$\begin{aligned} x(t) &= \delta(t) \\ \overset{transf.\ Laplace}{\longrightarrow} \quad y(p) &= F(p) \\ \overset{transf.\ Laplace}{\longrightarrow} \quad y(t) &= F(t) \ , \end{aligned} \tag{7.11}$$

or to a sudden jump:

$$\begin{aligned} x(t) &= \theta(t) \\ \overset{transf.\ Laplace}{\longrightarrow} \quad y(p) &= F(p)/p \\ \overset{transf.\ Laplace}{\longrightarrow} \quad y(t) &= \int_0^t F(\tau)d\tau \ . \end{aligned} \tag{7.12}$$

Here, $\theta(t)$ denotes the Heavyside function, which is 1 for $t > 0$ and 0 else. The time-dependent function, which describes the pulse response is often used as a symbol for a specific control loop element.

The pulse response works in a similar way as the Green's function procedure: Wanting to know how a loop control element F transforms a given input signal $x(t)$ into an output signal $y(t)$, i.e., $y(t) = F(t) \star x(t)$, we produce a rapid pulse leading to the output,

$$y_\delta(t) = F(t) \star \delta(t) = F(t) \ . \tag{7.13}$$

Now, once we know $F(t)$, the response to arbitrary input signals can be computed via,

$$y(t) = y_\delta(t) \star x(t) \ . \tag{7.14}$$

7.1.4 Bode diagram and polar diagram

The *Bode diagram* illustrates the transfer function in the spectral domain on a bilogarithmic scale separating the amplitude spectrum from the phase spectrum [see Fig. 7.2(a-b)]. Frequency regions, where $|F(p)|$ or $\varphi(p)$ vary particularly strongly are nicely emphasized in the polar representation [see Fig. 7.2(c-d)].

For LTI systems $F(p)$ is always a rational function and can, hence, be represented by its poles and zeros in the complex plane,

$$F(p) = A\frac{(p-a_1)(p-a_2)...(p-a_n)}{(p-b_1)(p-b_2)...(p-b_n)} \ . \tag{7.15}$$

With this, $F(p)$ is analytical and conform, i.e., multiple curves in the p-plane are represented in an isogonal way in the $F(p)$-plane. In order to avoid that the eigenfunctions e^{pt} oscillate and diverge, it is necessary that all the poles and zeros are in the left halfplane.

7.1.5 Algebra of transfer circuits

A technical realization of a signal transfer circuit is illustrated by a signal flux diagram, which itself corresponds to the formalism of linear operators. As shown in Fig. 7.3, signals can be

- (a) added $(f_1 + f_2)(t) \equiv f_1(t) + f_2(t)$,

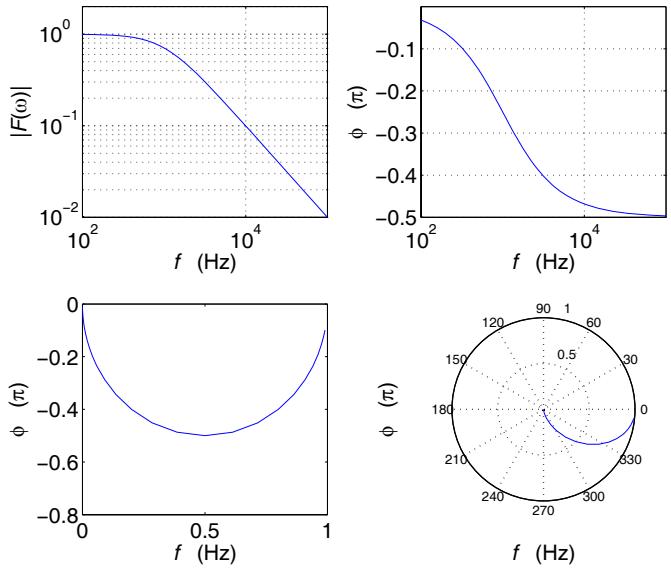

Figura 7.2: Diagrama de Bode.

- (b) multiplied $(f_1 \cdot f_2)(t) \equiv f_1(t) \cdot f_2(t)$,
- (c) doubled $f_1(t) = f_2(t)$,
- (d) transformed $f_2(t) = F[f_1](t) \equiv F(f_1(t))$,
- (e) connected in parallel $(F_1 + F_2)[f(t)] \equiv F_1[f(t)] + F_2[f(t)]$,
- (f) connected in series $(F_1 \circ F_2)[f(t)] \equiv F_1[F_2[f(t)]]$,

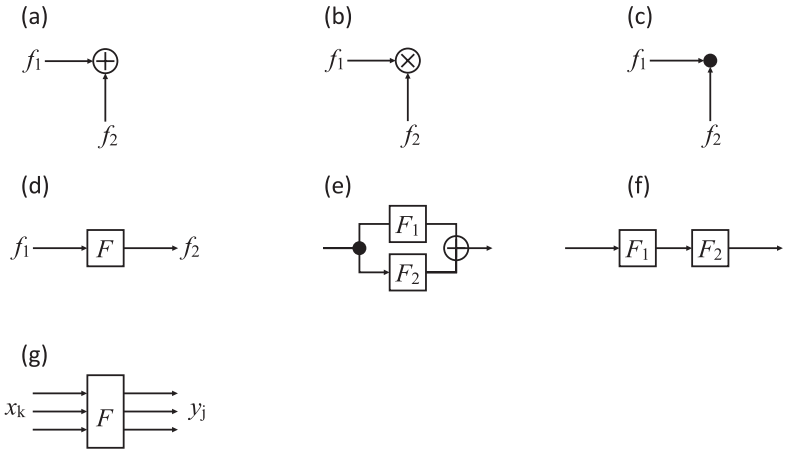

Figura 7.3: Circuitos LTI.

Mathematically, the functions $f(t)$ form a *vector space* and the operators $F[f]$ a *ring*. The linear operators generally are defined implicitly by a system of differential equations. The particular case of linear systems is considerably simpler. The general circuit shown in Fig. 7.3(g) corresponds to the differential equation,

$$0 = F[x_1, .., x_k, \partial_t x_1, .., \partial_t x_k, y_1, .., y_j] \ . \tag{7.16}$$

The linearity $F[\lambda f_1 + \mu f_2] = \lambda F[f_1] + \mu F[f_2]$ warrants that this equation becomes,

$$0 = [1 + \partial_t + ... + \int dt + ...]y_k = [1 + \partial_t + ... + \int dt + ...]x_j \ . \tag{7.17}$$

Note that the multiplication, the derivation, and the integration are linear operators in the same sense as the Fourier and the Laplace transformation.

Linear differential equations can be Laplace transformed. The corresponding transfer function is,

$$F(p) = F(-\delta + i\omega) \equiv \frac{\mathcal{L}y(t)}{\mathcal{L}x(t)} \ . \tag{7.18}$$

In the Laplace-transformed space the operations multiplication, derivation, and integration are all replaced by multiplications:

$$\mathcal{L}[\lambda + \partial_t + ... + \int dt + ...] = \lambda + p + ... + \frac{1}{p} \ . \tag{7.19}$$

With this, the control loop elements and the additive nodes can be used to completely represent a control circuit.

The characteristic responses of components are frequently non-linear (e.g. transistor). For small signal amplitudes, these response functions, and also multiplication points (e.g. mixers) can be linearized by Taylor expansion up to first order,

$$y_0 + \Delta y = F[x_{01} + \Delta x_1, ..., x_{0k} + \Delta x_k] = F[x_{01}, ..., x_{0k}] + \left(\frac{\partial F}{\partial x_1}\right)_0 \Delta x_1 + ... + \left(\frac{\partial F}{\partial x_k}\right)_0 \Delta x_k \ , \tag{7.20}$$

with $y_0 = 0 = F[x_{01}, ..., x_{0k}]$ giving,

$$\Delta y = \left(\frac{\partial F}{\partial x_1}\right)_0 \Delta x_1 + ... + \left(\frac{\partial F}{\partial x_k}\right)_0 \Delta x_k \ . \tag{7.21}$$

For example for a multiplication point,

$$\Delta y = K_1 \Delta x_1 + K_2 \Delta x_2 \ . \tag{7.22}$$

7.1.6 Regulators

For many circuits, it is sufficient to restrict to combinations of resistive (proportional), capacitive (integral), and inductive (differential) circuits. Then, the general case of a control regulator is that of a $PID - T_1...T_n$-element, meaning that:

$$T_2^2 \ddot{y} + T_1 \dot{y} + y = K_D \dot{x} + K_P x + K_I \int dt x = K_P \left(x + T_v \dot{x} + \frac{1}{T_n} \int dt x \right) \ , \tag{7.23}$$

corresponding to the transfer function,

$$F(p) = \frac{K_D p + K_P + K_I/p}{1 + T_1 p + T_2^2 p^2} = \frac{(1 + T_v p + 1/T_n p)}{1 + T_1 p + T_2^2 p^2} \ . \tag{7.24}$$

In literature, two notations are used for the constants. They are linked via: $K_D \equiv K_P T_v$ and $K_I \equiv K_P / T_n$. The stationary behavior is obtained setting the delays to zero: $T_n \equiv 0$.

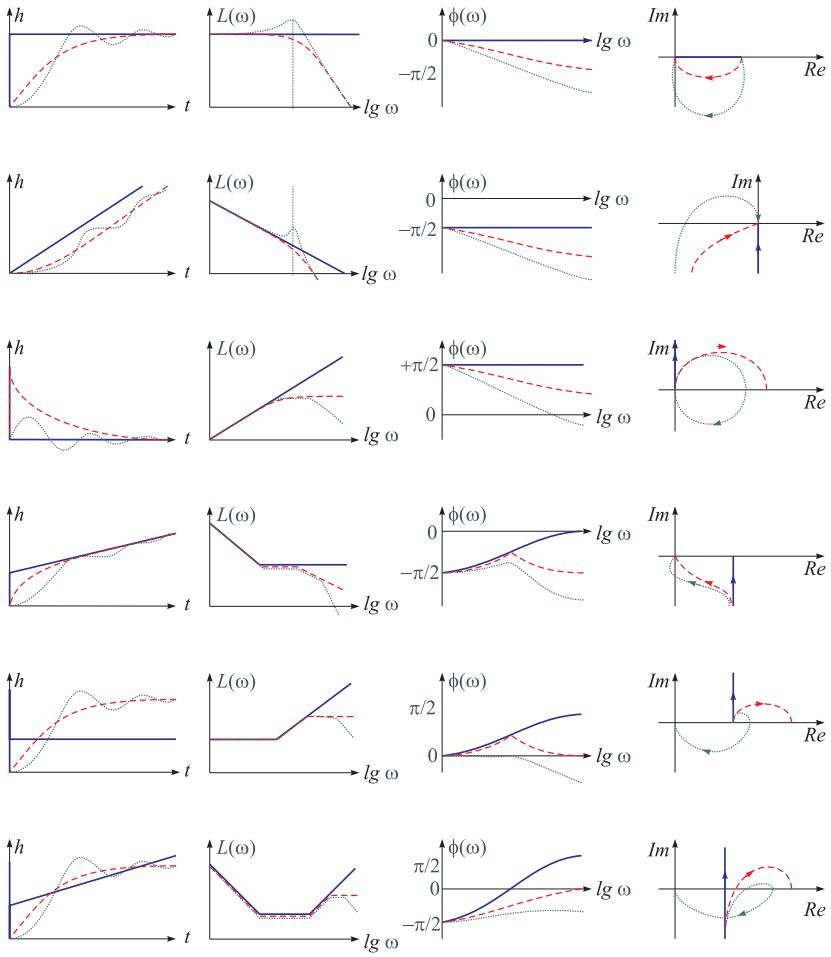

Figura 7.4: Transfer function $h(t) = \frac{y(t)}{x_w}$, Bode diagram amplitude $L(\omega) = 20 \lg |F_R|$ and phase $\varphi = \arctan \frac{Im\ F_R}{Re\ F_R}$, and polar representation $F(i\omega) = \mathrm{Re}\ F_R + i\mathrm{Im}\ F_R$ of the most common regulators. With delay time (—), $T_2 = T_1 = 0$, first order with delay time (- - -), $T_2 = 0 \neq T_1$, and second order $(\cdots)$, $T_2 \neq 0 \neq T_1$. From top to bottom, the diagrams show the regulators P, I, D, PI, PD, and PID, described by the equations (7.23) and (7.24).

For example, for a *proportional regulator*, we have,

$$y = K_P x_w \qquad \text{e} \qquad F_R = K_P \ , \tag{7.25}$$

for an *integral regulator* with time delay T_1, we have,

$$T_1 \dot{y} + y = K_I \int x_w dt \qquad \text{e} \qquad F_R = \frac{K_I}{p(1 + pT_1)} \ , \tag{7.26}$$

or for a *PID regulator* without delay, we have,

$$y = K_P x_w + K_D \dot{x}_w + K_I \int x_w dt \qquad \text{e} \qquad F_R = K_P + \frac{K_I}{p} + K_D p \ . \tag{7.27}$$

Since there are three basic operations (multiplication with 1, p and $1/p$), in the end, all rational circuit elements can be reduced to an addition and concatenation of proportional $F(p) =$

K_P, integral $F(p) = K_I/p$, and differentials elements, $F(p) = K_D p$. In particular, $PID-T_1...T_n$ circuits can be constructed by putting in parallel P, I, and D regulators concatenated with delay elements T_1. The possibility of feedback opens other possibilities (see Fig. 7.5(a)].

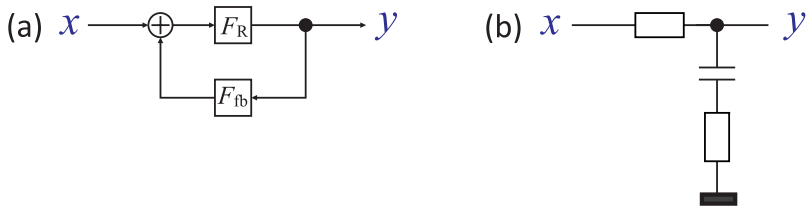

Figura 7.5: (a) Circuit with feedback, (b) low-pass filter circuit.

We consider the example of a low-pass filter exhibited in Fig. 7.5(b) and described by the equation,

$$F(i\omega) = \frac{R + i\omega L + 1/i\omega C}{R_i + R + i\omega L + 1/i\omega C} \ . \tag{7.28}$$

I.e., we have a $PID - T_1T_2$ circuit.

Another example, is the dead time circuit,

$$y(t) = x(t - T_t) \quad \text{e} \quad F(p) = e^{-pT_t} \ . \tag{7.29}$$

We have,

$$F(i\omega) = e^{-i\omega T_t} F_0 \quad \text{e} \quad |F(i\omega)| = F_0 \quad \text{e} \quad \varphi(i\omega) = -\omega T_t \ . \tag{7.30}$$

Hence, dead time circuits produce phase shifts, which are proportional to the dead time interval T_t.

7.1.7 Heuristic rules for the Bode diagram

Any deviation of the amplitude spectrum from $n \cdot 6$dB/octave to $(n+1) \cdot 6$dB/octave causes a retardation in the phase spectrum of 90°. At the cut-off frequency, where the inclination changes its behavior, the phase shift is just 45°. A deviation to higher/lower inclinations shifts the phase by ±90°. (This does not hold for some phase-shifting circuits).

7.1.8 Transfer function of feedback circuits

Fig. 7.5 shows the idea underlying the feedback,

$$F(p) = \frac{1}{1/F_R - F_{fb}} \ . \tag{7.31}$$

For example, for $F_R = 1/T_1 p$ e $F_{fb} = -1$ he have,

$$F(p) = \frac{1}{1 + T_1 p} \ , \tag{7.32}$$

which corresponds to a delay element (or high-pass filter).

For F_r being a proportional element, we say that the feedback rigid, for F_r being differential, the feedback is anticipating, and for F_r being integral, the feedback is delaying.

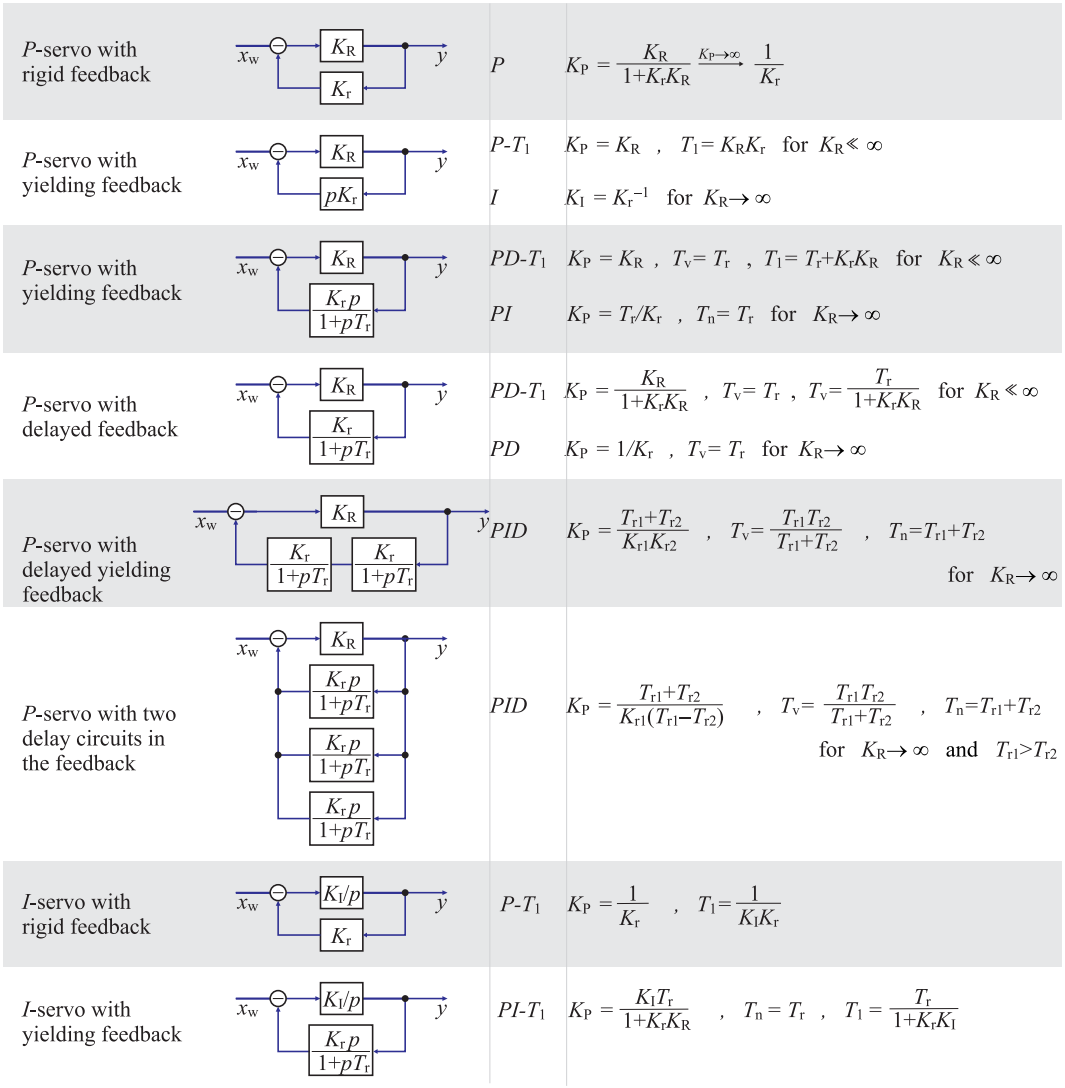

Figura 7.6: Some examples for feedback regulators. The columns show from left to right: the nomenclature, the circuit diagram, the behavior, and the constants of the LTI system.

7.1.9 Stability of feedback circuits

As discussed above, the transfer function of the feedback circuit is,

$$H(p) = \frac{F(p)}{1 + F(p)F_{fb}(p)} \ . \tag{7.33}$$

The *open loop gain* é $V(p) = F(p)F_{fb}(p)$. The circuit is stable, when for all the eigenfunctions e^{pt}, that do not decay with $Re\ p \geq 0$, the transfer function of the feedback circuit is finite, $H(p) < \infty$.

An equivalent criterion is the *Nyquist criterion*: *The curve $V(i\omega)$ to $\omega \in [0;\infty[$ must always bypass the point of instability at $Re\ p = -1$ leaving it on the left side. That is, considering negative frequencies, the curve should not circle this point.* Fig. 7.7 shows an example.

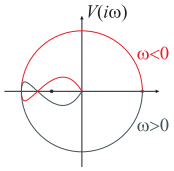

Figura 7.7: Illustration of the Nyquist criterion.

7.1.10 Noise reduction via feedback circuits

The idea of *locking*, whether mechanical or electronic, is to bring a given physical (control) signal X to a predetermined value W and lock it there. To achieve this goal, one needs a *regulator* to adequately neutralize the impact of perturbations. Fig. 7.8 shows the scheme of a simple control.

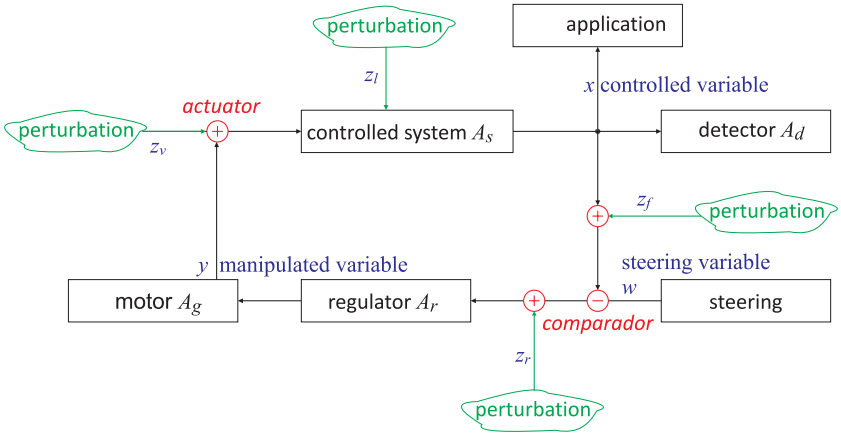

Figura 7.8: General idea of a locking circuit.

For a control to work, it needs to know in which direction to act and when the control point is reached. Therefore, each control needs a slope (*discriminator*) crossing zero. This can be implemented by comparing the signal X delivered by the detector A_d with a reference signal W. The error signal $W - X$ is then processed by a controller A_R, and the control signal Y is passed, via the actuator A_g, to the controlled device A_S. The controlled device (and obviously all other components of the circuit) are subject to perturbations Z. The transfer functions form a closed control circuit,

$$Y = A_g A_r (W - Z) X = A_d A_s (Y + Z) \ . \tag{7.34}$$

Consequently

$$X = \frac{A_g A_r A_d A_s}{1 + A_g A_r A_d A_s} W + \frac{A_d A_s}{1 + A_d A_s A_d A_s} Z \ . \tag{7.35}$$

We call $V \equiv A_g A_r A_d A_s$ the *loop amplification* of the feedback, such that,

$$X = \frac{A_g A_r A_d A_s}{1 + V} W + \frac{A_d A_s}{1 + V} Z \ . \tag{7.36}$$

If $V(p) = V_0$ is a proportional regulator, the differential equation corresponding to (7.37) gives $x \nrightarrow 0$ to $t \to 0$ (that is, $p \to 0$). Hence, we do not have stationary behavior. In contrast, if $V(p) = V_0/p$ is an integral regulator, the differential equation corresponding to (7.37) gives $x \to 0$ for $t \to 0$ (that ie, $p \to 0$). Hence, we have stationary behavior.

Regulators P have little phase lag, but the controlled variable can not be zeroed. On the other hand, regulators I have finite control speed, but the controlled variable can be zeroed. Regulators PI (putting in parallel P and I) have a reaction time $T_n = K_P/K_I$; that is, the jump response is advanced by T_n in comparison to the regulator I.

In the temporal regime we can summarize that regulators

- D are characterized by the absence of memory, but they are very fast,
- P have no idea of the amplitude of their impact,
- I increase their impact in time until the error disappears.

The formula (7.35) shows that noise suppression becomes all the better, as the amplification of the controller A_r is higher. However, with the amplification of the controller, also the amplification of the closed control circuit increases, and this necessarily causes phase shifts, which lead to oscillations in the circuit.

Like any real system, the controlled device behaves as a low-pass at high frequency. In other words, the device can only respond to external perturbations with finite speed. This delay of the response leads to a phase shift that can reverse the sign of the signal X and transform a negative feedback into a positive feedback. Now, in the case that there are high frequency perturbations, for which the amplification of the closed control circuit is > 1, these perturbations can be amplified to form oscillations. These oscillations, which occur at the bandwidth of the closed loop gain are called *servo oscillations*.

The transfer function of a low-pass with the cut-off frequency ω_g is

$$A_s = \frac{1}{1 + f/f_g} \ . \tag{7.37}$$

The simplest types of control loops are the *proportional control* $A_r = A$ and the "PI control" (proportional-integral) $A_r = \frac{A}{1+f_g/f}$.

7.1.10.1 Noise sources

Noise can enter a systems in various places, as shown in Fig. 7.8. For this diagram, we have (with the loop gain),

$$x = \frac{1}{1 + V_0}[z_l + z_v - V_0(z_r + z_f - w)] \ . \tag{7.38}$$

We assume that the controlled system is of the $P-T_2$ type and the servo regulator of the $P-T_1$ type. In the stationary state, $P \to 0$ and $V_0 = K_{ps1}K_{ps2}K_{pr}$, we obtain,

$$x = \frac{1}{1 + V_0} z_l + \frac{K_{ps2}K_{ps1}}{1 + V_0} z_v - \frac{V_0}{1 + V_0}(z_r + z_f - w) \ . \tag{7.39}$$

Repeating the calculation, but with an integrator I, we get,

$$x = -z_r - z_f + w \ . \tag{7.40}$$

This means, that the *perturbations entering between the measurement point and the input of the regulator are not eliminated*! Hence, the detector (which generally works with very low signals) should not introduce or let penetrate noise, because this affects the variable to be controlled: Any variation of the steering variable, at the integral regulator, will be transmitted 1 to 1.

7.1.11 MIMO control systems

So far, we have discussed *single-input single-output control system*s (*SISO*), which is the simplest and most common type, in which one output is controlled by one control signal. Examples are the temperature control or an audio system, in which the control input is the input audio signal and the output is the sound waves from the speaker.

In contrast, *multiple-input multiple-output control system*s (*MIMO*) are found in more complicated systems. For example, modern large telescopes such as the Keck and MMT have mirrors composed of many separate segments each controlled by an actuator. The shape of the entire mirror is constantly adjusted by a MIMO active optics control system using input from multiple sensors at the focal plane, to compensate for changes in the mirror shape due to thermal expansion, contraction, stresses as it is rotated and distortion of the wavefront due to turbulence in the atmosphere.

Another example are ultra-stable laser systems stabilized by combinations of fast actuators with low dynamic range and slow actuators with large dynamic range.

Capítulo 8

Data sheets

DB The following pages contain the data sheets of the main components used in this course.

HL6722G

AlGaInP Laser Diode

opnext
Powered by HITACHI

ODE-208-220E (Z)

Rev.5
Mar. 2005

Description

The HL6722G is a 0.67 µm band AlGaInP index-guided laser diode with a multi-quantum well (MQW) structure. It is suitable as a light source for bercode scanner, and various other types of optical equipment. Hermetic sealing of the package assures high reliability.

Features

- Visible light output at wavelengths up to 680 nm
- Single longitudinal mode
- Continuous operating output: 5 mW CW
- Low voltage operation: 2.7 V Max
- Low current operation: 32 mA Typ
- Built-in monitor photodiode

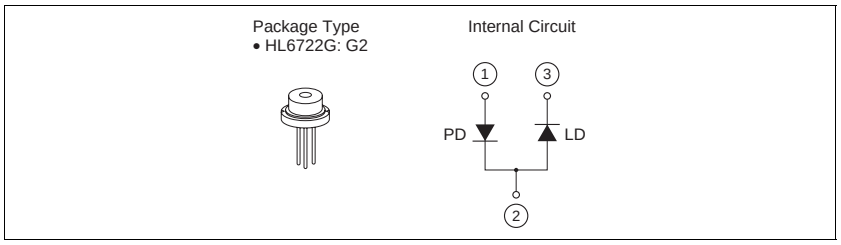

opnext
Powered by HITACHI

Figura 8.1: Data sheet for the diode laser from Thorlabs, model Hitachi HL6722G.

Coaxial

Amplifier

ZHL-2-8

50Ω Medium High Power 10 to 1000 MHz

ZHL-2-8X

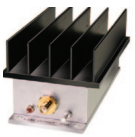

ZHL-2-8

SMA version shown

Features

- wideband, 10 to 1000 MHz
- high IP3, +38 dBm typ.
- medium high power, 29 dBm min.

Applications

- VHF/UHF
- test equipment
- cellular
- instrumentation
- laboratory

CASE STYLE: T34

Connectors	Model	Price	Qty.
BNC	ZHL-2-8	$525.00 ea.	(1-9)
BNC	ZHL-2-8X	$515.00 ea.	(1-9)
SMA	ZHL-2-8-S	$535.00 ea.	(1-9)
SMA	ZHL-2-8X-S	$525.00 ea.	(1-9)

Electrical Specifications

MODEL NO.	FREQ. (MHz)		GAIN (dB)			MAXIMUM POWER OUTPUT (dBm)		DYNAMIC RANGE		VSWR (:1) Max.		DC POWER	
	f_L	f_U	Min.	Typ.	Flatness Max.	(1 dB Compr.) Min.	Input (no damage)	NF (dB) Typ.	IP3 (dBm) Typ.	In	Out	Volt (V) Nom.	Current (A) Max.
ZHL-2-8	10	1000	31	35	±1.0	+29	+5	10.0	+38	2.0	2.0	24	0.6
ZHL-2-8X*	10	1000	31	35	±1.0	+29	+5	10.0	+38	2.0	2.0	24	0.6

* Heat sink not included
Open load is not recommended, potentially can cause damage.
With no load derate max input power by 20 dB

To order without heat sink, add suffix X to model number. Alternative heat sinking and heat removal must be provided by the user to limit maximum temperature to 65°C, in order to ensure proper performance. For reference, this requires thermal resistance of user's external heat sink to be 1.35°C/W Max.

Maximum Ratings

Operating Temperature	-20°C to 65°C
Storage Temperature	-55°C to 100°C
DC Voltage	+25V Max.

Permanent damage may occur if any of these limits are exceeded.

Outline Drawing

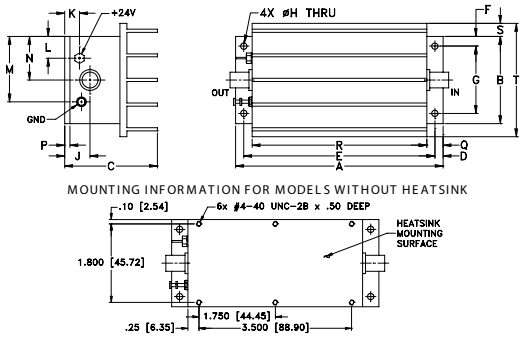

Figura 8.2: Data sheet for the rf-amplifier from MiniCircuits, model ZHL-2-8.

Coaxial

Voltage Controlled Oscillator

ZOS-100+

Dual Output 50 to 100 MHz

CASE STYLE: BR386

Connectors	Model	Price	Qty.
SMA	ZOS-100+	$119.95	(1-9)

+ RoHS compliant in accordance with EU Directive (2002/95/EC)

The +Suffix has been added in order to identify RoHS Compliance. See our web site for RoHS Compliance methodologies and qualifications.

Features

- octave bandwidth
- linear tuning, 4.5 MHz/V typ.
- excellent harmonic suppression, -29 dBc typ.
- rugged shielded case
- protected by US Patent, 6,943,629

Applications

- auxiliary output freq. monitoring
- load insensitive source

Electrical Specifications

FREQUENCY (MHz)		POWER OUTPUT (dBm) Typ.		TUNING VOLTAGE (V)		PHASE NOISE (dBc/Hz) SSB at offset frequencies: Typ.			PULLING (MHz) pk-pk (open/short)	PUSHING (MHz/V)	TUNING SENSITIVITY (MHz/V)	HARMONICS (dBc)		3 dB MODULATION BANDWIDTH (MHz)	DC OPERATING POWER	
Min.	Max.	Main	Aux.	Min.	Max.	10 kHz	100 kHz	1 MHz	Typ.	Typ.	Typ.	Typ.	Max.	Typ.	Vcc (volts)	Current (mA) Max.
50	100	+9	-12	1	16	-111	-131	-143	0.026	0.25	4.5	-29	-20	0.1	12	140

Maximum Ratings

Operating Temperature	-55°C to 85°C
Storage Temperature	-55°C to 100°C
Absolute Max. Supply Voltage (Vcc)	+16V
Absolute Max. Tuning Voltage (Vtune)	+18V

all specifications: 50 ohm system
Permanent damage may occur if any of these limits are exceeded.

electrical schematic

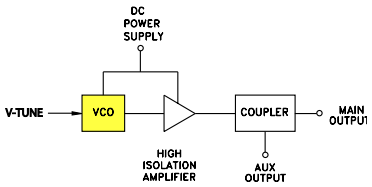

Outline Drawing

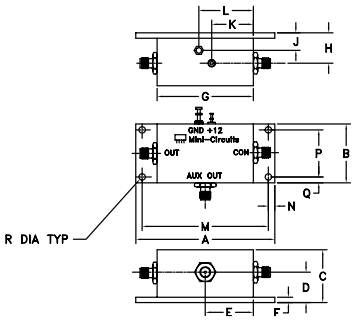

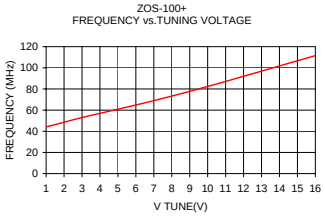

Outline Dimensions (inch / mm)

A	B	C	D	E	F	G	H	J	K	L	M	N	P	Q	R	wt
3.25	1.38	1.25	.71	1.13	.125	2.25	.71	.41	.98	1.28	2.950	.15	1.100	.14	.150	grams
82.55	35.05	31.75	18.03	28.70	3.18	57.15	18.03	10.41	24.89	32.51	74.93	3.81	27.94	3.56	3.81	180

Figura 8.3: Data sheet for the Voltage-Controlled Oscillator (VCO) from Minicircuits, model ZOS-100+.

Coaxial

Voltage Variable Attenuator

ZX73-2500+

50Ω 10 to 2500 MHz

FEMALE SMA shown

CASE STYLE: GD958

SMA INPUT	Connectors OUTPUT	Model	Price	Qty.	Case
FEMALE	FEMALE	ZX73-2500-S+	$49.95	(1-9)	GD958
MALE	FEMALE	ZX73-2500M-S+	$49.95	(1-9)	GD1163

+ RoHS compliant in accordance with EU Directive (2002/95/EC)

The +Suffix has been added in order to identify RoHS Compliance. See our web site for RoHS Compliance methodologies and qualifications.

Maximum Ratings

Operating Temperature	-55°C to 85°C
Storage Temperature	-55°C to 85°C
Absolute Max. Supply Voltage (V+)	12V
Absolute Max. Control Voltage (Vcrtl)	20V
Absolute Max. RF Input Level	+20 dBm

Permanent damage may occur if any of these limits are exceeded.

Features

- Broadband, 10-2500 MHz
- IP3, +43 dBm typ.
- 40 dB attenuation @ 1500 MHz
- Good VSWR at in /out ports over attenuation range
- No external bias and RF matching network required
- Shielded case
- Protected by US Patent 6,790,049

Applications

- Variable gain amplifier
- Power level control
- Feed-forward amplifiers
- ALC circuits

Outline Drawing (GD958)

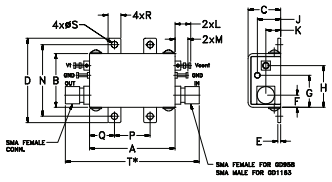

Outline Dimensions (inch / mm)

A	B	C	D	E	F	G	H	J
1.20	.75	.46	1.18	.04	.17	.45	.59	.33
30.48	19.05	11.68	29.97	1.02	4.32	11.43	14.99	8.38

K	L	M	N	P	Q	R	S	T	wt.
.21	.22	.18	1.00	.50	.35	.18	.106	1.88	grams
5.33	5.59	4.57	25.40	12.70	8.89	4.57	2.69	47.75	35.0

Note:

* T dimension is 2.05 inch (52.07 mm) for GD1163 Case Style.

Electrical Specifications (T_{AMB}= 25°C)

FREQ. (MHz)		MIN. INSERTION LOSS, dB (+15V)		MAX. ATTENUATION dB (0V)		INPUT POWER (dBm)	CONTROL Voltage (V)	CONTROL Current (mA)	IP3 (dBm)	RETURN LOSS[1] (dB)	POWER SUPPLY Voltage (V)	POWER SUPPLY Current (mA)
Min.	Max.	Typ.	Max.	Typ.	Min.	Max.		Max.	Typ.	Typ.		Max.
10	500	3.0	4.6	55	41	+20	0 - 17	30	43	20	+3 to +5	5
500	1500	3.3	5.0	40	30	+20	0 - 17	30	43	20	+3 to +5	5
1500	2500	4.0	6.2	37	25	+20	0 - 17	30	44	20	+3 to +5	5

Notes:
Rise/Fall time: 14μSec/25μSec Typ.
Switching Time, turn on/off: 14μSec/25μSec Typ.
[1] Improved R. Loss in/out performance can be achieved at certain frequencies by choosing a V+ between +3V to +5V

Equivalent Schematic

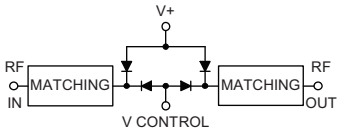

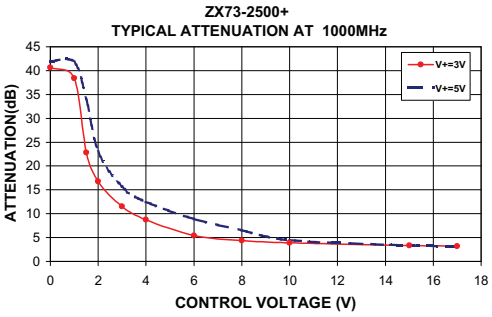

Figura 8.4: Data sheet for the voltage-controlled variable attenuator from Minicircuits, model ZX73-2500+.

Plug-In

Power Splitter/Combiner

PSC-2-1+
PSC-2-1

2 Way-0° 50Ω 0.1 to 400 MHz

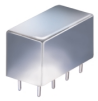

CASE STYLE: A01
PRICE: $14.20 ea. QTY. (1-9)

+ RoHS compliant in accordance with EU Directive (2002/95/EC)

The +Suffix identifies RoHS Compliance. See our web site for RoHS Compliance methodologies and qualifications.

Maximum Ratings

Operating Temperature	-55°C to 100°C
Storage Temperature	-55°C to 100°C
Power Input (as a splitter)	1W max.
Internal Dissipation	0.125W max.

Pin Connections

SUM PORT	1
PORT 1	5
PORT 2	6
GROUND	2,3,4,7,8
CASE GROUND	2,3,4,7,8

Features

- wideband, 0.1 to 400 MHz
- low insertion loss, 0.4 dB typ.
- rugged welded construction

Applications

- VHF/UHF
- federal & defense communications

Outline Drawing

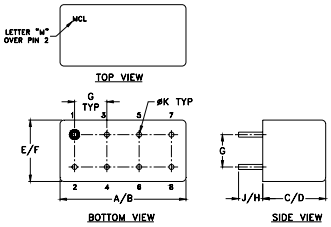

Outline Dimensions (inch / mm)

A	B	C	D	E	F
.770	.800	.385	.400	.370	.400
19.56	20.32	9.78	10.16	9.40	10.16
G	H	J	K		wt
.200	.20	.14	.031		grams
5.08	5.08	3.56	0.79		5.2

Electrical Specifications

FREQ. RANGE (MHz)	ISOLATION (dB)						INSERTION LOSS (dB) ABOVE 3.0 dB						PHASE UNBALANCE (Degrees)			AMPLITUDE UNBALANCE (dB)		
	L		M		U		L		M		U		L	M	U	L	M	U
f_L-f_U	Typ.	Min	Typ.	Min	Typ.	Min	Typ.	Max.	Typ.	Max.	Typ.	Max.	Max.	Max.	Max.	Max.	Max.	Max.
0.1-400	20	15	25	20	25	20	0.2	0.6	0.4	0.75	0.6	1.0	2.0	3.0	4.0	0.15	0.2	0.3

L = low range [f_L to 10 f_L] M = mid range [10 f_L to f_U/2] U= upper range [f_U/2 to f_U]

Typical Performance Data

Frequency (MHz)	Insertion Loss (dB) S-1	Insertion Loss (dB) S-2	Amplitude Unbalance (dB)	Isolation (dB)	Phase Unbalance (deg.)	VSWR S	VSWR 1	VSWR 2
0.10	3.23	3.23	0.00	24.82	0.01	1.16	1.37	1.37
5.00	3.14	3.14	0.00	35.64	0.01	1.10	1.11	1.11
20.00	3.18	3.17	0.00	35.33	0.03	1.11	1.10	1.10
40.00	3.18	3.18	0.00	34.39	0.02	1.12	1.10	1.10
60.00	3.22	3.22	0.00	33.16	0.02	1.12	1.09	1.09
80.00	3.24	3.24	0.00	31.85	0.04	1.13	1.09	1.09
100.00	3.24	3.24	0.00	30.68	0.05	1.13	1.09	1.09
150.00	3.28	3.27	0.00	28.37	0.04	1.14	1.08	1.08
175.00	3.31	3.30	0.01	27.46	0.07	1.14	1.07	1.07
200.00	3.32	3.31	0.01	26.72	0.05	1.15	1.07	1.07
225.00	3.32	3.31	0.01	26.14	0.02	1.15	1.06	1.06
250.00	3.37	3.36	0.01	25.65	0.05	1.15	1.06	1.06
300.00	3.41	3.38	0.03	24.88	0.10	1.15	1.06	1.06
350.00	3.47	3.44	0.03	24.40	0.06	1.16	1.08	1.07
400.00	3.50	3.46	0.04	23.86	0.05	1.18	1.10	1.09

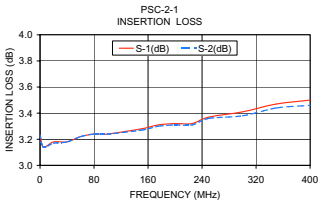

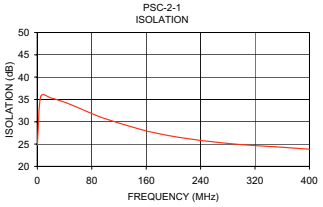

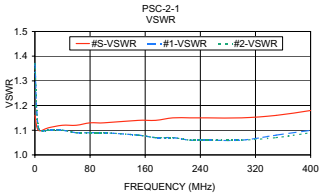

electrical schematic

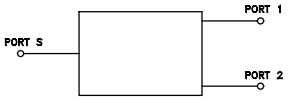

Mini-Circuits®
ISO 9001 ISO 14001 CERTIFIED

ALL NEW minicircuits.com

P.O. Box 350166, Brooklyn, New York 11235-0003 (718) 934-4500 Fax (718) 332-4661 For detailed performance specs & shopping online see Mini-Circuits web site

The Design Engineers Search Engine Provides ACTUAL Data Instantly From MINI-CIRCUITS At: www.minicircuits.com

RF/IF MICROWAVE COMPONENTS

REV. A
M98898
PSC-2-1
HY/TD/CP
070202

Figura 8.5: Data sheet for the power divider from Minicircuits, model PSC-2-1.

Plug-In

Frequency Mixer

SRA-2CM+

Level 7 (LO Power +7 dBm) 5 to 1000 MHz

CASE STYLE: A01
PRICE: $18.20 ea. QTY (1-9)

+ RoHS compliant in accordance with EU Directive (2002/95/EC)

The +Suffix has been added in order to identify RoHS Compliance. See our web site for RoHS Compliance methodologies and qualifications.

Maximum Ratings

Operating Temperature	-55°C to 100°C
Storage Temperature	-55°C to 100°C
RF Power	50mW
IF Current	40mA

Pin Connections

LO	8
RF	1
IF	3,4^
GROUND	2,5,6,7
CASE GROUND	2,5,6,7

^ pins must be connected together externally

Features

- excellent conversion loss, 5.27 dB typ.
- good L-R isolation, 35 dB typ. L-I isolation, 30 dB typ.
- rugged welded construction
- hermetic

Applications

- VHF/UHF
- cellular
- defense & federal communications
- ISM/GSM

Outline Drawing

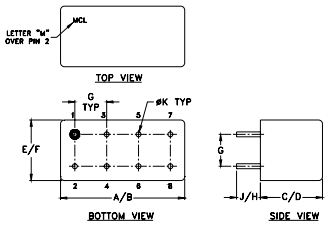

Outline Dimensions (inch / mm)

A	B	C	D	E	F
.770	.800	.385	.400	.370	.400
19.56	20.32	9.78	10.16	9.40	10.16
G	H	J	K		wt
.200	.20	.14	.031		grams
5.08	5.08	3.56	0.79		5.2

Electrical Specifications

FREQUENCY (MHz)		CONVERSION LOSS (dB)				LO-RF ISOLATION (dB)						LO-IF ISOLATION (dB)					
		Mid-Band			Total Range	L		M		U		L		M		U	
LO/RF f_L-f_U	IF	$\bar{X}$	σ	Max.	Max.	Typ.	Min.	Typ.	Min.	Typ.	Min.	Typ.	Min.	Typ.	Min.	Typ.	Min.
5-1000	DC-1000	5.27	.04	7.0	8.5	60	50	35	30	30	25	50	45	30	25	25	20

1 dB COMP.: +1 dBm typ.

L = low range [f_L to 10 f_L]
m= mid band [2f_L to f_U/2]

M = mid range [10 f_L to f_U/2]

U = upper range [f_U/2 to f_U]

Typical Performance Data

Frequency (MHz)		Conversion Loss (dB)	Isolation L-R (dB)	Isolation L-I (dB)	VSWR RF Port (:1)	VSWR LO Port (:1)
RF	LO	LO +7dBm	LO +7dBm	LO +7dBm	LO +7dBm	LO +7dBm
5.00	35.00	7.36	67.00	67.00	5.03	4.09
38.13	68.13	5.59	54.82	53.34	1.40	3.04
71.27	41.27	5.30	49.15	48.13	1.31	2.99
137.53	107.53	5.33	46.10	45.22	1.27	2.83
200.00	170.00	5.35	42.68	41.91	1.24	2.82
236.93	206.93	5.27	41.09	40.29	1.24	2.72
303.20	273.20	5.28	39.42	38.94	1.24	2.76
336.33	306.33	5.42	39.72	36.88	1.26	2.77
402.60	372.60	5.63	38.13	35.49	1.30	2.85
468.86	438.86	5.62	37.15	35.09	1.37	2.84
535.13	505.13	5.87	35.49	32.57	1.45	2.97
568.26	538.26	6.01	35.26	31.27	1.50	2.96
634.53	604.53	6.17	36.03	29.46	1.61	3.10
700.79	670.79	6.68	38.00	30.29	1.70	3.21
767.06	737.06	6.49	38.00	29.92	1.85	3.09
800.19	770.19	6.11	39.26	28.34	2.01	3.03
833.33	803.33	6.37	39.87	27.52	2.08	3.08
899.59	869.59	6.80	40.23	26.99	2.32	3.39
965.86	935.86	6.86	42.61	25.65	2.53	3.58
1000.00	969.00	7.10	44.90	24.17	2.76	3.76

Electrical Schematic

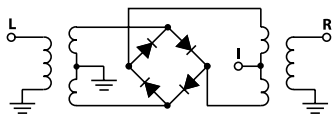

Figura 8.6: Data sheet for the mixer from Minicircuits, model SRA-2CM+.

SPECIFICATIONS				
AO Medium				TeO2
Acoustic Velocity				4.2 mm/µs
Active Aperture*	2.5	mm 'L' X	1	mm 'H'
Center Frequency (Fc)				80 MHz
RF Bandwidth	20 MHz @	-10 dB	Return Loss	
Input Impedance				50 Ohms Nominal
VSWR @ Fc				1.3 :1 Max
Wavelength				442-633 nm
Insertion Loss				4 % Max
Reflectivity per Surface				1 % Max
Anti-Reflection Coating				MIL-C-48497
Optical Power Density				250 W/mm^2
Contrast Ratio				1000 :1 Min
Polarization				90 ° To Mounting Plane

PERFORMANCE VS WAVELENGTH				
Wavelength (nm)	**442**	**488**	**515**	**633**
Saturation RF Power (W)	0.27	0.33	0.36	0.55
Bragg Angle (mr)	4.2	4.6	4.9	6
Beam Separation (mr)	8.4	9.2	9.8	12

PERFORMANCE VS BEAM DIAMETER			
Beam Diameter (µm)	**200**	**300**	**500**
at Wavelength (nm)	633	633	633
Diffraction Efficiency (%)	80	83	85
Rise Time (nsec)	34	49	80
	15.9	10.6	6.3
	10	5	1

Figura 8.7: Data sheet for the acousto-optic modulator (AOM) from Crystal Technologies, model AOMO 3080-120.

Silicon PIN Photodiodes - Large Area, Fast Response Time – 400 nm to 1100 nm

The FFD series devices are high-quality, large-area, high-speed, N-type Si PIN photodiodes in hermetically sealed TO packages designed for the 400 nm to 1100 nm wavelength range. The FND-100Q has a quartz window to enhance UV responsivity.

Preamplifiers

Preamplifier modules incorporating these photodiodes are available on a custom basis.

Si PINs – Large Area, Fast Response

Typical Characteristics @ T = 22º C

Part #	Standard Package	Photo Sens. Diam. (mm)	Resp. @ 900 nm (A/W)	Dark Current Id (nA)	Spect. Noise Curr. Dens. In (fW/√Hz)	Cap. @ 100 kHz Cd (pF)	Response Time tr (ns)	NEP @ 900 nm (fW/√Hz)	Bias Volt (V)
FFD-040B	Y	1	0.58	1	18	1.8	2	31	15
FFD-100	B	2.5	0.58	2	25	8.5	3.5	44	15
FFD-200	C3	5.1	0.58	4	36	30	5	62	15
FND-100Q	B	2.5	0.58	10	60	8.5	2	100	90

Typical Applications

Laser detection systems, fast pulse detection, instrumentation, and high-speed switching.

Figura 8.8: Data sheet for the photo diode from Perkin Elmers FDD100.

Detectors

Silicon Epitaxial PIN Photodiodes - High Speed – 400 nm to 1100 nm

The C30736 series of high-speed epitaxial silicon PIN photodetectors provide fast response and good quantum efficiency in the spectral range between 400 nm and 1100 nm. These devices are optimized for high-speed, high volume and low cost applications. Standard sizes include 0.25 mm, 0.5 mm, 1.0 mm, 1.5 x 1.5 mm, and custom sizes can be accomodated depending on volume required. Available in plastic surface mount packages and in chip form.

Silicon Epitaxial PIN Photodiodes

Typical Characteristics @ T = 22º C

Part #	Standard Package	Photo Sens. Diam. (mm)	Resp. @ 870 nm (A/W)	Dark Current @2V Id (nA)	Spect. Noise Curr. Dens. In (fW/√Hz)	Cap. @ 100 kHz Cd (pF)	Response Time tr (ns)	NEP @ 870 nm (fW/√Hz)	Bias Volt (V)
C30736-1	Chip form	0.20	0.55	0.05	6	0.75	0.3	11	2
C30736-2	Chip form	0.50	0.55	0.10	10	1.5	0.5	18	2
C30736-3	Chip form	1.5 x 1.5	0.55	0.50	50	14	0.3	91	2

Silicon PIN Photodiodes - Standard N-Type – 400 nm to 1100 nm

The C308XX series devices are high-quality N-type Si PIN photodiodes in hermetically sealed TO packages designed for the 400 nm to 1100 nm wavelength region.

Si PINs – Standard N-Type

Typical Characteristics @ T = 22º C

Part #	Standard Package	Photo Sens. Diam. (mm)	Resp. @ 900 nm (A/W)	Dark Current Id (nA)	Spect. Noise Curr. Dens. (fA/√Hz)	Cap. @ 100 kHz Cd (pF)	Response Time tr (ns)	NEP @ 900 nm (fW/√Hz)	Bias Volt (V)
C30807E	A	1	0.6	1	18	2.5	3	30	45
C30808E	B	2.5	0.6	3	31	6	5	52	45
C30822E	C	5	0.6	5	40	17	7	67	45
C30809E	C3	8	0.6	7	47	35	10	79	45
C30810E	D	11.4	0.6	30	98	70	12	163	45

Typical Applications

Laser detection systems, photometry, data transmission, instrumentation, and high-speed switching.

Silicon PIN Photodiodes - Large Area, Fast Response Time – 400 nm to 1100 nm

The FFD series devices are high-quality, large-area, high-speed, N-type Si PIN photodiodes in hermetically sealed TO packages designed for the 400 nm to 1100 nm wavelength range. The FND-100Q has a quartz window to enhance UV responsivity.

Preamplifiers

Preamplifier modules incorporating these photodiodes are available on a custom basis.

Si PINs – Large Area, Fast Response

Typical Characteristics @ T = 22º C

Part #	Standard Package	Photo Sens. Diam. (mm)	Resp. @ 900 nm (A/W)	Dark Current Id (nA)	Spect. Noise Curr. Dens. In (fW/√Hz)	Cap. @ 100 kHz Cd (pF)	Response Time tr (ns)	NEP @ 900 nm (fW/√Hz)	Bias Volt (V)
FFD-040B	Y	1	0.58	1	18	1.8	2	31	15
FFD-100	B	2.5	0.58	2	25	8.5	3.5	44	15
FFD-200	C3	5.1	0.58	4	36	30	5	62	15
FND-100Q	B	2.5	0.58	10	60	8.5	2	100	90

Typical Applications

Laser detection systems, fast pulse detection, instrumentation, and high-speed switching.

Figura 8.9: Data sheet for the photo diode from Perkin Elmers C30822E.

19-0350; Rev 0; 12/94

MAXIM

Precision, Dual-Supply, SPST Analog Switches

General Description

The MAX320/MAX321/MAX322 are precision, dual, SPST analog switches designed to operate from ±3V to ±8V dual supplies. The MAX320 has two normally open (NO) switches and the MAX321 has two normally closed (NC) switches. The MAX322 has one NO and one NC switch. Low power consumption (1.25mW) makes these parts ideal for battery-powered equipment. They offer low leakage currents (100pA max) and fast switching speeds (t_{ON} = 150ns max, t_{OFF} = 100ns max).

The MAX320 series, powered from ±5V supplies, offers 35Ω max on-resistance (R_{ON}), 2Ω max matching between channels, and 4Ω max R_{ON} flatness.

These switches also offer 5pC max charge injection and a minimum of 2000V ESD protection per Method 3015.7.

For equivalent devices specified for single-supply operation, see the MAX323/MAX324/MAX325 data sheet. For quad versions of these switches, see the MAX391/MAX392/MAX393 data sheet.

Applications

Battery-Operated Systems	Sample-and-Hold Circuits
Heads-Up Displays	Guidance and Control Systems
Audio and Video Switching	Military Radios
Test Equipment	Communications Systems
±5V DACs and ADCs	PBX, PABX

Features

- **Low On-Resistance, 35Ω max (16Ω typical)**
- **R_{ON} Matching Between Channels <2Ω**
- **R_{ON} Flatness <4Ω**
- **Guaranteed Charge Injection <5pC**
- **Bipolar Supply Operation (±3V to ±8V)**
- **Low Power Consumption, <1.25mW**
- **Low Leakage Current Over Temperature, <2.5nA at +85°C**
- **Fast Switching, t_{ON} <150ns, t_{OFF} <100ns**
- **Guaranteed Break-Before-Make (MAX322 only)**

Ordering Information

PART	TEMP. RANGE	PIN-PACKAGE
MAX320CPA	0°C to +70°C	8 Plastic DIP
MAX320CSA	0°C to +70°C	8 SO
MAX320CUA	0°C to +70°C	8 µMAX
MAX320C/D	0°C to +70°C	Dice*
MAX320EPA	-40°C to +85°C	8 Plastic DIP
MAX320ESA	-40°C to +85°C	8 SO
MAX320EJA	-40°C to +85°C	8 CERDIP**
MAX320MJA	-55°C to +125°C	8 CERDIP**

Ordering Information continued at end of data sheet.

** Contact factory for dice specifications.*

*** Contact factory for availability.*

Pin Configurations/Functional Diagrams/Truth Tables

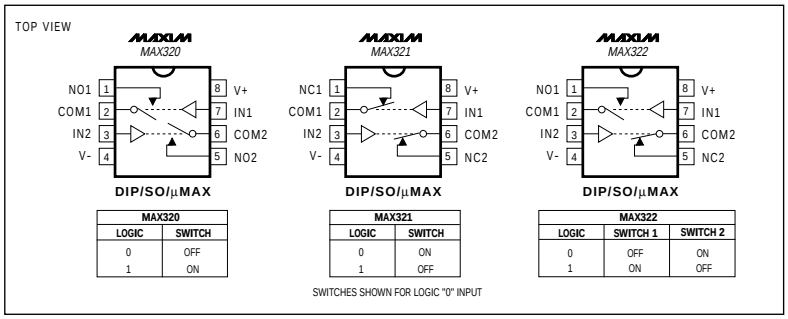

MAX320	
LOGIC	SWITCH
0	OFF
1	ON

MAX321	
LOGIC	SWITCH
0	ON
1	OFF

MAX322		
LOGIC	SWITCH 1	SWITCH 2
0	OFF	ON
1	ON	OFF

SWITCHES SHOWN FOR LOGIC "0" INPUT

Figura 8.10: Data sheet for the digital switch MAX322 from Maxim.

National Semiconductor

August 2000

LM741
Operational Amplifier

General Description

The LM741 series are general purpose operational amplifiers which feature improved performance over industry standards like the LM709. They are direct, plug-in replacements for the 709C, LM201, MC1439 and 748 in most applications.

The amplifiers offer many features which make their application nearly foolproof: overload protection on the input and output, no latch-up when the common mode range is exceeded, as well as freedom from oscillations.

The LM741C is identical to the LM741/LM741A except that the LM741C has their performance guaranteed over a 0˚C to +70˚C temperature range, instead of −55˚C to +125˚C.

Features

Connection Diagrams

Metal Can Package

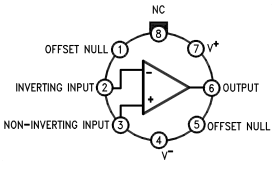

00934102

Note 1: LM741H is available per JM38510/10101

Order Number LM741H, LM741H/883 (Note 1), **LM741AH/883 or LM741CH**
See NS Package Number H08C

Dual-In-Line or S.O. Package

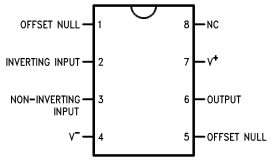

00934103

Order Number LM741J, LM741J/883, LM741CN
See NS Package Number J08A, M08A or N08E

Ceramic Flatpak

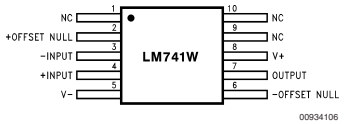

00934106

Order Number LM741W/883
See NS Package Number W10A

Typical Application

Offset Nulling Circuit

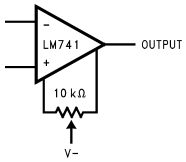

00934107

Figura 8.11: Data sheet for the operational amplifier LM741 from National Semiconductor.

ANALOG DEVICES

Low-Noise, Precision Operational Amplifier

OP27

FEATURES

Low Noise: 80 nV p-p (0.1 Hz to 10 Hz), 3 nV/√Hz
Low Drift: 0.2 μV/°C
High Speed: 2.8 V/μs Slew Rate, 8 MHz Gain Bandwidth
Low V_{OS}: 10 μV
Excellent CMRR: 126 dB at V_{CM} of ±11 V
High Open-Loop Gain: 1.8 Million
Fits 725, OP07, 5534A Sockets
Available in Die Form

GENERAL DESCRIPTION

The OP27 precision operational amplifier combines the low offset and drift of the OP07 with both high speed and low noise. Offsets down to 25 μV and drift of 0.6 μV/°C maximum make the OP27 ideal for precision instrumentation applications. Exceptionally low noise, e_n = 3.5 nV/√Hz, at 10 Hz, a low 1/f noise corner frequency of 2.7 Hz, and high gain (1.8 million), allow accurate high-gain amplification of low-level signals. A gain-bandwidth product of 8 MHz and a 2.8 V/μsec slew rate provides excellent dynamic accuracy in high-speed, data-acquisition systems.

A low input bias current of ±10 nA is achieved by use of a bias-current-cancellation circuit. Over the military temperature range, this circuit typically holds I_B and I_{OS} to ±20 nA and 15 nA, respectively.

The output stage has good load driving capability. A guaranteed swing of ±10 V into 600 Ω and low output distortion make the OP27 an excellent choice for professional audio applications.

(Continued on page 7)

PIN CONNECTIONS

TO-99
(J-Suffix)

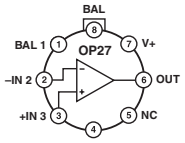

8-Pin Hermetic DIP
(Z-Suffix)
Epoxy Mini-DIP
(P-Suffix)
8-Pin SO
(S-Suffix)

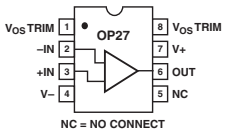

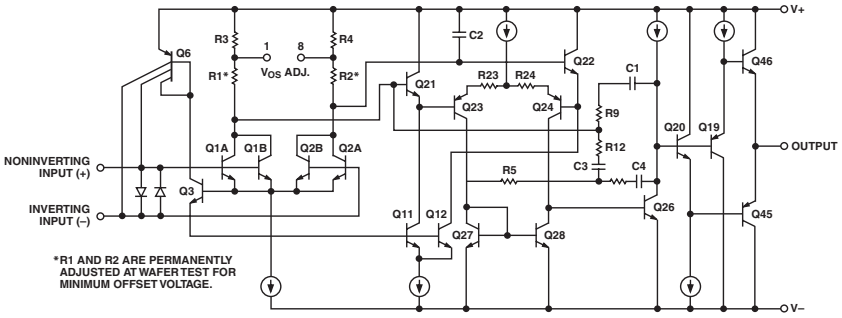

Figure 1. Simplified Schematic

Figura 8.12: Data sheet for the operational amplifier OP27 from Analog Devices.

Referências Bibliográficas

[1] B. Agate, B. Stormont, A. J. Kemp, C. T. A. Brown, U. Keller, and W. Sibbett, *Simplified cavity designs for efficient and compact femtosecond cr:lisaf lasers*, Opt. Comm. **205** (2002), 207.

[2] W. B. Davenport and W. L. Root, *Random, signals and noise*, McGraw-Hill Book Company Inc. (1958).

[3] D. S. Elliott, Rajarshi Roy, and S. J. Smith, *Extracavity laser bandshape and bandwidth modification*, Phys. Rev. A **26** (1982), 12, ⊙.

[4] O. Föllinger, *Regelungstechnik: Einführung in die methoden und ihre anwendung*, Hütig, 2008.

[5] J. D. Gaskill, *Linear systems, fourier transforms and optics*, John Wiley & sons, 1978.

[6] R. Holzwarth, Th. Udem, T. W. Hänsch, J. C. Knight, W. J. Wadsworth, and P. St. J. Russell, *Optical frequency synthesizer for precision spectroscopy*, Phys. Rev. Lett. **85** (2000), 2264.

[7] R. Holzwarth, M. Zimmermann, Th. Udem, T. W. Hänsch, P. Russbüldt, K. Gäbel, R. Poprawe, J. C. Knight, W. J. Wadsworth, and P. St. J. Russell, *White-light frequency comb generation with a diode-pumped cr:lisaf laser*, Opt. Lett. **26** (2000), 1376.

[8] S. Inouye, A. P. Chikkatur, D. M. Stamper-Kurn, J. Stenger, D. E. Pritchard, and W. Ketterle, *Superradiant rayleigh scattering from a bose-einstein condensate*, Science **285** (1999), 571, ⊙.

[9] D. Jaksch, S. A. Gardiner, K. Schluze, J. I. Cirac, and P. Zoller, *Uniting bose-einstein condensates in optical resonators*, Phys. Rev. Lett. **86** (2001), 4733, ⊙.

[10] D. J. Jones, S. A. Diddams, J. K. Ranka, A. Stentz, R. S. Windeler, J. L. Hall, and S. T. Cundiff, *Carrier-envelope phase control of femtosecond mode-locked lasers and direct optical frequency synthesis*, Science **288** (2000), 635.

[11] H. Kogelnik and X. Y. Li, *Laser beams and resonators*, Appl. Opt. **5** (1966), 155.

[12] Mann, Schiffelgen, and Froriep, *Einführung in die regelungstechnik*, Hanser-Verlag München, 2009.

[13] O. D. Mücke, R. Ell, A. Winter, Jung-Won Kim, J. R. Birge, L. Matos, and F. X. Kärtner, *Self-referenced 200 mhz octave-spanning ti:sapphire laser with 50 attosecond carrier-envelope phase jitter*, Opt. Exp. **13** (2005), 5163, ⊙.

[14] A. Pikovsky, M. Rosenblum, and J. Kurths, *Synchronization: A universal concept in nonlinear sciences*, Cambridge, University press (2001).

[15] H. R. Telle, B. Lipphardt, and J. Stenger, *Kerr-lens, mode-locked lasers as transfer oscillators for optical frequency measurements*, Appl. Phys. B **74** (2002), 1.

[16] Jun Ye, H. Schnatz, and L. W. Hollberg, *Optical frequency combs: From frequency metrology to optical phase control*, IEEE J. Sel. Top. QE **9** (2003), 1041.

Índice Remissivo